ORGANIC COMPOUNDS AS BUILDING BLOCKS IN MOLECULE-BASED MAGNETIC MATERIALS

by

Jordan Louis Arthur

A dissertation submitted to the faculty of
The University of Utah
in partial fulfillment of the requirements for the degree of

Doctor of Philosophy

Department of Chemistry

University of Utah

May 2012

The University of Utah Graduate School

STATEMENT OF DISSERTATION APPROVAL

The dissertation of **Jordan Louis Arthur**

has been approved by the following supervisory committee members:

Joel S. Miller	, Chair	**12/01/11** Date Approved
Thomas G. Richmond	, Member	**12/01/11** Date Approved
Ilya Zharov	, Member	**12/01/11** Date Approved
Jennifer Heemstra	, Member	**12/01/11** Date Approved
Amy M. Barrios	, Member	**12/01/11** Date Approved

and by **Henry S. White**, Chair of the Department of **Chemistry**

and by Charles A. Wight, Dean of The Graduate School.

ABSTRACT

Organic ligands have become an integral part of molecule-based magnetic systems. Incorporation of organic compounds into molecule-based magnets enables control of the physical properties and the blending of phenomena, e.g., photomagnetism. Understanding how to construct molecule-based magnetic systems with organic compounds should lead to new classes of readily functionalized materials.

The magnetic behavior of the dimeric form of *N*,*N*'-ethylenebis(salicylideniminato)cobalt(II) (Co^{II}(salen)) was reinvestigated as the dimer was seen to exhibit magnetic tristability associated with the dinuclear site. The singlet (S = 0) ground state arises from the antiferromagnetic coupled pair of the Co^{II} ions, each being in the single-ion (S = 1/2) electron configuration. The triplet (S = 1) excited state arises from ferromagnetic coupling of the Co^{II} S = 1/2 ions. As the temperature increases, the thermal energy populates both the singlet and triplet states. This leads to increases in the $\chi T(T)$ approaching the Curie behavior for the two Co^{II} S = 1/2 doublets at higher temperature.

In contrast to salen-like compounds, spin-carrying radical organic ligands have been seen to enhance magnetic properties. Reactions of *N*,7,7-tricyanoquinonemethanimine (TCQMI), which forms a radical, with precedented cationic building-blocks of molecular magnets have shown mixed results. The expected structural motif of 1-D chains of alternating $[TCQMI]^{\bullet -}$ and $[FeCp^*_2]^+$ showed weak magnetic ferrimagnetic ordering at low temperatures with a T_c of 3.4.

The reaction of TCQMI with $M^{II}(CO)_x$ compounds leads to amorphous materials which showed either weak ferromagnetic coupling or paramagnetic behavior at low temperatures. These results indicate that TCQMI is incompatible with forming magnetic systems where direct bonding to metal centers is encountered. Further evidence of the unsuitability of TCQMI was encountered in the reaction with MnTPP(py) (TPP = Tetraphenylporphinato; py = pyridine). The resulting structure consisted of 1-D chains with MnNCNMn linkages of warped MnTPP and a σ-$[TCQMI]_2^{2-}$ dimer.

The reaction of MnTPP(py) with TCQMI is in contrast with that of typical DCNQIs. The structure $[Mn^{III}TPP][Me_2DCNQI]$ has been determined by Rietveld refinement of the X-ray powder diffraction method. The nonsolvated structure is composed of linear (1-D) chains of alternating $[Mn^{III}TPP]^+$ and μ-$[Me_2DCNQI]^{\bullet-}$.

This dissertation is dedicated to my beautiful wife, Crystal, and to my parents. Your support and faith in me has made all the difference. And, to my son, Theodore, whom I have known only a few days, but am so excited to have in my life.

TABLE OF CONTENTS

LIST OF TABLES

LIST OF FIGURES

LIST OF SCHEMES

LIST OF SYMBOLS AND ABBREVIATIONS

H	applied magnetic field
B	internal magnetic field
M	magnetization
χ_v	magnetic susceptibility per volume
Oe	Oersted
χ	magnetic susceptibility
C	Curie constant
T	temperature
K	Kelvin
N	Avogadro's number
g	Landé g value
S	spin quantum number
μ_B	Bohr magneton
k_B	Boltzmann's constant
J	magnetic exchange parameter
θ	Weiss constant
χ^{-1}	inverse molar susceptibility
T_c	critical temperature
MFT	Mean-Field Theory, self-consistent field theory
z	number of nearest neighbors

ω	frequency of the ac field
χ'	in-phase ac susceptibility
χ''	out-of-phase ac susceptibility
Hz	Hertz
ZFC	zero-field-cooled
FC	field-cooled
T_b	bifurcation temperature
T	Tesla
M_{sat}	saturation magnetism
M_{rem}	remnant magnetization
H_{cr}	coercive field
1-D	one-dimensional
2-D	two-dimensional
3-D	three-dimensional
TCNE	tetracyanoethylene
TCNQ	7,7,8,8-tetracyano-*p*-quinodimethane
salen	*N*,*N*'-ethylenebis(salicylideniminato)
(O)LEDS	(organic) light-emitting diodes
TTF	tetrathiofulvalene
TCQMI	*N*, 7,7-tricyanoquinomethanimine
DCMBQ	*p*-(dicyanomethylene)benzoquinone
CDTQI	*N*,7-cyano-2,3-ditertbutlyquinoimine
CDCQI	*N*,7-cyano-2,3-dichloroquinoimine
MeOH	methanol

EtOH	ethanol
n-PrOH	*n*-propanol
IR	infra red
NMR	nuclear magnetic resonance
QD	quantum design
MHz	megahertz
MPMS	magnetic properties measurement system
SQUID	superconducting quantum interference device
DC	direct current
AC	alternating current
PPMS	physical properties measurement system
cm	centimeter
TGA	thermogravimetric analysis
TA	Thermal Analysis
DSC	differential scanning calorimetry
C	Celsius
hr	hour
g	gram
mol	mole
cm	centimeter
calcd	calculated
obsd	observed
EA	elemental analysis
emu	electromagnetic unit

min	minute
χ_G	Pauling unit
H	hydrogen
s	singlet
d	doublet
m	multiplet
THF	tetrahydrofuran
aq	aqueous
EtOAc	ethyl acetate
Å	angstrom
TLC	thin-layer chromatography
$CHCl_3$	chloroform
(P)XRD	(powder) crystal X-ray diffraction
H_2SO_4	Sulfuric acid
t-Bu	*tert*-butyl
UV-Vis	Ultraviolet-visible
$[NBu_4][PF_6]$	tetrabutylammonium hexafluorophosphate
V	volt
SCE	standard calomel electrode
$FeCp_2$	ferrocene
M	molar
DCNQI	dicyano-*p*-quinoimine
MeCN	acetonitrile
Me_3TCQMI	3,4,6,-trimethyl- *N,*7,7-tricyanoquinomethanimine

Me_4TCQMI	3,4,6,7-tetramethyl- *N,*7,7-tricyanoquinomethanimine
Me_4TCNQ	2,3,5,6-tetramethyl-7,7,8,8-*p*-benzoquinonedimethane
$FeCp^*_2$	decamethylferrocene
HCBD	hexacyanobutadiene
HCTMCP	hexacyanotrimethylenecyclopropane
Cp*	pentamethylcyclopentadiene
py	pyridine
MnTPP	manganese(III) tetraphenylporphyrin
μ_n	bridging to n species, n bridging interactions

ACKNOWLEDGMENTS

As I begin an attempt to name all of those who have contributed to my work as a graduate student at the University of Utah, I realize how impossible it is to mention everyone who has had an impact on me these past years. Of course, I must express my love and admiration to my wife, Crystal, for her love and support, as well as for her faith in me. She has made this possible. I must also acknowledge my new son, Theodore. While he may not have contributed much intellectually to my research, he has been a never-ending source of motivation to push forward. I must also recognize my family, especially my parents, for their love and support. They taught me to love learning and discovery and gave me the confidence and drive to continue with school. Their example and confidence have been invaluable.

Most importantly to this work itself, I must acknowledge the contribution of Professor Joel S. Miller. While serving as my dissertation advisor, his expertise in chemistry has taught me how to bridge the worlds of organic molecules and magnetism. He has made this work possible through his patient instruction, wisdom, and guidance. He has served as an example of scientific integrity and devotion to instructing the next generation of researchers.

I must also recognize the many contributions of the faculty and staff of the University of Utah. I would like to especially acknowledge those I have learned personally from at this institution, Dr. Keck, Dr. Sigman, Dr. Looper, and Dr. Louie, for the insight into organic and organometallic chemistry, and Dr. Flynn for instruction on

spectroscopy. I would also like to acknowledge the input of those on my graduate committee, Dr. Richmond, Dr. Zharov, Dr. Heemstra, and Dr. Barrios, for their input and guidance in conducting my research. I must also mention the amazing staff at the University: Jo Hoovey, Dale Heisler, Dennis Edwards, Dennis Romney, Kevin Teaford, James Mueller, and Sue Wolfe. Their contributions and support carry the work forward.

I would like to thank our collaborators for their efforts and contributions. Dr. Peter Stephens and Saul Lapidus at SUNY-Stony Brook and Brookhaven National Laboratory have provided the structures derived from powder X-ray diffraction seen in this dissertation. Additionally, the single crystal X-ray diffraction analysis of compounds was performed and the structures provided by Dr. Arnold Rheingold at the University of California, San Diego.

I must also mention the support and contribution of the members, previous and current, of the Miller research group. I would like to especially acknowledge Dr. Mahika Weeraskare for her guidance and instruction during my early days in the group. Also, I would like to acknowledge Zach Fox and Hoa-lan Vo for their work on portions of the material presented in this dissertation. I would also like to acknowledge the remaining members of the Miller Group: Dr. Bretni Kennon, Dr. William Shum, Chris Kareis, Amber McConnell, Dr. Endrit Shurdha, Jack DaSilva, Preston Erickson, Joshua Sussman, Joshua Bell, Andrew Simonson, Chris Hardcastle, and Kevin Siegel. Their insight, advice, and friendship have made the past years all the more worthwhile.

Finally, I would like to thank the University of Utah for the support provided by the Graduate Research Fellowship as well as the U.S Department of Energy for their grant for the research of novel materials. This support has fueled this research and allowed me the freedom and time to explore applications of molecular magnetism.

CHAPTER 1

INTRODUCTION TO MAGNETISM AND INCORPORATION OF ORGANIC LIGANDS IN MAGNETIC SYSTEMS

Introduction and Background on Magnetism

Magnetism has captivated the imagination of mankind from the earliest recorded encounters with the phenomenon.[1] The seemingly supernatural ability of ordinary looking lodestone to attract similar stones through the exertion of an invisible force led ancient man to ascribe mystical properties to magnetism. In fact, the prevalence of these beliefs has continued to the present day and is readily observable in marketing campaigns in catalogues and on the internet.

A burgeoning field within the study of magnetism is the synthesis and characterization of molecule-based magnetic systems.[2] The possible applications of molecule-based magnets span a wide area. Molecule-based magnetic materials have sparked a large amount of interest due to their potential to store data in bytes at the molecular level[3] as well as serve as sensors and switches.[4] These systems may be comprised solely of organic components[5] or, more commonly, incorporate organic molecules into structures containing metal sites. Organic ligands may contribute directly to the overall magnetic response[1,2,6] or tune the properties of the metal centers.[7] Systems

that incorporate organic materials have become increasing popular as conventional materials often require the use of rare-earth metals, the supply of which may be limited by both scarcity and access. Regardless of the materials comprising these systems, they all adhere to the same fundamental magnetic theory.

Magnetic Theory

Magnetism is defined as the response of materials to an applied magnetic field. It arises from the fundamental property of electrons referred to as spin. As electrons are charged particles, their spin and orbital motion create a magnetic dipole moment. These moments can be conceptualized as subatomic magnets, exhibiting poles with equal, but opposite magnetization. Electrons exist in two fundamental orientations, paired or unpaired. These different orientations give rise to two distinct types of magnetism, diamagnetism and paramagnetism (Figure 1.1).

When electrons are paired, the spins of the two electrons interact strongly, coupling together according to the Pauli exclusion principle.[8] The field generated by the paired electrons repels an externally applied field, giving rise to a diamagnetic response. When unpaired electrons are exposed to an applied field, the spin interacts with the external field, exhibiting magnetic permeability. The spins are attracted towards the field, giving rise to a paramagnetic response.

These two types of magnetism are not mutually exclusive. Due to the occurrence of paired electrons in the inner orbitals of compounds, all materials possess a diamagnetic contribution. However, the diamagnetic response is generally several orders of magnitude weaker than the paramagnetic contribution. Thus, an attractive response overwhelms the repulsive force. Therefore, paramagnetism is seen for materials with unpaired electrons

Diamagnetic

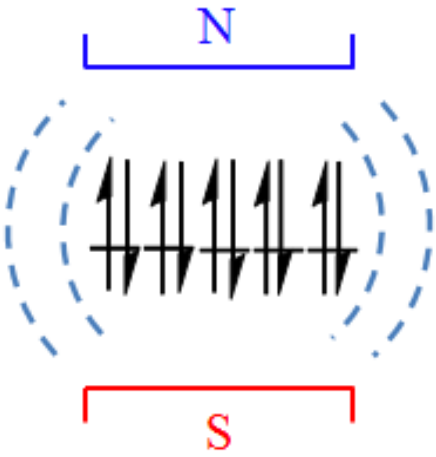

Paired Electrons

Repels Applied Field

Ubiquitous

Paramagnetic

Unpaired Electrons

Attracts Applied Field

Figure 1.1. Diagram distinguishing between diamagnetic behavior and paramagnetic behavior

despite the presence of a diamagnetic contribution.

The type of magnetism a material possesses can be determined by its interaction with an applied field. As all materials are either diamagnetic or paramagnetic, they will always effect, to some degree, the magnitude of an applied field. The difference is expressed as:[9]

$$\Delta H = B - H_0 \tag{1.1}$$

where B is the induced field inside the sample and H_0 is the free-field value. A negative ΔH value indicates a diamagnetic response while a positive ΔH value indicates a paramagnetic material. This can be easily observed in laboratory experiments through application of the Guoy method[10] as well as through modern instrumentation.

A more common (and useful) way to quantify the magnetic response is as the molar magnetic response of a material per unit of volume while in an applied field. This value is referred to as the magnetization (M) and can be defined as:[9]

$$M = \chi_v H \tag{1.2}$$

where H is the applied field in Oersted (Oe), and χ_v is the magnetic susceptibility per volume. Magnetic susceptibility (χ) is defined as the degree to which a material responds to, or is receptive to, an external magnetic field.

The susceptibility of a sample may display temperature dependency due to internal interactions. The nature of the dependency provides important information about the magnetic state of the sample, particularly in how spins interact with each other. In a purely paramagnetic sample, the spins are considered to be sufficiently isolated such that

no interaction is observed. Pierre Curie showed[9a] that the magnetic susceptibility displays inverse proportionality with temperature. He declared the relationship of the susceptibility to temperature in the Curie law, which states:[9a]

$$\chi = C / T \tag{1.3}$$

where T is the temperature in Kelvin (K) and C is defined as:

$$C = \frac{Ng^2 \mu_B{}^2 S(S+1)}{3k_B} \tag{1.4}$$

where N = Avogadro's number, g = Landé g value, S = spin quantum number, μ_B = Bohr magnetron, and k_B = Boltzmann's constant. In an ideal paramagnetic system, the Curie law provides a reasonable approximation of the behavior. However, many systems exhibit deviation from this law. Exceptions to the Curie law may arise if spins are in close proximity to each other and begin to interact. This magnetic exchange is referred to as coupling.

Coupling behavior can be thought of as a competition between the exchange energy, represented by J/k_B, and the thermal energy, k_B/T. At high temperatures (relative to the magnetic system), the thermal energy dominates, favoring randomization of the spins. As the temperature decreases, thermal energy decreases and the magnetic exchange energy begins to exert itself, favoring alignment of the spins. While this is occurring, the spins are described as coupling with each other.

This interaction can be modeled by the inclusion of a parameter in the Curie law, giving rise to the Curie-Weiss law. The Curie-Weiss law states:[9a]

$$\chi = \frac{C}{T - \theta} \tag{1.5}$$

where θ, the Weiss constant, describes the nature and magnitude of the coupling. As spins are described as being up or down, the coupling of the spins can occur in two fashions. If the spins align in the same direction (both up or both down), they enhance the susceptibility as they reinforce each other; the sum being greater than the parts. While this is relatively rare, it is the magnetic phenomenon most individuals are familiar with. More commonly, the spins align antiparallel, canceling each other out.

Coupling can be diagnosed by referencing the $\chi T(T)$ plot (Figure 1.2). Paramagnetic systems exhibit a flat line while ferromagnetic and antiferromagnetic systems deviate in a positive or negative manner, respectively. The Weiss constant (θ) can be most easily determined from the x-intercept, or abscissa, of the inverse susceptibility (χ^{-1}) vs. temperature plot (Figure 1.3). Positive values indicate ferromagnetic coupling, while negative values indicate antiferromagnetic coupling.

As stated above, most often spins align in an antiparallel manner. The greater stability encountered by this form of coupling, as with diamagnetism, contributes to the high prevalence of this phenomenon. As would be expected, this type of coupling leads to a reduction in the sum of the magnetic susceptibility and is evidenced by a negative value-intercept and negative Weiss constant.

At a certain temperature, termed the Curie temperature (T_c), the coupling becomes strong enough that the spins are considered to be locked in place. Mathematically, T_c is often calculated through the Mean-Field Theory[9] (MFT, also commonly known as self-consistent field theory):

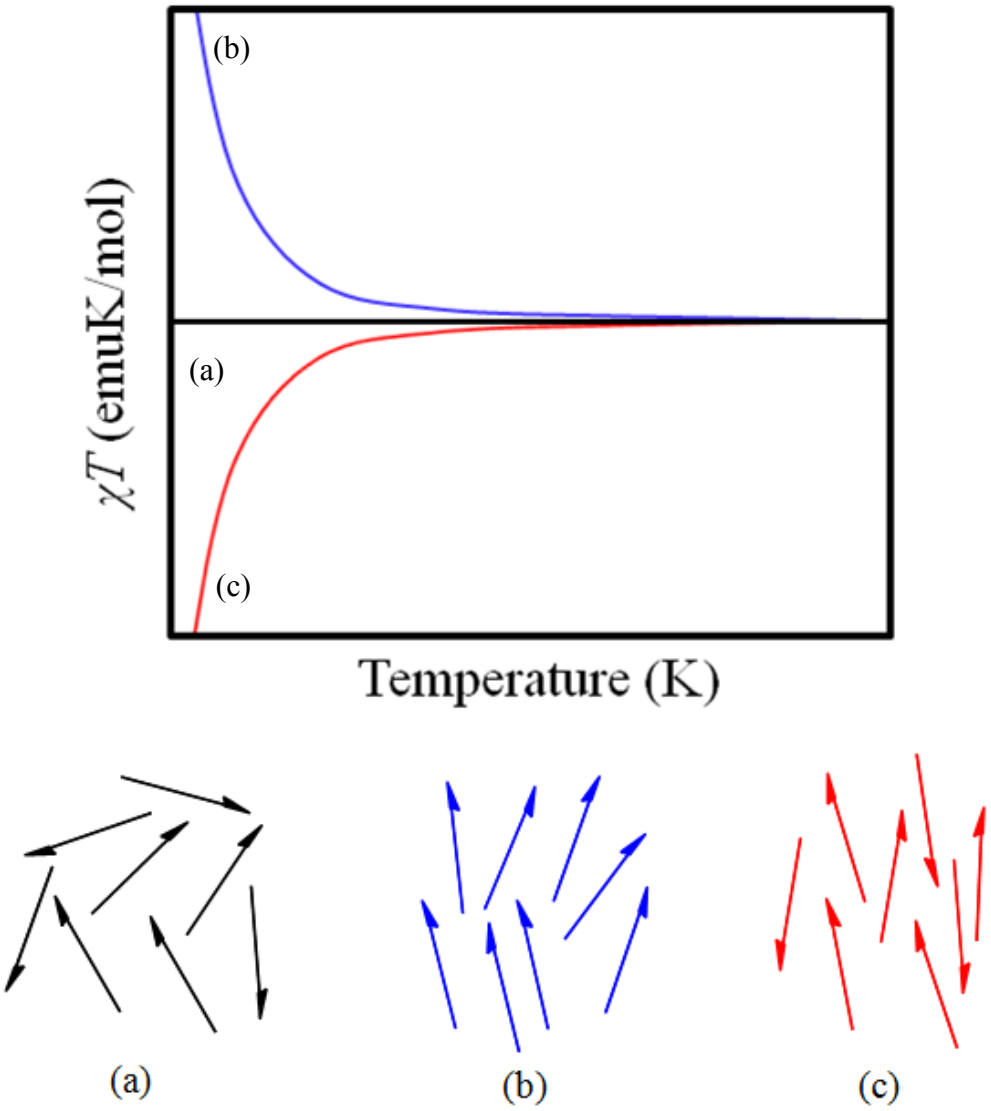

Figure 1.2. Idealized $\chi T(T)$ plot and orientation diagram of spins for paramagnetic (a), ferromagnetic (b), and antiferromagnetic (c) coupling.

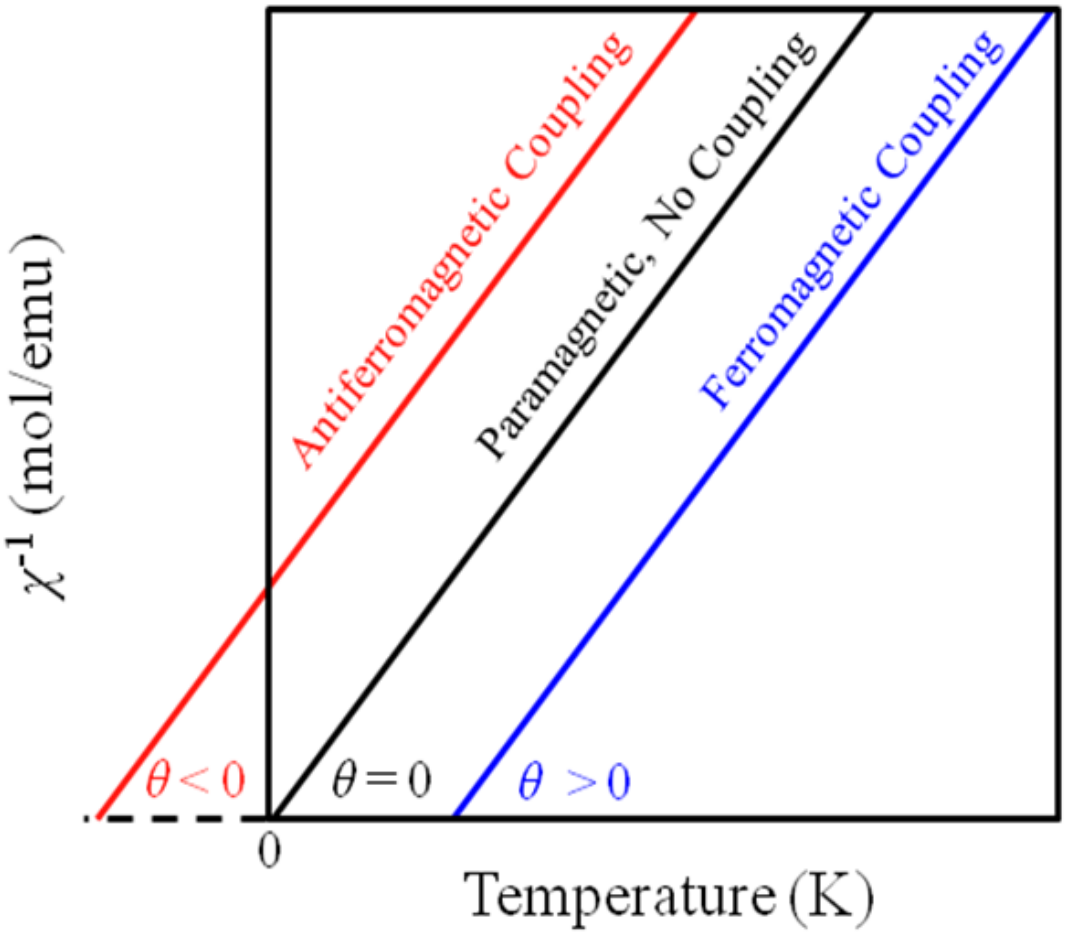

Figure 1.3. Example of $1/\chi(T)$ indicating idealized example of paramagnetic, ferromagnetic, and antiferromagnetic.

$$T_C = \frac{2JzS(S+1)}{3k_B} \tag{1.6}$$

where J is the exchange parameter, and z represents the number of nearest neighbors of the designated spin. S and k_B represent the spin quantum number and the Boltzmann constant, respectively. At this point, the spins are considered to be magnetically ordered.

Ordering can occur in several fashions (Figure 1.4). As with coupling, the ordering of the spins sites can occur in a ferromagnetic (parallel) or antiferromagnetic (antiparallel) manner. However, a new type of ordering, ferrimagnetic, is possible. Ferrimagnetic ordering is closely related to antiferromagnetism, but the number of spins aligning antiparallel to each other is nonequivalent. As seen in antiferromagnetism, this effect exhibits a reduced susceptibility in comparison to what might have been expected.

Magnetic Measurements

Determination of possible applications of a magnetic materials, as well as increasing understanding of magnetic compounds, is accomplished through detailed characterization of the internal nature of the magnet and its response to external magnetic fields. As noted above, two important factors involved are the orientation of the systems' spins as well as the effect of temperature and an applied field on the spin orientation. Several different magnetic measurements can be run to better characterize the materials. One of the most important magnetic characteristics is ordering. Whether a material orders or not, and the ordering temperature, dictate the practical applications of a material.

Magnetic ordering is a second-order phase transition, the transition occurring as the material moves from being paramagnetic to (anti)ferromagnetic. The intrinsic importance of ordering has resulted in the development of several different tests to best

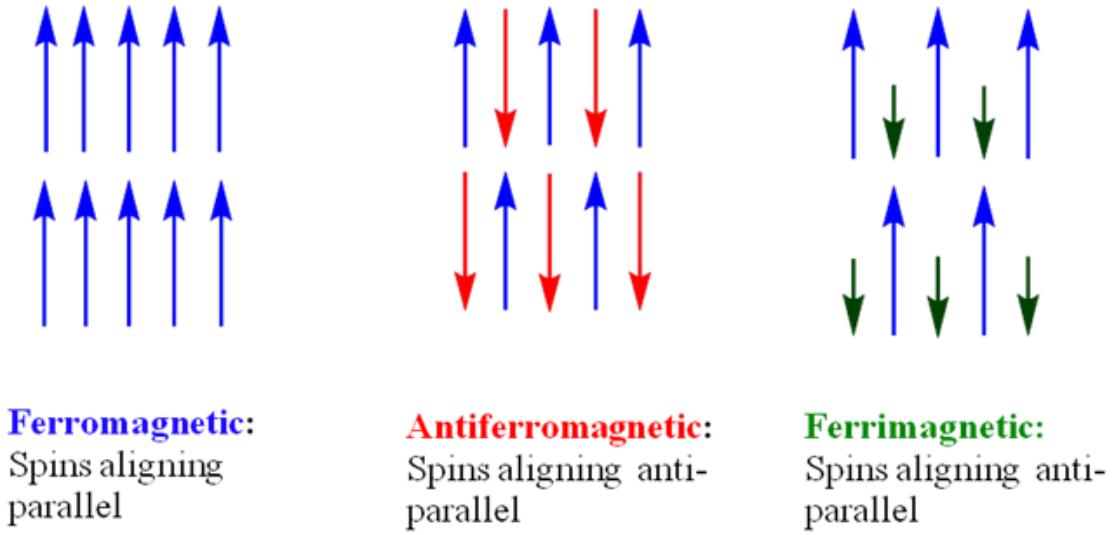

Figure 1.4. Examples of common types of ordering observed in magnetic systems.

quantify the phenomenon. It should be noted that the experiment used to determine the Curie temperature is chosen by the researcher and is often dependent on the instrumentation available.

Perhaps the most sensitive measurement available for determining the T_c is heat capacity,[9b] though the difficulty in physically performing the measurement makes the process unwieldy and less attractive. A much more common experiment is an alternating current (ac) measurement. Above the critical temperature, unpaired electrons respond readily to an alternating magnetic field of low intensity (≤ 3 Oe). However, as the temperature is cooled to and below the ordering temperature, the interaction of the electrons with each other begins to overwhelm their response to the weak field and the electrons essentially become "stuck" in their ordered confirmation. The response is detected by the presence of an uncompensated moment observed in χ as a function of the ac field as:[10]

$$\chi(\omega) = \chi'(\omega) + i\chi''(\omega) \tag{1.7}$$

where ω represents the frequency of the ac field in hertz (Hz) and χ' is the real, in-phase element of the susceptibility and χ'' is the imaginary, out-of-phase component. These are observed as peaks in the susceptibility vs. temperature measurements (Figure 1.5).

In addition to detecting order in systems, ac measurements can also be applied to distinguish between the types of ordering observed. Peaks in both the χ' and χ'' occur in both ferromagnetic and ferrimagnet ordering, whereas only a peak in the χ' occurs in the case of antiferromagnetic ordering. Also, frequency dependency can appear, where changes in the frequency of the applied ac field shift the location and magnitude of the χ'

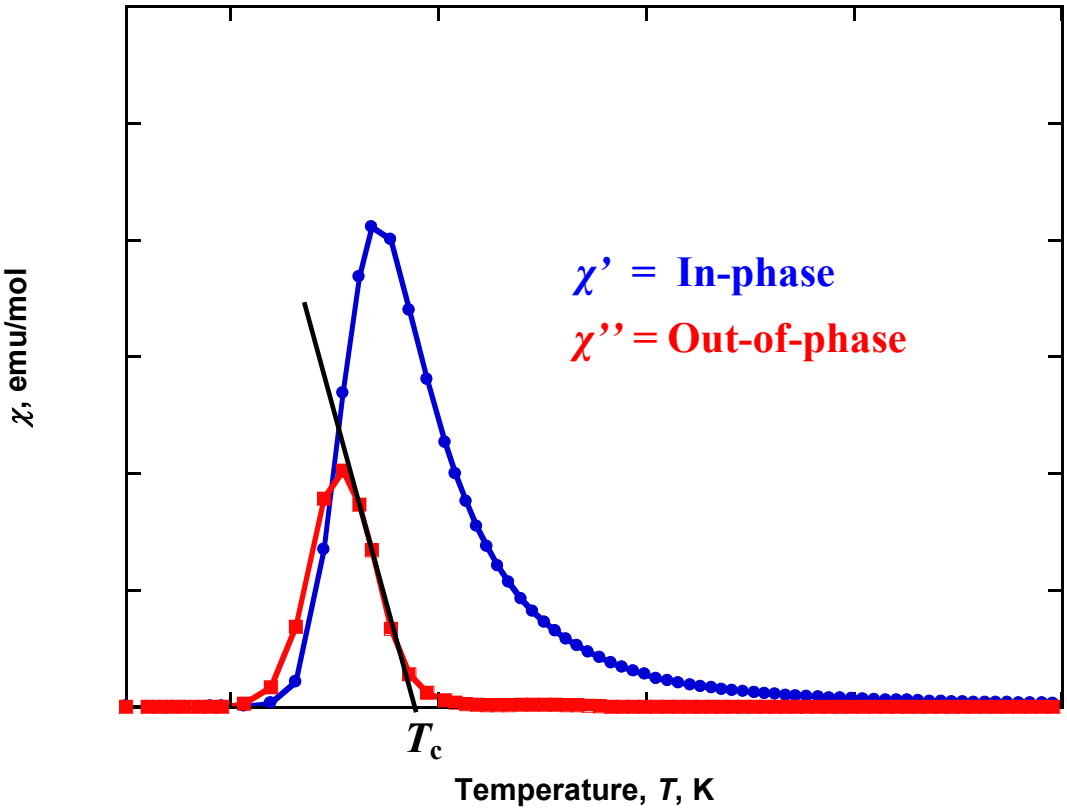

Figure 1.5. Ac susceptibility detailing in χ' (in-phase, ●) and χ'' (out-of-phase, ■). T_c is defined as the x-intercept of the χ'' component of the ac susceptibility.

and χ'' peaks (Figure 1.6). This response can indicate the presence of spin-glass or superparamagnetic states within the sample.[11]

Other useful magnetic analyses commonly performed are the zero-field-cooled (ZFC) and field-cooled (FC) measurements. The zero-field-cooled experiment is conducted by carefully zeroing the magnetic field of the magnetometer before placing the sample in the magnetometer and cooling it below the critical temperature. Once below the T_c, the sample is then subjected to a weak field (generally less than 10 Oe) and the susceptibility is measured as the sample is heated to above T_c. The field-cooled measurement is then conducted by cooling the sample below the T_c once more, at which point the magnetic field is applied. The sample is then once again heated above the T_c and the susceptibility is measured.

The ZFC data allow the determination of the magnetic ground state, the shape of the curve being used to assign the material as an antiferromagnet, a ferromagnet, or a ferrimagnet. The FC data allow examination of the excited state of the material. Comparison of the ZFC and FC magnetization data can also yield the Curie temperature as the material cooled in zero-field will display reduced magnetization (tendency to disorder) due to the lack of an applied field. The data taken from the FC sample will have enhanced magnetization as the field will favor a more ordered state. As the two sets of data are overlaid, a divergence can be detected. This is termed the bifurcation temperature (T_b) (Figure 1.7). This point represents the onset of ordering of the sample and can be provide valuable information on the location of T_c.

Another important parameter to measure for magnetic systems is their response to varying magnetic fields. This measurement, termed an $M(H)$ (Figure 1.8), is conducted by cooling the sample below the T_c and then increasing the field from zero to a

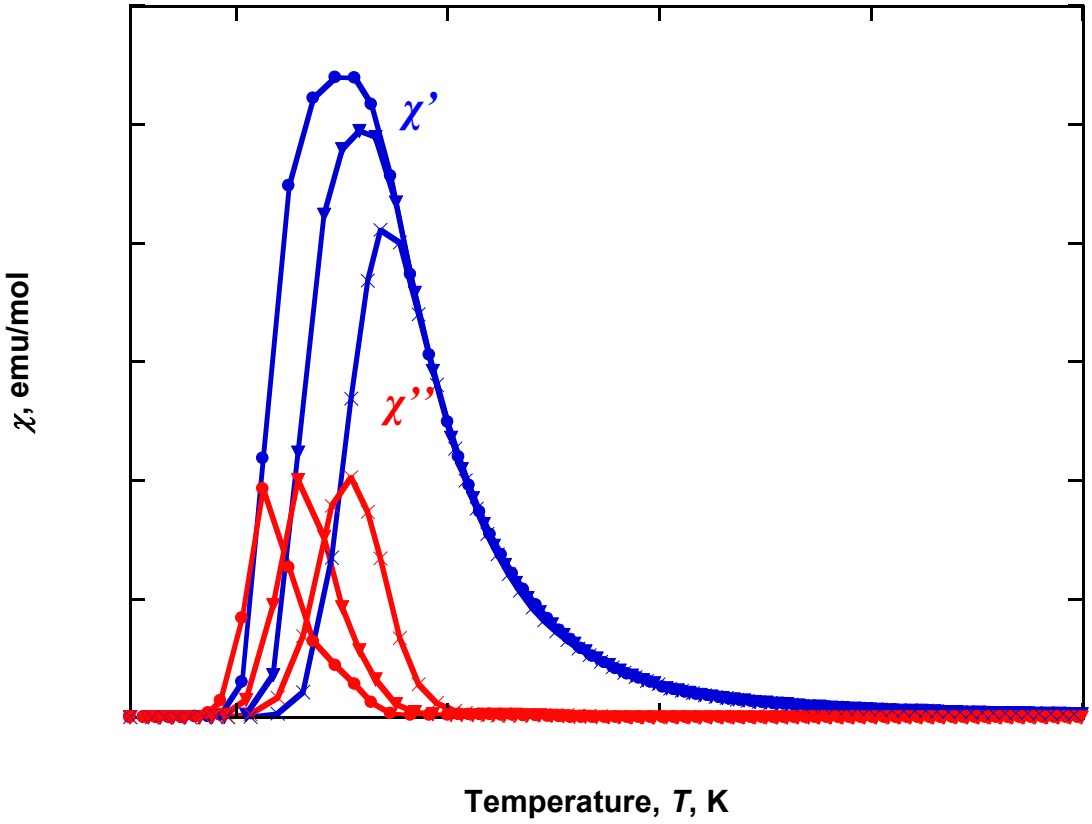

Figure 1.6. Frequency dependency observed in magnetic sample in the χ' and χ'' components when sampled as 10 (**x**), 100 (▼), and 1000 (●) Hz.

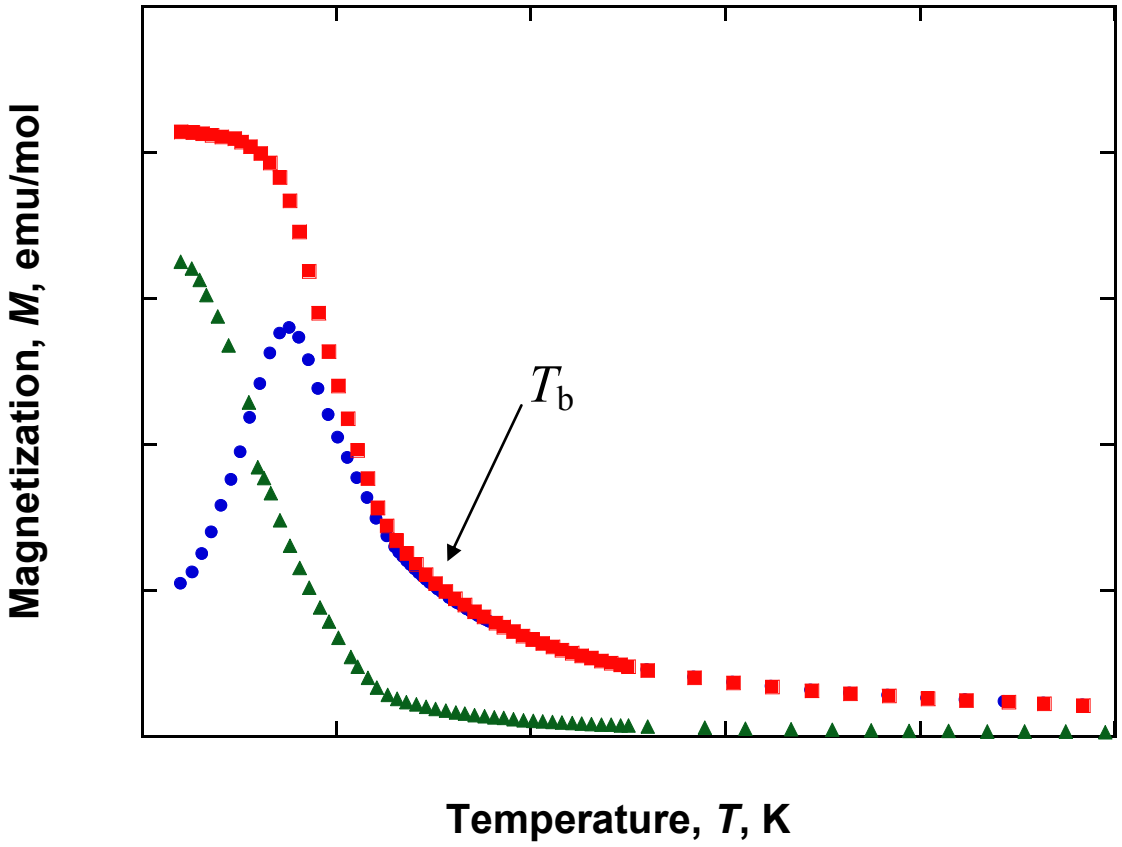

Figure 1.7. Zero-field-cooled(●), field-cooled (■) and remnant (▲) magnetization plot. The bifurcation temperature (T_b) is indicated by an arrow.

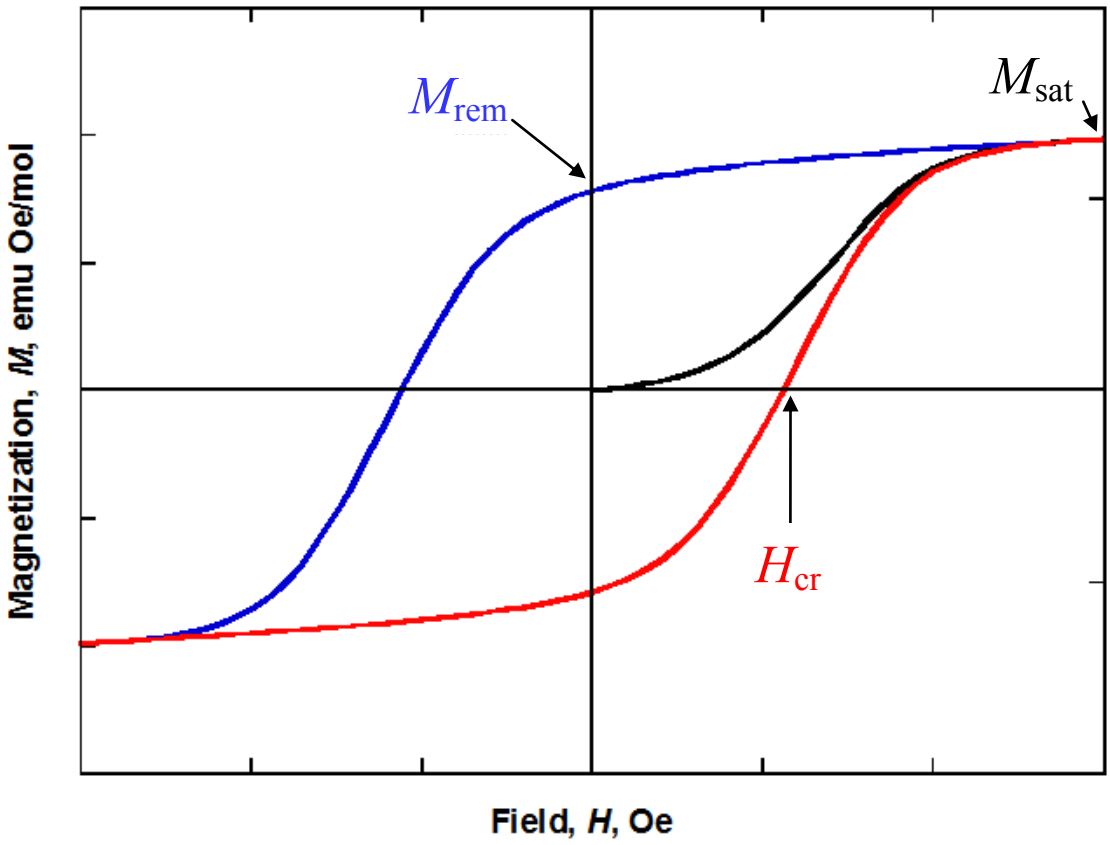

Figure 1.8. $M(H)$ plot showing hysteresis-loop with saturation magnetization (M_{sat}), remnant magnetization (M_{rem}) and coercive field (H_{cr}) indicated with arrows.

sufficiently high field (typically 50 to 90 kOe (Oersted)). This measurement can determine the saturation magnetization (M_{sat}) or the magnetization value where the spins are fully aligned. The saturation magnetization gives valuable insight into the behavior and composition of the system. The field is then decreased until it is equal to, but the opposite of, the high field (-50 or -90 kOe). The field is then increased to the maximum positive value again.

In a paramagnetic system, the curves would be expected to overlap. The onset of ordering, however, creates microdomains within the system. These microdomains aligned upon the initial increase in field strength. When the field is reversed to the negative maximum, the microdomains resist realignment. This creates a lag in response such that the response does not overlap over the initial curve. The magnetization is not zero at zero-field. The value of the magnetization at zero-field is referred to as the remnant magnetization (M_{rem}). The field strength required to return the magnetization to zero is termed the coercive field (H_{cr}) (Figure 1.8).

The coercivity of a sample, or the field required to return the magnetization to zero once it has reached saturation, is important when the applications of the compound are considered. Materials displaying high coercivities (requiring strong fields to return the magnetization to zero) are labeled as hard magnets and retain their magnetic field. These compounds are useful in data storage applications as they are highly resistant to demagnetization. Compounds with low coercivities, or soft magnets, where relatively weak fields removed magnetization, readily lose their magnetic field. Soft magnets have applications in systems that involve rapidly changing fields, such as power converters, transformer, and another other technology where the material must respond readily to abrupt shifts in field strength and direction.

Molecule-based Magnets

While magnets can be found in devices as varied as telecommunications satellites and railroad crossing guards, the structural diversity and composition of conventional magnets is surprising limited. While the materials comprising magnets can be varied among a number of metals and alloys, virtually all magnets used today have the same well-known structures. The lack in variation arises from the processes used in the synthesis of magnets. These processes involved in forming materials with stronger retentivity (resistance to loss of magnetism) involve heating the materials to high temperatures at intense pressures in strong magnetic fields. Under these conditions, control over the reactions is virtually nonexistent, leading to formation of the most stable thermodynamic product.

Molecule-based magnets are attractive as they can be synthesized in ambient temperatures and pressures.[1,2] Additionally, the use of organic components allows for more control over the structure and can allow the formation of materials that blend magnetic properties with light,[12] pressure,[13] and heat sensitivity.[14] Development of molecule-based magnets has been pursued due to the potential of such materials in providing advanced magnetic storage devices to reduce the memory medium size.

From an industrial standpoint, molecule-based magnets are attractive due to their mild synthetic conditions, often at ambient pressure and room-temperature. However, organic magnets still have significant obstacles to overcome before practical applications can be realized. Major drawbacks to these materials are lower magnetic density (when compared to conventional magnets) due to poor overlap between orbitals and less-than-desirable spin coupling.[1b] Additionally, many of the systems are not air stable and typically order at low temperatures. However, recent investigations of molecular magnets

have shown that the implementation of organic ligands in magnetic systems has allowed for the manipulation of the magnetic properties.

Organic Building Blocks

The use of organic ligands in molecule-based magnetic systems has highlighted different roles the ligand may play in the overall structure.[1,2,6,7] First, the ligands may serve as tuning scaffolds. They work to bridge metal sites, giving rise to 1-D,[15] 2-D,[16] and 3-D[17] superstructures while creating a favorable ligand-field to enhance desirable properties from the metals. Prussian Blue and its analogues, which typically employ cyanide as the bridging ligand, serve as prime examples of this type of compound.[7]

The second way in which organic ligands play a role are as spin carriers.[1,2,6] In this case, ligands form radical species, typically anions. The unpaired spins of the radicals couple with the spins on the metal sites ferro-, antiferro-, or ferrimagnetically to give rise to improved properties. Tetracyanoethylene (TCNE) and 7,7,8,8-tetracyano-*p*-quinonedimethane (TCNQ) are two of the most commonly encountered ligands that perform this role.[18] It should be noted that these ligands may also bond to metal sites to form networks of various dimensionalities, making the two roles not mutually exclusive.[17]

The third way in which organic ligands figure into molecule-based magnetic materials are as the sole constitutes.[19] Though much more rare than the two previously listed cases, some molecule-based magnetic systems have been constructed purely through cooperation between organic radicals. Typical constituents of these frameworks include nitroxides and similar compounds.[19] Though attractive, due to the ease of synthesis and lack of potentially rare and expensive metals, these compounds typically

order at very low temperatures, though some examples of higher-temperature ordering have been seen.[20]

My research has focused on projects involving the first two types of molecule-based magnets. The first project focuses on the use of *N*,*N*'-ethylenebis(salicylideniminato) (salen) ligands complexed to cobalt(II) centers to favor temperature-dependent tristability involving both a singlet-triplet transition and spin crossover to an excited quartet state. The second project focuses on the synthesis of asymmetric ligands bearing nitrile functional groups to form radical anions.

Salen as a tuning ligand. An important role organic ligands play in molecule-based magnetic systems is to tune magnetic phenomena. Magnetic materials have become the preferred data storage medium and rely on bistability to record information in binary code. To this end, molecule-based materials that exhibit bistability are being pursued with the goal of developing smaller, more efficient memory systems.[21]

Examples of phenomena capable of producing bistablility, where two stable states exist in molecular systems, include spin crossover,[22] valence tautomerization,[23] and photo-chromism.[24] Metal-salen complexes have been extensively studied as potential synthetic oxygen carriers as well as catalysts in numerous organic reactions. While investigating technologically important magnetic materials, a series of functionalized Co^{II}(salen) compounds were reviewed. They were seen to exhibit interesting magnetic properties[25] and possess potential as memory storage devices.

While the majority of the research has focused on bistable systems, materials based on Co^{II}(salen) have been seen to display three stable, reversible states. Further studies in our group were performed to examine the magnetic properties of a series of Co^{II}(salen) derivatives (Figure 1.9). During the course of these studies, the temperature-

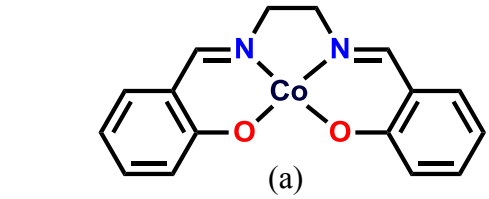

(a)

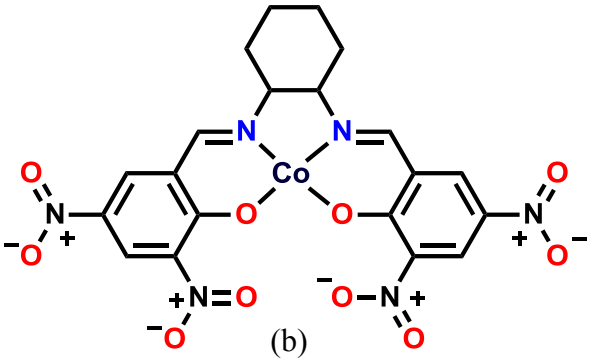

(b)

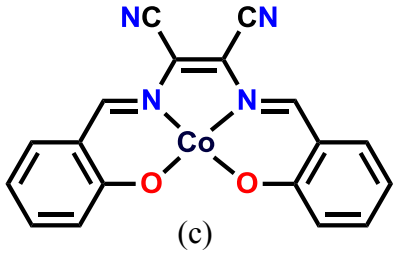

(c)

Figure 1.9. Co^{II}(Salen) (a) and derivatives Co^{II}(salen-$(NO_2)_4$ (b) and Co^{II}(salen-$(CN)_2$) (c)

dependent susceptibility (χT) of the unsubstituted salen dimer was seen to indicate a singlet ground state with an excited triplet state above the ground state.[25] Evidence of an additional state was seen above 300 K. Further investigations were carried out involving the synthesis of several substituted Co(salen) compounds in the search for further examples of tristable materials. Of the investigated compounds, it was seen that the tetranitro compound with a cyclohexyldiamine backbone and an unsubstituted salicylaldehyde compound with a diaminomaleononitrile backbone showed similar behavior (Figure 1.9).

The possibility of tristable materials was interesting as it would lead to exciting applications in the fields of molecule-based switches and memory storage materials. Investigation of these phenomena, as well as additional research into related compounds exhibiting these behavior was undertaken.

Asymmetrical nitrile cyanocarbon acceptors. The use of organic or organometallic compounds in applications typically reserved for metal or semiconductor materials is a burgeoning field of research.[26] A prime example of these applications is found in the increasing prevalence of organic light-emitting diodes (OLEDs) over more conventional light-emitting diodes (LEDs) or liquid crystal displays (LCDs).[26c,d] As the name suggests, OLEDS are close counterparts of the traditional LEDs and produce light in much the same way. However, the use of organic molecules over the metals and inorganic materials in LED displays leads to several advantages including faster response time,[27] improved brightness[28] and power efficiency,[29] as well as lighter, more flexible materials.[30]

In an analogous fashion, organic molecules as novel and vital components in magnetic systems have been receiving increasing interest for many years. The use of

organic materials in magnetic applications was envisioned from the discovery that alternating chains of $TCNQ^{\bullet-}$ and a tetrathiofulvalene cation ($TTF^{\bullet+}$) contained a low-temperature magnetic phase and were capable of conducting current.[31] Further work led to the discovery that the cyanocarbon acceptor TCNE formed the first room-temperature magnetic material when reacted with vanadium hexacarbonyl, $V(CO)_6$.[2,6,32]

The prevalence of cyanoacceptors as constituents in magnetic systems is due to the stabilization of radicals by the electron-withdrawing nitrile groups. This allows the radical electron to reside in a π^* orbital of the compound. Additionally, the nitrile groups serve as sites for coordination to metal cations, allowing extended 2-D[16] and 3-D[17] networks to form. The unpaired spin on the radical anion is capable of interacting with spins on the metal sites, with the goal of encouraging coupling between the spins, leading to enhanced magnetization.

The success of $V(TCNE)_2$ as a room-temperature molecule-based magnet inspired further research. While TCNE is an ideal cyanocarbon component in many ways, there are drawbacks. TCNE and similar cyanocarbon acceptors possess four nitriles and form homoleptic complexes of $M^{II}(TCNE)_2$ stoichiometry with octahedral M^{II} ions. The resulting combination leads to exclusion of a fourth of the nitrile groups, and is suspected of fostering disorder.[33] To date, structures of $V^{II}(TCNX)_2$ have eluded determination. In an attempt to synthesize a compound with three nitrile groups that would still serve as a good acceptor, the asymmetric ligand *N*,7,7-tricyanoquinomethanime (TCQMI)[34] (Figure 1.10) was investigated. The compound was also attractive as it would serve to expand the library of molecule-based materials to include asymmetric radical anions. In order to better explore the properties of asymmetric nitrile acceptors, *p*-(dicyanomethylene)benzoquinone (DCMBQ), *N*,7-cyano-2,3-di-*tert*-butlyquinonimine

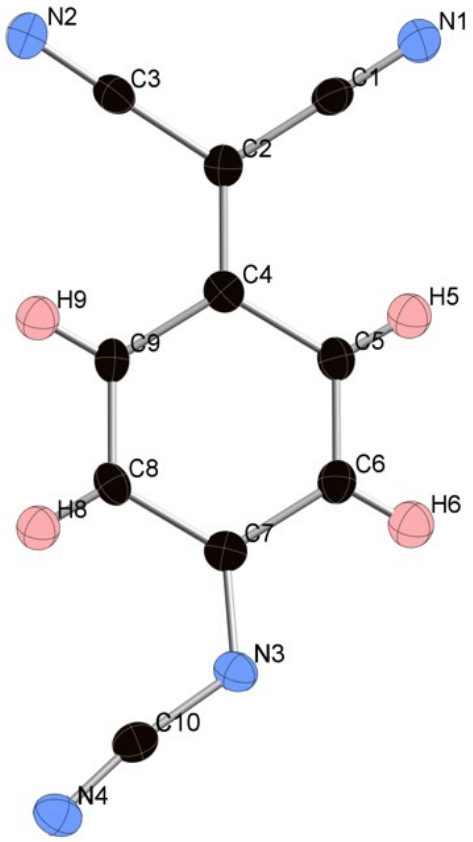

Figure 1.10. Structure of *N*,7,7-Tricyanoquinomethanimine, TCQMI.

(CDTQI), and *N*,7-cyano-2,3-dichloroquinonimine (CDCQI) were synthesized and characterized as potential cyanocarbon acceptors.

References

(1) (a) Miller, J.S. *Inorg. Chem*. **2000**, *39*, 4392. (b) *Magnetism: Molecules to Materials I-IV*, Miller, J.S. and Drillon, M. Eds., Wiley-VCH, Weinheim, New York, **2001-2002**. (c) Yoshihara, D.; Karasawa, S.; Koga, N. *J. Am. Chem. Soc.*, **2008**, *130*, 10460. (d) Stickley, K.R.; Selby, T.D.; Blackstock, S.C. *J. Org. Chem*., **1997**, *62*, 448.

(2) (a) Miller, J. S. *Chem. Soc. Rev.* **2011**, *40*, 3266. (b) Bousseksou, A.; Molnár, G.; Salmon, L.; Nicolazzi, W. *Chem. Soc. Rev.* **2011**, *40*, 3313. (c) Robertson, N.; Yee, G. T. *Molecular Materials*: John Wiley&Sons Ltd.: Chichester, UK, 2010, pp 143-209. (d) Min, K. S. *Hwahak Kyoyuk*, **2008**, *35*, 14.

(3) Giusti, A.; Charron, G.; Mazerat, S.; Compain, J.-D.; Mialane, P.; Dolbecq, A.; Riviere, E.; Wernsdorfer, W.; Ngo, B. R.; Keita, B.; Nadjo, L.; Filoramo, A.; Bourgoin, J. -P.; Mallah, T. *Angew. Chem. Int. Ed. Engl.* **2009**, *48***,** 4949.

(4) (a) Kahn, O. Launay, J. P. *Chemtronics* **1988**, *3*, 140. (b) Leibeling, G.; Demeshko, S.; Dechert, S. Meyer, F. **2005**, *Angew. Chem. Int. Ed.* **2005**, *44*, 7111. (c) Gütlich, P.; Garcia, Y.; Woike, T. *Coord. Chem. Rev.* **2001**, *219*, 839. (d) Sato, O. *Acc. Chem. Res.* **2003**, *36*, 692.

(5) (a) Takeda, K.; Yoshida, Y.; Inanaga, Y.; Kawae, T.; Shiomi, D. Ise, T.; Kozaki, M.; Okada, K.; Sato, K.; Takui, T. *Phys. Rev. B* **2005**, *72*, 024435. (b) Awaga, K.; Inabe, T.; Nagashima, U.; Maruyama, Y. *J. Chem. Soc. Chem. Comm.* **1989**, 1617. (c) Awaga, K.; Maruyama, Y. *Chem. Phys. Lett.* **1989**, *158*, 556.

(6) (a) Miller, J. S.; Calabrese, J. C.; Harlow, R. L.; Dixon, D. A.; Zhang, J. H.; Reiff, W. M.; Chittipeddi, S.; Mark, C.; Selover, A.; Epstein, A. J. *J. Am. Chem. Soc.***1990**, *112,* 5496. (b) Zhang, J.; Ensling, J.; Ksenofontov, V.; Gütlich, P.; Epstein, A. J.; Miller, J. S. *Angew. Chem., Int. Ed.* **1998**, *37*, 657. (c) Werner, H. -P.; Von Schütz, J. U.; Wolf, H. C.; Kremer, R.; Gehrke, M.; Aumüller, A.; Erk, P.; Hünig, S. *Solid State Comm.* **1988**, *65*, 809. (d) Tanaka, J.; Katayama, C.; Kumagai, H.; Saito, G.; Enoki, T.; Inokuchi, H. *Mol. Cryst. Liq. Cryst.* **1985**, *125*, 223. (e) O'Hare, D.; Rai-Chaudhuri, A.; Murphy, V. *J. Chem. Soc., Dalton Trans.* **1993**, *20*, 3071.

(7) (a) Ohkoshi, S.-i.; Hashimoto, K. *Phys. Rev. B* **1999**, *60*, 12820. (b) Tokoro, H.; Ohkoshi, S.-i.; *Dalton Trans.* **2011**, *40*, 6825. (c) Earnshaw, A.; Hewlett, P.C.; King, E. A.; Larkworthy, L. F. *J. Chem. Soc. A* **1968**, 241

(8) (a) Pauli, W. *Z. Physik* **1925**, *31*, 765. (b) Jordan, P.; Wigner, E. *Z. Physik*, **1928**, *47*, 631. (c) Heisenberg, W. *Ann. Physik* **1931**, *10*, 888.

(9) (a) Kahn, O. *Molecular Magnetism*: VCH Publishers Inc.: New York, NY, 1993, pp 1-17. (b) Palacio, F. *Molecular Magnetism: From Molecular Assemblies to the Devices*: NATO ASI Series (Kluwer Acad. Publ.), vol. E321, pp 5-63.

(10) Carlin, R. L., *Magnetochemistry*: Springer-Verlag: Berlin, Germany, 1986, pp 312-317.

(11) Mydosh, J., *Spin Glass*: Taylor and Francis: Washington, DC, 1993, pp 66-67.

(12) Oshio, H. in Abstracts of Papers, 229th ACS National Meeting, San Diego, CA, United States, March 13-17, 2005 (2005) (b) Tripathi, G. S. *Ind. J. Phys. A*, **2003**, *77*, 543.

(13) Yakhmi, J. V. *Bull. Mater. Sci.* **2009**, *32*, 217.

(14) (a) Murray, K.S.; Van den Bergen, A.; Kennedy, B.J.; West, B.O. *Aust. J. Chem*., **1986**, *39*, 1479. (b) Murray, K.S.; Sheahan, R.M. *Chem. Phys. Lett.*, **1973**, *22*, 406.

(15) (a) Her, J.-H.; Stephens, P. W.; Bagnato, J. D.; Miller, J. S. *J. Phys. Chem. C* **2010**, *114*, 20614. (b) Ribas-Ariño, J.; Novoa, J. J.; Miller, J. S. *J. Mater. Chem.* **2006**, *16*, 2600.

(16) Fujisaki, T.; Nakazawa, Y.; Oguni, M.; Nakata, K.; Yamashita, M.; Lecren, L.; Miyasaki, H. *J. Phys. Soc. Jpn.* **2007**, *76*, 105602/1.

(17) Stone, K. H.; Stephens, P. W.; McConnell, A. C.; Shurdha, E.; Pokhodnya, K. I.; Miller, J. S. *Adv. Mater.* **2010**, *22*, 2514.

(18) (a) Pokhodnya, K. I.; Petersen, N.; Miller, J. S. *Inorg. Chem.* **2002**, *41*, 1996. (b) Vickers, E. B.; Selby, T. D.; Thorum, M. S.; Taliaferro, M. L.; Miller, J. S. *Inorg. Chem.* **2004**, *43*, 6414. (c) Miller, J. S.; Epstein, A. J.; Reiff, W. M. *Chem. Rev*. **1988**, *88*, 201. (d) Miller, J. S.; Epstein, A. J.; Reiff, W. M. *Acc. Chem. Res*. **1988**, *21*, 114.

(19) (a) Sugano, T.; Kurmoo, M.; Uekusa, H.; Ohashi, Y.; Day, P. *J. Solid State Chem.* **1999**, *145*, 427. (b) Train, C.; Norel, L.; Baumgarten, M. *Coord. Chem. Rev.* **2009**, *253*, 2342.

(20) Banister, A. J.; Bricklebank, N.; Lavender, I.; Rawson, J. M.; Gregory, C. I.; Tannner, B. K.; Clegg, W.; Egglewood, M. R. J.; Palacio, F. *Angew. Chem., Int. Ed*. **1996**, *35*, 2533.

(21) (a) Minkin, V. I. *Russ. Chem. Bull., Int. Ed.* **2008**, *57*, 687. (b) Li, H.; Jin. Z.; Li, N.; Xu, Q.; Gu, H.; Lu, J.; Xia, X.; Wang, L. *J. Mater. Chem.* **2011**, *21*, 5860. (c) Ling, Q. D.; Song, Y.; Lim, S. L.; Teo, E. Y. H.; Tan, Y. P.; Zhu, C. X.; Chan, D. S. H.; Kwong, D. L.; Kang, E. T.; Neoh, K. G. *Angew. Chem., Int. Ed.* **2006**, *45*, 2947. (d) Xie, L. H.; Ling, Q. D.; Hou, X. Y.; Huang, W. *J. Am. Chem. Soc.* **2008**, *130*, 2120. e. Li, Y. B.; Sinitskii, A.; Tour, J. M. *Nat. Mater.* **2008**, *7*, 966.

(22) *Spin Crossover in Transition Metal Compounds*; Gütlich, P.; Goodwin, H. A.,

Eds.; Springer: New York, 2004; Vol *1-3*.

(23) Shultz, D. A., *Magnetism-Molecules to Materials*; Miller, J. S., Drillion, M., Eds.; Wiley-VCH: Weinheim, Germany, 2001; Vol. *2*, p 281.

(24) (a) *Photochromism*: *Molecules and Systems*; Dürr, H., Bouas-Laurent, H., Eds.; Elsevier: Amsterdam, The Netherlands, 1990; p 64. (b) Organic Photochromic and Thermochromic Compounds. *Main Photochromic Families*; Crano, J. C., Guglielmetti, R., Eds.; Plenum Publishers: New York, 1999; Vol. *1*.

(25) Min, K. S.; Arthur, J.; Shum, W. W.; Bharathy, M.; zur Loye, H. -C.; Miller, J. S. *Inorg. Chem.* **2009**, *48*, 4593.

(26) (a) Samuel, I. D. W.; Turnball, G. A. *Chem. Rev.* **2007**, *107*, 1272. (b) Tsumura, A.; Koezuka, H.; Ando, T. *Appl. Phys. Lett.* **1986**, *49*, 1210. (c) Tang, C. W.; VanSlyke, S. A. *Appl. Phys. Lett.* **1987**, *51*, 913. (d) Burroughes, J. H.; Bradley, D. D. C.; Brown, A. R.; Marks, R. N.; Mackay, K.; Friend, R. H.; Burns, P. L.; Holmes, A. B. *Nature* **1990**, *347*, 539.

(27) (a) Matsueda, Y. *Nippon Gazo Gakkaishi* **2008**, *47*, 452. (b) Kranzelbinder, G.; Meghdadi, F.; Tasch, S.; Leising, G.; Fasoli, L.; Sampietro, M. *Synth. Metals* **1999**, *102*, 1073.

(28) Inigo, A. R.; Underwood, J. M.; Silva, S. R. P. *Carbon*, **2011**, *49*, 4211.

(29) (a) Lee, J. -H.; Ho, Y. -H.; Chen, K. -Y.; Lin, H. -Y.; Fang, J. -H.; Hsu, S. -C.; Lin, J. -R.; Wei, M. -K. *Optics Express* 2008, 16(26), 21184-21190.

(30) Gustafsson, G.; Cao, Y.; Treacy, G. M.; Klavetter, F.; Colaneri, N.; Heeger, A. J. *Nature*, **1992**, *357*, 477.

(31) (a) Bloch, A. N.; Ferraris, J. P.; Cowan, D. O.; Poehler, T. O. *Sold State Commun.* **1973**, *13*, 753. (b) Holczer, K.; Gruner, G.; Miljak, M.; Cooper, J. *Solid State Commun.* **1977**, *24*, 97. (c) Shirotani, I.; Onodera, A.; Anzai, H. *Solid State Chem.* **1981**, *36*, 246. (d) Mukherjee, B.; Mukherjee, M. *Langmuir* **2011**, *27*, 11246.

(32) (a) Miller, J. S.; Manriquez, J. M.; Yee, G. T.; Epstein, A. J. *Chim. Ind.* **1992**, *74*, 845. (b) Zhou, P.; Long, S. M.; Miller, J. S.; Epstein, A. J. *Phys. Lett. A* **1993**, *181*, 71. (c) Epstein, A. J.; Miller, J. S. *Mol. Cryst. Liq. Cryst.* **1993**, *233*, 171.

(33) Matsuura, H.; Miyake, K.; Fukuyama, H. *J. Phys. Soc. Jpn* **2010**, *79*, 034712.

(34) (a) Bryce, M. R.; Davies, S. R.; Grainger, A. M.; Hellberg. J.; Hursthouse, M. B.; Mazid, M. Bachmann, R.; Gerson, F. *J. Org. Chem.* **1991**, *57*, 1690. (b) Iwatsuki, S.; Itoh, T. T.; Itoh, H. *Chem. Lett.* **1988**, *17*, 1187. (c) Arthur, J. L.; Moore, C. E.; Rheingold, A. L.; Miller, J. S. *Inorg. Chem.* **2011**, *50*, 2735.

CHAPTER 2

TRISTABILITY OF CO^{II}(SALEN)-BASED (SALEN = *N*,*N*'-ETHYLENEBIS(SALICYLIDENIMINATO) COMPOUNDS

Introduction

Molecule-based electronics have received a great deal of interest due to their potential to overcome the current limits of silicon-based circuits.[1] Bistable molecule-based materials that respond to external stimuli, in particular, have application as vital components in molecule-based sensors, switches, actuators, and information storage.[2] Transition between the stable states occurs in response to external stimuli. Technologically important stimuli include electric fields, temperature, pressure, and light. Phenomena identified as initiating a reversible transition between states include spin crossover,[3] valence tautomerism,[4] and photochromism.[5]

Spin crossover behavior is encountered when the electronic structure of a metal changes from a low-spin to high-spin state by variation in external stimuli. The transition from low-spin to high-spin changes the number of paired electrons and results in an observable change in the magnetization. Compounds exhibiting spin crossover behavior

---

have been identified as suitable bistable materials.[2b,e] Likewise, valence tautomers exhibit spin-state changes resulting from an intramolecular oxidation-reduction reaction and have been explored as bistable materials. Spin crossover behavior has been observed for many materials, including a family of Schiff bases coordinated to cobalt ions, where the most prominent constituent is ethylenebis(salicylideniminato)cobalt(II).

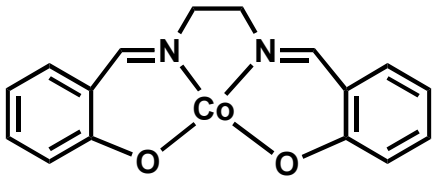

Co^{II}salen

We reinvestigated the magnetic behavior of the dimeric form of *N*,*N*'-ethylenebis(salicylideniminato)cobalt(II) (Co^{II}(salen))[6] as we saw the compound exhibited unusual magnetic behavior. The structure of Co^{II}(salen) has been well established.[7] The compound exists in both monomeric and dimeric forms (Figure 2.1). Monomeric Co^{II}(salen) has a distinct 4-coordinate Co^{II} center and C_{2v} symmetry.[8] The dimeric form, $[Co^{II}(salen)]_2$, **1**, has pentacoordinate Co^{II} with the phenolic oxygen of an adjacent Co^{II}(salen) moiety occupying the axial position,[9] and overall possesses C_i symmetry.[10]

Monomeric Co^{II}(salen) exhibits both paramagnetic and diamagnetic behavior as an isolated dimer[11] and superoxo-bound species.[12] In contrast, the dimer ($[Co(salen)]_2$) displays a singlet ($S = 0$) ground state with a triplet ($S = 1$) excited state. Additionally, at higher temperatures, the population of a quartet state ($S = 3/2$) is observed.[6,13] Hence, $[Co(salen)]_2$ has three stable spin-states, and is tristable. This is attributed to its

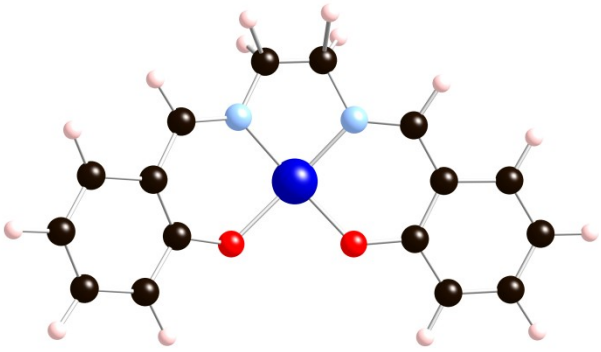

(a)

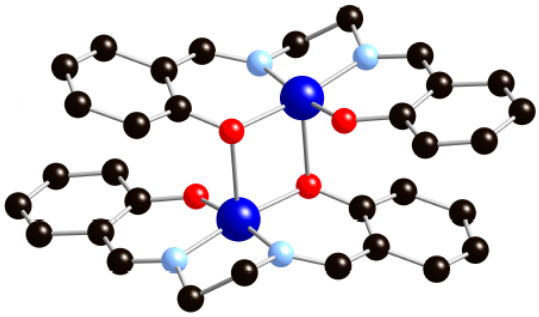

(b)

Figure 2.1. Structure of monomeric (a) and dimeric (b) (hydrogen atoms removed for clarity) Co^{II}(salen).

dimeric structure, with both $Co^{II}N_2O_3$ centers being five-coordinate. Tristable materials could lead to exciting developments in molecule-based switches and memory storage.

To better understand the genesis of the magnetic behavior of $[Co(salen)]_2$ and to identify compounds that exhibit similar behavior, as the dimeric structure was associated with this tristability, several salen-substituted Co(II) complexes were synthesized. As analogous dimers based on the parent salen compound have not been observed, 1,2-diaminocyclohexane, and diaminomaleonitrile were chosen as Schiff base backbones. These groups were chosen as their synthesis is described in the literature,[14,15] and as a means to encourage crystallization due to their greater steric bulk.

Hence, to understand and control the tristability, $[Co(salen)]_2$, **1**, was reinvestigated and the following Co^{II}(salen)-based compounds were sought and targeted for study: bis(3,5-di-*tert*-butylsalicylidene)-1,2-cyclohexanediaminato(2-)cobalt(II)], **2**, *N*,*N*'-bis(3-chlorosalicylidene)-1,2-cyclohexanediaminato(2-)cobalt(II), **3**, *N*,*N*'-bis(3,5-dichlorosalicylidene)-1,2-cyclohexanediaminato(2-)cobalt(II), **4**, *N*,*N*'-bis(3-nitrosalicylidene)-1,2-cyclohexanediaminato(2-)cobalt(II), **5**, *N*,*N*'-bis(3,5-dinitrosalicylidene)-1,2-cyclohexanediaminato(2-)cobalt(II), **6**, and [*N*,*N*'-diaminomaleonitrilebis(salicylideniminato(2-)cobalt(II)], **7** (Figure 2.2).

Experimental

Synthesis. Solvents used included methanol (MeOH), ethanol (EtOH), 1-propanol (*n*-PrOH), and water (H_2O). The alcohols were dried and sparged with N_2 prior to use. Ethylene diamine was obtained from Sigma-Aldrich and was purified by distillation. 1,2-cyclohexanediamine was purchased from Acros Organics and distilled at atmospheric pressure and stored away from light. Diaminomaleonitrile was purchased

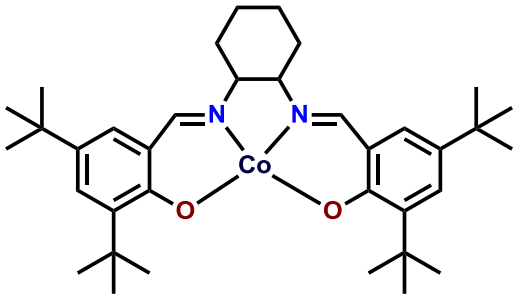

2

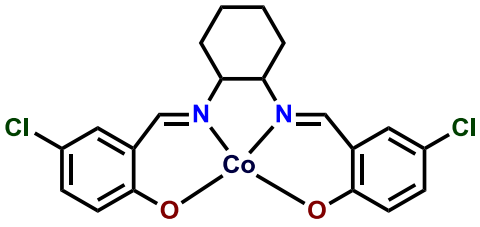

3

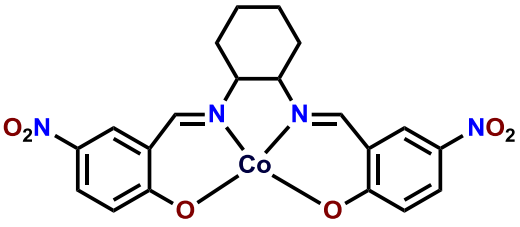

4

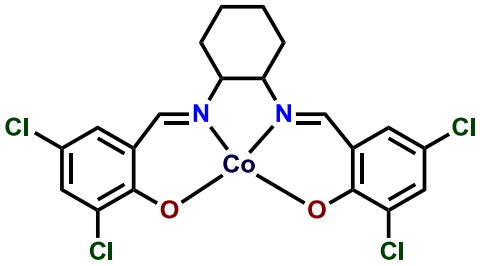

5

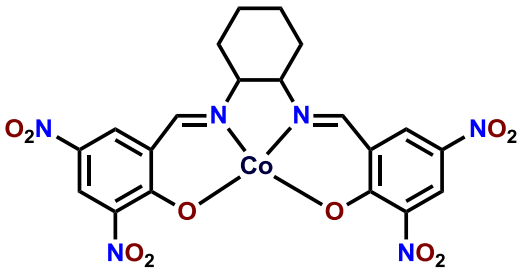

6

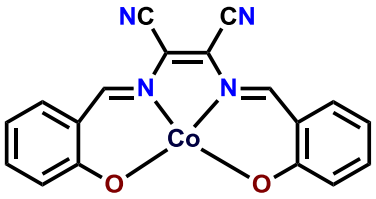

7

Figure 2.2. Structures of Co^{II}(salen) analogues **2**, **3**, **4**, **5**, **6**, and **7**.

from Sigma-Aldrich and used without further purification. Unsubstituted salicylaldehyde was purchased from Sigma-Aldrich and dried by stirring over $CaCO_3$ and then purified by distillation under high vacuum on a Vigeraux column. 5-Chlorosalicylaldehyde (Alfa Aesar), 5-nitrosalicylaldehyde (Alfa Aesar), 3,5-dichlorosalicylaldehyde (Arcos Organics), and 3,5-dinitrosalicylaldehyde (Avocado Research Chemicals Ltd.) were used without further purification. The compounds $[Co^{II}(salen)]_2$, **1**, and bis(3,5-di-*tert*-butylsalicylidene)-1,2-cyclohexanediaminato(2-)-cobalt(II)], **2**,[16] were gifts from colleagues. $Co(OAc)_2 \bullet 4H_2O$ was purchased from Baker Chemical Company and dehydrated by heating to 140°C for several hours according to the method described by Tsurata and coworkers.[15]

The Schiff bases were synthesized following the method outlined by Bailes and Calvin,[14] with the substitution of MeOH, EtOH, or *n*-PrOH for the listed alcohol made in some situations. Coordination of Co(II) to the Schiff bases was achieved following the general procedure outlined by Tsurata and coworkers.[15] Reaction times, temperatures, and solvents were also adjusted as needed and are detailed below.

Physical methods. Infrared spectra (IR) (± 1 cm^{-1}) were taken using a Bruker Tensor 37 spectrometer equipped with a liquid N_2 cooled detector. NMR spectra were recorded on a 300 MHz Varian Unity 300 Spectrometer equipped with a Nalorac Quad-probe ($^1H/^{19}F$, $^{13}C/^{31}P$) or equivalent. Low- to room-temperature magnetic susceptibilities were measured in applied fields of 1000 Oe between 5 and 400K on a Quantum Design (QD) Magnetic Properties Measurements System (MPMS) superconducting quantum interference device (SQUID) equipped with a reciprocating samples measurement system, low-field option, and continuous low-temperature control with enhanced thermometry features as previously described.[18] Samples were ground to powder and

loaded in gelatin capsules, sealed with grease. The direct current (dc) magnetization temperature dependence was obtained by cooling in zero-field and then data were collected upon warming in a 5 Oe field.

The diamagnetic contribution from the sample holder was corrected for, as well as the core diamagnetic corrections noted below. A home-built brass sample holder (7.9 cm in length with an outer diameter of 0.30 cm) was used for the magnetic measurement. The paramagnetic contribution from the sample holder was subtracted from the overall magnetic moment using a point-by-point background subtraction.

Thermogravimetric analysis (TGA) was conducted on a TGA 2050 TA instrument. The instrument was stored in a Vacuum Atmospheres DriLab glove box filled with nitrogen, though the samples tested were not expected to be noticeably air sensitive. Typical runs were conducted from 25 to 400°C. Differential scanning calorimetry (DSC) was conducted on a TA Instruments DSC 2910 Modulated DSC with a MDSC Cell Heat Exchange Assembly. The experiment was run for a single cycle from 20 to 400°C and then back to 20°C at a rate of 2.5°C/min. Data were analyzed with Universal Analysis (version 4.4) software. Elemental analysis (EA) was performed by Desert Analytics, Tucson, AZ.

[*N,N*'-ethylenebis(salicylideniminato)cobalt(II)] dimer (1). The dimer was received as a gift from a colleague. Structure was confirmed by IR and magnetic data.[9,10] IR (KBr; cm^{-1}); $\nu_{C\text{-}H}$ 3053, 3020, 2959 cm^{-1}, $\nu_{C=N}$ 1607 cm^{-1} $\nu_{C=C}$ 1529, 1450 cm^{-1}. The diamagnetic correction of -166 x 10^{-6} emu/mol was used.

[*N,*N'-Bis(3,5-di-*tert*-butylsalicylidene)-1,2-cyclohexanediaminato (2-) cobalt(II)] (2). The complex was received as a gift from a colleague. IR (KBr; cm^{-1}); $\nu_{C\text{-}H}$ 2952, 2867 cm^{-1}, $\nu_{C=N}$ 1595 cm^{-1} $\nu_{C=C}$ 1527, 1465 cm^{-1}. Elemental Analysis (EA) Calcd

(obsd) for 1: C 71.62 (71.67), H 8.68 (8.72), N 4.64 (4.72). The diamagnetic correction of -366 x 10^{-6} emu/mol was used.

[*N*,*N*'-Bis(5-chlorosalicylidene)-1,2-cyclohexanediaminato (2-) cobalt(II)] (3). The Schiff base was formed by dissolving 2.00 g (12.80 mmol) 5-chlorosalicylaldehyde in MeOH, forming a yellow solution. The reactions were then heated to 60°C. Once boiling was achieved, a solution of 729 mg (6.39 mmol) (±)-*trans*-1,2-cyclohexanediamine dissolved in 10 mL MeOH was added dropwise via syringe over the course of 10 min. A yellow precipitate formed almost immediately. The reaction was then stirred for ~2 hr, after which time the solution was cooled to room-temperature. The yellow solid was collected on a frit, washed with cold EtOH, and dried under reduced pressure [Yield: 1.78 g (71.0%)] IR (KBr; cm^{-1}); ν_{C-H} 2926, 2852 cm^{-1}, $\nu_{C=N}$ 1632 cm^{-1}, $\nu_{C=C}$ 1573, 1478 cm^{-1}.

Next, 110.5 mg (0.282 mmol) of the resulting Schiff base ligand was suspended in EtOH, the reaction was then placed under nitrogen and heated to 60°C with stirring. To the slurry, 50 mg (0.282 mmol) of cobalt(II) acetate was added as a solid. A red-brown solid resulted almost immediate and the slurry was stirred for an additional 2 hr. The red-brown solid was then collected on a frit and washed with EtOH and dried under strong vacuum. [yield: 120 mg (94.7%)] IR (KBr; cm^{-1}); ν_{C-H} 2936, 2857cm^{-1}, $\nu_{C=N}$ 1601 cm^{-1}, $\nu_{C=C}$ 1521, 1447 cm^{-1}. EA Calcd (obsd) for 2: C 53.19 (53.59), H 4.05 (4.01), N 6.25 (6.05). The diamagnetic correction of -242 x 10^{-6} emu/mol was used.

[*N*,*N*'-Bis(3,5-dichlorosalicylidene)-1,2-cyclohexanediaminato (2-) cobalt(II)] (4). The Schiff base was synthesized by solvating 2.00 g (10.5 mmol) 3,5-dichlorosalicylaldehyde in EtOH. To this, a solution of 0.598 g (5.24 mmol) of (±)1,2-cyclohexanediamine dissolved in EtOH was added dropwise, resulting in a yellow

precipitate. The stirring solution was then heated to 60°C for 0.5 hr before being cooled to room-temperature. The resulting precipitate was then collected on a frit, washed with cold EtOH and air dried. [Yield: quantitative] IR (KBr; cm^{-1}); ν_{C-H} 2939, 2862 cm^{-1}, $\nu_{C=N}$ 1632 cm^{-1}, $\nu_{C=C}$ 1570, 1452 cm^{-1}.

Next, 1.00 g (2.17 mmol) of the yellow precipitate was suspended in 10 mL of *n*-PrOH heated to 60°C and 385 mg (2.17 mmol) of cobalt acetate was added as a solid. The reaction was stirred at 60°C for 1 hr , during which time a brown precipitate formed. After 1 hr, the reaction was cooled to room-temperature, the precipitate filtered off, washed with *n*-PrOH, and dried under strong vacuum. The precipitate was sticky and stopped up the frit so acetone was used to wash the product. The same was then redried under strong vacuum. [Yield: 950 mg (84.7%)] IR (KBr; cm^{-1}); ν_{C-H} 2939, 2861 cm^{-1}, $\nu_{C=N}$ 1600 cm^{-1}, $\nu_{C=C}$ 1514, 1436 cm^{-1}. EA Calcd (obsd) for 3: C 46.45 (46.74), H 3.12 (2.95), N 5.42 (5.42). The diamagnetic correction of -276 x 10^{-6} emu/mol was used.

[*N*,*N*'-Bis(5-nitrosalicylidene)-1,2-cyclohexanediaminato (2-) cobalt(II)] (5). The Schiff base was formed by dissolving 2.00 g (11.96 mmol) of 5-nitrosalicylaldehyde and 683 mg (5.98 mmol) of (±)1,2-cyclohexanediamine in 30 mL of EtOH, under an inert N_2 atmosphere, with stirring. The reaction was then heated to 60°C and stirred for 2 hr, during which time a yellow/orange solid precipitated. After 2 hr, the solution was cooled to room-temperature and the precipitate was then collected on a frit and air dried. [Yield: 2.10 g (85.0%)] IR (KBr; cm^{-1}); ν_{C-H} 3065, 2954, 2865 cm^{-1}, $\nu_{C=N}$ 1652 cm^{-1}, $\nu_{C=C}$ 1554 cm^{-1}, $\nu_{N=O}$ 1619, 1309 cm^{-1}.

Next, 117 mg (0.282 mmol) of the yellow/orange Schiff base precipitate was dissolved in 20 mL of EtOH and 50 mg (0.282 mmol) of $Co(OAc)_2$ was added. The solution was stirred for 2 hr at 60°C. The resulting brown slurry was then cooled to room

temperature and the solid was collected on a frit, washed with EtOH, and dried under vacuum. [Yield: 120 mg (87%).] IR (KBr; cm^{-1}): ν_{C-H} 3065, 2938, 2864 cm^{-1}, $\nu_{C=N}$ 1599 cm^{-1}, $\nu_{C=C}$ 1498 cm^{-1}, $\nu_{N=O}$ 1543, 1317 cm^{-1}. EA Calcd (obsd) for 4: C 51.18 (51.50), H 3.87 (3.60), N 11.92 (11.94). The diamagnetic correction of -231 x 10^{-6} emu/mol was used.

[*N*,*N*'-Bis(3,5-dinitrosalicylidene)-1,2-cyclohexanediaminato (2-) cobalt(II)] (6). The Schiff base was formed by dissolving 500 mg (2.36 mmol) of 3,5 dinitrosalicylaldehyde in 20 mL of EtOH, forming an orange solution. Next, 134 mg (1.17 mmol) of (±)-*trans*-1,2-cyclohexanediamine was solvated in 12 mL of EtOH, forming a clear, colorless solution. The salicylaldehyde solution was then place under a N_2 atmosphere and heated to reflux (~70°C). The EtOH solution of diaminocyclohexane was then added dropwise to the refluxing solution over the course of 0.5 hr. Orange precipitate was seen to crash out of the solution near the end of addition. The slurry was stirred at reflux for an additional 1.5 hr, and then cooled to room-temperature. The precipitate was collected on a frit and washed with ethanol and ether, yielding a bright orange solid. The solid was then dried under strong vacuum. [Yield: 550 mg (94.0%)] IR (KBr; cm^{-1}); ν_{C-H} 3087, 2958, 2865 cm^{-1}, $\nu_{C=N}$ 1652 cm^{-1}, $\nu_{C=N}$ 1619 cm^{-1}, $\nu_{N=O}$ 1554, 1339 cm^{-1}.

Next, 200 mg (0.398 mmol) of the orange Schiff base was dissolved in 20 mL of *n*-PrOH. The resulting orange solution was then placed under a N_2 atmosphere and heated to 60°C. Next, 71 mg (0.398 mmol) of $Co(OAc)_2$ was added as a solid, causing the orange solution to turn a dark red/brown color. The reaction was stirred at 60°C for 1 hr. The reaction was then cooled to room-temperature and filtered through a frit. The resulting brown solid was then collected on a frit, washed several times with *n*-PrOH and

dried under vacuum. [Yield: 210 mg (93%).] IR (KBr; cm^{-1}): ν_{C-H} 3079, 2942, 2862 cm^{-1}, $\nu_{C=N}$ 1599 cm^{-1}, $\nu_{C=C}$ 1560 cm^{-1}, $\nu_{N=O}$ 1525, 1331 cm^{-1}. EA Calcd (obsd) for 5: C 42.95 (43.10), H 2.88 (2.99), N 15.03 (14.88). The diamagnetic correction of -255 x 10^{-6} emu/mol was used.

[*N*,*N*-bis[[(2-hydroxyphenyl)methylene]amino]-2-butenedinitrilato (2-)-cobalt(II)] • 0.5 EtOH • 1.2 H_2O (7). The Schiff base was formed by dissolving 1.01 g (9.34 mmol) of diaminomaleonitrile in 150 mL of hot MeOH. The resulting solution was then filtered to remove nonsolvated starting material. Next, the solution was heated to ~60°C and 1.94 mL (18.21 mmol) of salicylaldehyde was added dropwise over the course of 15 min, resulting in an orange precipitate. The reaction was then stirred for 2 hr before being cooled in freezer. The solid was then filtered off and washed with cold H_2O and cold MeOH. The dried solid was next recrystallized from boiling MeOH, giving a microcrystalline orange solid. [Yield: 1.09 g (34.2%)] IR (KBr; cm^{-1}): ν_{C-H} 2963 cm^{-1}, $\nu_{C\equiv N}$ 2243, 2207 cm^{-1}, $\nu_{C=N}$ 1624 cm^{-1}, $\nu_{C=C}$ 1606, 1498 cm^{-1}.

A slurry of 0.72 g (2.3 mmol) of the orange solid was formed in 10 mL of EtOH heated to 60°C. An excess of cobalt acetate tetrahydrate (0.71 g; 4.0 mmol) was dissolved in 5 mL of water and added dropwise over the course of 10 min, forming a dark brown slurry. The reaction was then stirred at 60°C overnight before being cooled to room temperature and filtered under reduced pressure. The resulting solid was dark purple and fibrous. The purple solid was collected on a frit and washed with cold EtOH. The solid was recrystallized from hot toluene, without noticeable change in the color or texture. [Yield: 0.25 g (29%)] IR (KBr, cm^{-1}) ν_{C-H} 2952 cm^{-1}, $\nu_{C\equiv N}$ 2216 cm^{-1}, $\nu_{C=N}$ 1605 cm^{-1}, $\nu_{C=C}$ 1574, 1514 cm^{-1}. EA Calcd (obsd) for 6: C 54.54 (54.61), H 4.00 (3.71), N 13.51 (13.41). The diamagnetic correction of -119 x 10^{-6} emu/mol was used.

Results and Discussion

This research was conducted in an attempt to better understand the source of the magnetic behavior of the Co^{II}(salen) dimer and to identify compounds which exhibited similar behavior as the dimeric structure was associated with this tristability. As no Co^{II} dimers of analogous compounds synthesized from the parent salen compound have been observed, 1,2-diaminocyclohexane and diaminomaleonitrile were used as alternative backbones as a means to encourage crystallization of the product without negatively impacting the magnetic properties. The magnetic behavior and structure did not indicate dimers for any of the compounds[6] except the tetranitro derivative with the 1,2-diaminocyclohexane backbone (**6**) and the product of the unfunctionalized salen and 1,2-diaminomaleonitrile (**7**). Similar magnetic data indicated the presence of tristability.

The syntheses of all of the substituted-salen compounds were conducted by established reaction schemes.[14,15] Formation of the Schiff bases was established through diagnostic signals in the IR spectrum. The appearance of the bands around 1638 ± 14 cm^{-1} in all of the compounds indicated the formation of the C=N bond from condensation of the amine with the aldehyde. The recorded values were in good agreement with values previously reported in the literature.[18] Additionally, the spectra were shown to all possess absorptions from 2940 to 2970 cm^{-1}, >1620 cm^{-1}, and 1500 to 1600 cm^{-1}, consistent with alkenyl ν_{C-H}, conjugated $\nu_{C=N}$, and aromatic $\nu_{C=C}$ stretching, respectively.

Formation of the Co(II) complexes from the Schiff bases was more difficult to ascertain from the IR spectra, as little change in the mid-IR could be detected. There was a recognizable shift of ~20 cm^{-1} in the C=N stretch after complexation of the metal ion. This was accompanied by an obvious, dramatic color change. Coordination of the metal site was also confirmed through elemental analysis and magnetic studies of the

compounds.

The use of 1,2-diaminomaleonitrile, though magnetically interesting, led to lower yields of both the Schiff base and coordinated complex. The low yields were most likely the result of poor solubility of 1,2-diaminomaleonitrile and the resulting Schiff base in alcohols. Additionally, the cobalt complex of the maleononitrile Schiff base (**7**) was more difficult to dry, resulting in trapped solvent in the final compound.

None of the substituted Co^{II}(salen) compounds formed single crystals suitable for either single crystal X-ray diffraction or powder diffraction analysis to confirm their structure. A correlation between color and tristability was noted, however. Co(salen) complexes exhibiting tristability (**1**, **6**, and **7**) were dark-violet, appearing to be almost black. The functionalized Co(salen) compounds which did not exhibit tristability were red/orange to mustard brown.

Structure. The crystal structures of Co^{II}(salen) have been well studied.[7-10] The compound exists in monomeric and dimeric forms (Figure 2.1). The monomer exists as a distinct 4-coordinate structure[8] with the cobalt center lying in the plane (C_{2v} symmetry) of the Schiff base, or as a pentacoordinate species with any number of ligands occupying the axial position and exhibiting a number of polymorphs.[13,19] In the dimeric structure, phenolic oxygens of adjacent compounds occupy the axial position giving rise to C_i symmetry.[10]

IR and magnetic studies of the crystals of dimeric Co(salen) were in keeping with previous studies.[7b,10] Previous structures showed interdimer Co-O distances of 2.253 Å. The interdimer Co•••Co distance were shown to measure 3.12 Å. This length is about ~0.26 Å (10.3%) longer than direct Co•••Co bonding observed in other compounds and would typically preclude significant metal interactions[20] despite evidence for Co•••Co

interaction in the magnetic data.

Crystals suitable for powder X-ray analysis of the functionalized salen compounds **2-7** have not been obtained. The structure was assigned by reference to IR spectrum, elemental analysis, and magnetic data, though efforts are currently underway to solve the structures of these compounds.

Magnetic studies. The magnetic susceptibility, χ, for all compounds were measured between 5 and 300 K, and are reported as $\chi T(T)$ and $\chi^{-1}(T)$. All compounds were paramagnetic and did not exhibit evidence of magnetic ordering.

The room-temperature moment ($\chi T(T)$) of $[Co(salen)]_2$ (**1**) is 0.45 emuK/mol-Co, in agreement with behavior seen in the previous complexes[7,9] and within reason for low-spin $S = 1/2$ sites, if spin-orbit coupling is taken into account (Figure 2.3). However, the moment slowly decreases to 0.43 emuK/mol upon cooling to ~200 K and then continues to decrease to 0 emuK/mol upon cooling to 5 K (Figure 2.3). Above 300 K, the susceptibility begins to increase rapidly to 1.70 emuK/mol of Co at 550 K, though thermal decomposition occurs at 525 K. Evidence for decomposition is seen in the TGA as a significant loss of mass (Figure 2.4) and in the DSC data as a phase transition. Additional, the decomposition can be observed visually in a melt tube as the dark red/magenta crystals can be observed to crack and discolor.

The increase in $\chi T(T)$ from 5 to 200 K is indicative of thermal population of a triplet excited state from a singlet ground state. $\chi T(T)$ of $[Co(salen)]_2$ can be fit to the Bleaney-Bowers singlet-triplet expression, eq 2.1, per Co with good results, showing the efficacy of the dimer model ($H = -2JS_iS_j$), with $g = 2.26$ and $J/k_B = -30$ K (-21 cm^{-1}; -60 cal/mol), in good agreement with earlier work [$g = 2.4$; $J/k_B = -29$ K (-20 cm^{-1}; -58 cal/mol)].[7b] However, in the area above 200 K, the dimer model begins to break down as

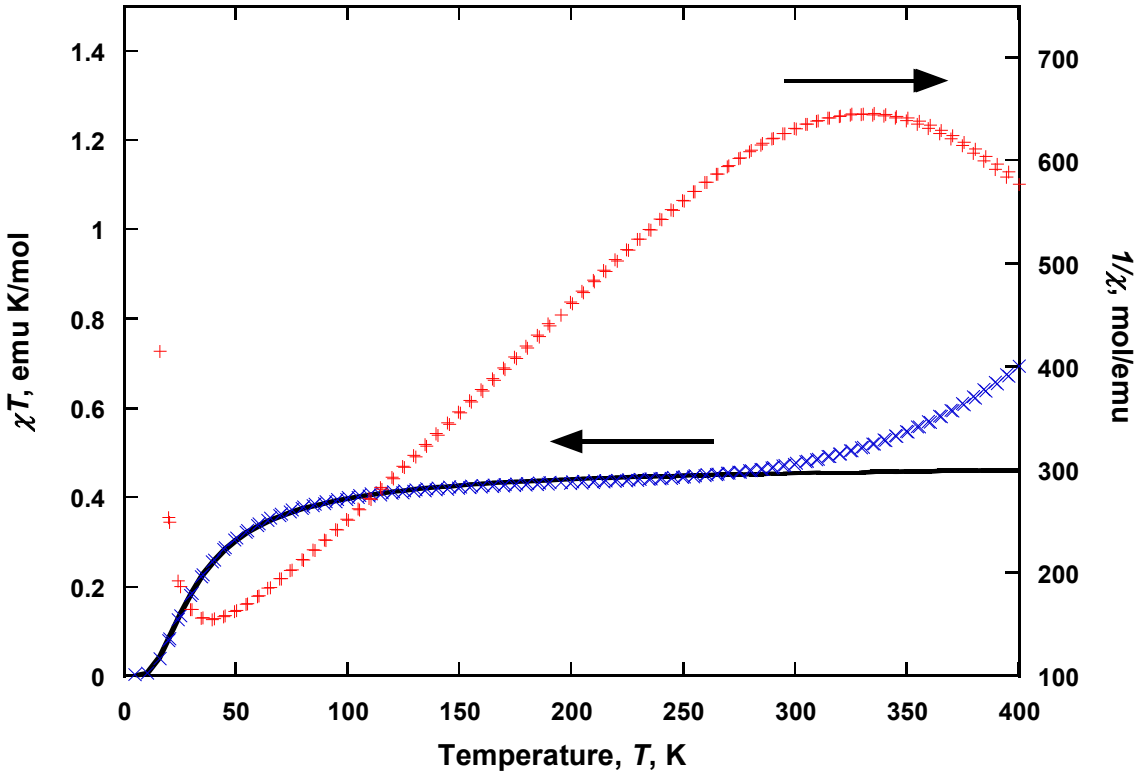

Figure 2.3. $\chi T(T)$ (x) and $1/\chi$ (T) (+) plot of $[Co(salen)]_2$, **1**. Solid line is fit to equation 2.1 below 200 K.

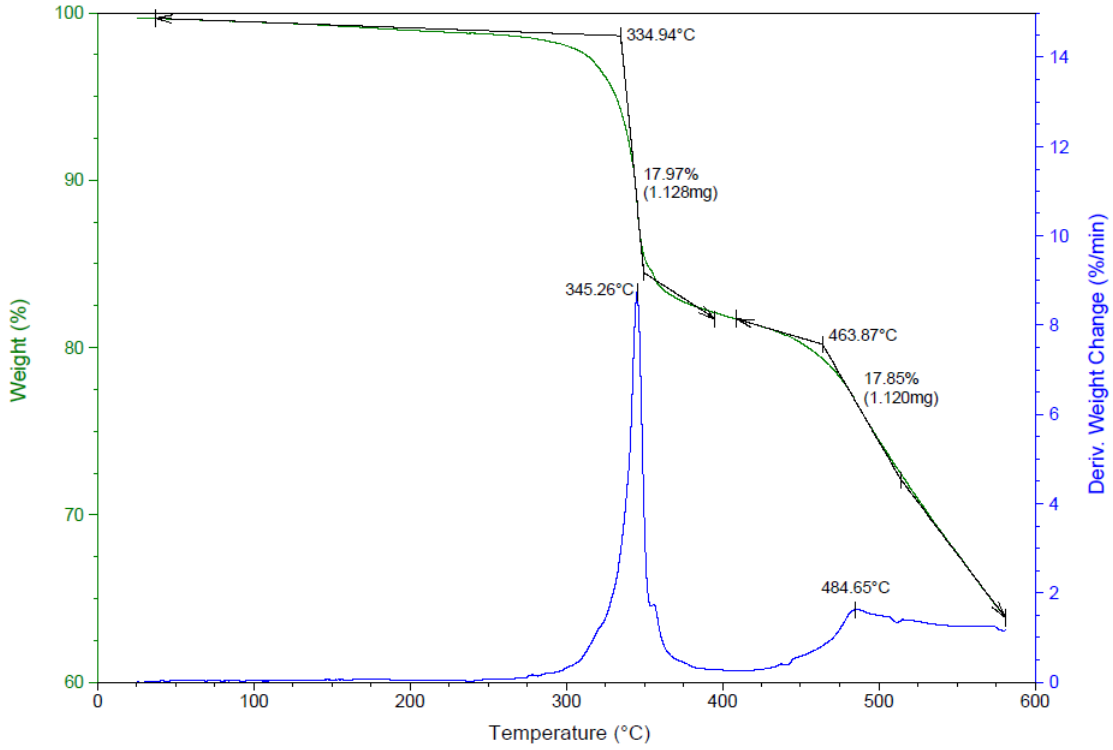

Figure 2.4. TGA of $[Co(salen)]_2$, **1**, indicating decomposition onset above 250°C.

the onset of spin crossover behavior is encountered.

$\chi T(T)$ increases much faster than would be expected from a Boltzmann population of the high-spin state at higher temperatures. This behavior is commonly encountered in spin crossover materials and is considered to be characteristic of the behavior,[21] but also means that the $\chi T(T)$ for this compound cannot be mathematically modeled above 200 K. Despite the occurrence of spin crossover behavior, the compound never exhibits a full saturated quartet state. The maximum theoretical value for χT for the high-spin 3/2 state is 2.39 emuK/mol for $g = 2.26$. The observed value of 1.70 emuK/mol is only 71% of the theoretical value at 600 K, indicating that temperatures greater than the decomposition temperature would be needed.

$$\chi T = \frac{N g^2 \mu_B{}^2}{k_B (3 + e^{-2J/k_B T})} \tag{2.1}$$

The spin crossover behavior observed for **1** is associated with a dinuclear site, not single-ion sites, as is well documented.[2] $\chi T(T)$ increases with heating until ~525 K, where thermal decomposition occurs. The singlet ($S = 0$) ground state arises from the antiferromagnetically coupled pair of Co^{II} ions, each being in the single-ion, low-spin $S = 1/2$ electron configuration, and the triplet ($S = 1$) excited state arises from ferromagnetic coupling of this pair of Co^{II} $S = 1/2$ ions. As the temperature increases, the thermal energy populates both the singlet and triplet states. This leads to $\chi T(T)$ approaching the Curie behavior for two Co^{II} $S = 1/2$ doublets at higher temperature as the exchange coupling, J, is less significant with respect to the thermal energy, $k_B T$ (Figure 2.5).

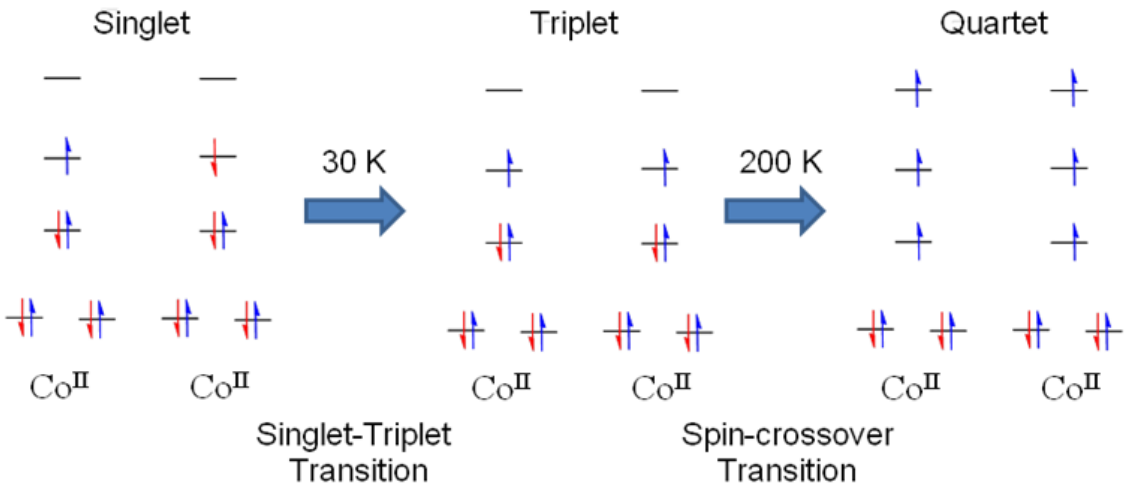

Figure 2.5. Orbital diagram representation of spin states involved in the singlet-triplet and spin crossover transitions of $[Co(salen)]_2$, **1**.

Of the following compounds studied, only **6** exhibited magnetic data analogous to that seen in dimeric Co(salen). Comparison of the $\chi T(T)$ plots of **1** and **6** indicated a strong agreement (Figure 2.6). The $\chi T(T)$ of **6** was 0.48 emuK/mol at 300 K, 6.7% higher than what was seen in our studies of **1**.[6] This is somewhat lower than would be expected, but is within reasonable agreement with the value expected for the $S = 1/2$, $g = 2.2$, system. Below 275 K, the susceptibility continues to decrease slowly until 180 K, where it reaches a plateau of ~0.42 emuK/mol. This was 2.4% lower than what was observed for **1** at that temperature. The moment continues to slowly decrease with decreasing temperature to 0.372 emuK/mol at 50 K. Below 50 K, the moment decreases rapidly to 0.218 emuK/mol at 5 K. This behavior reflects the temperature-dependent singlet-triplet transition behavior observed in **1**.

A fit of the $\chi T(T)$ data of **6** to the Bleaney-Bowers singlet-triplet expression (eq 2.1) (eq per Co ($H = -2J\mathbf{S}_i \bullet \mathbf{S}_j$), was conducted with $g = 2.10$ and $J/k_B = -7.5$ K. These values are lower in magnitude than those observed for **1**. The lower g-value is thought to arise from less spin anisotropy in **6**. The lower coupling values represent weaker coupling between the metal sites. This is evidenced by the earlier onset of the single-triplet transition, compared to **1**. This is attributed to longer Co•••Co distances, inhibiting the metal centers' ability to interact. Greater Co•••Co distances are supported by preliminary diffraction studies currently underway.

As with **1**, the model breaks down above the single-triplet plateau, ~180 K. This occurs 20 K lower in temperature than seen in $[Co(salen)]_2$, indicating an earlier onset of the spin crossover region. Earlier population of the quartet state is attributed to greater Co-N bond lengths, caused by the electron-withdrawing nitro-groups. Elongation of the bond length serves to weaken the ligand field strength which favors earlier population of

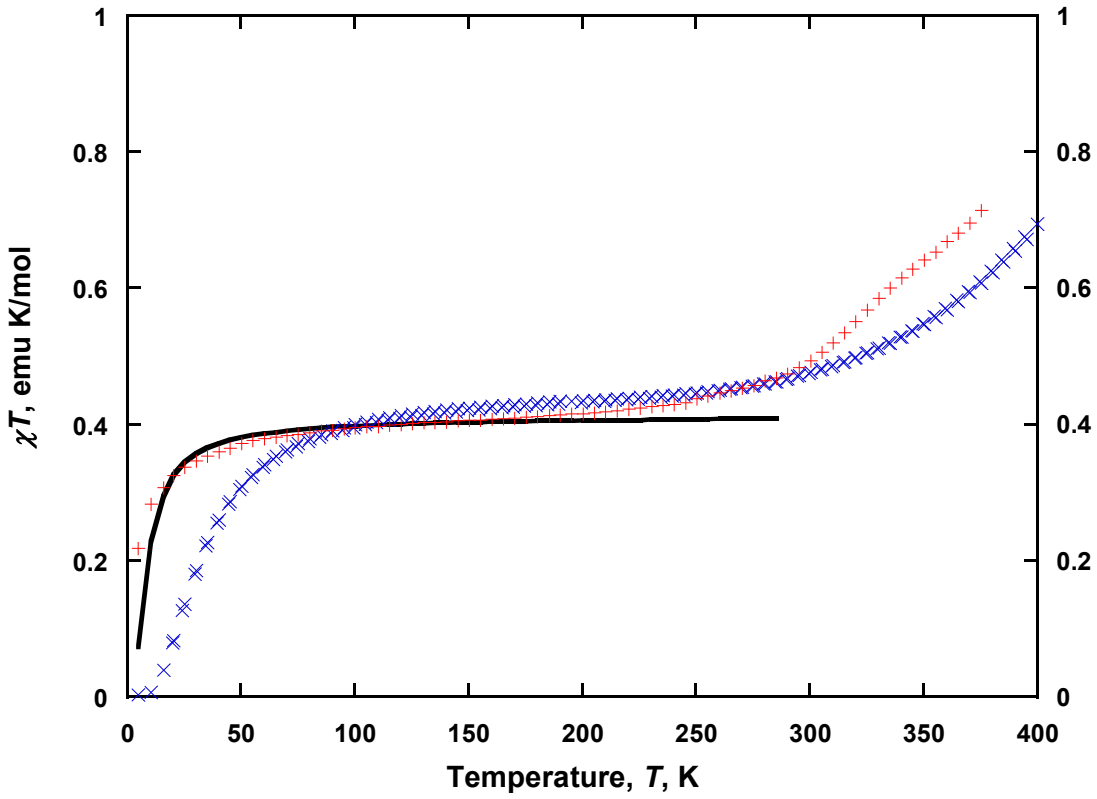

Figure 2.6. $\chi T(T)$ of $[Co(salen)]_2$ (**1**) (x) and $[Co(salen\text{-}(NO_2)_4)]_2$ (**6**) (+). Solid line is fit to eq 2.1 from 25 to 200 K.

the quartet state, and has been observed in related compounds. [22]

Above 320 K, $\chi T(T)$ shows the rate of increasing χT to increase again. This increase can be seen in the $1/\chi(T)$ data and corresponds to the start of gradual weight loss observed in a thermogravimetric analysis of the compound (Figure 2.7). An overlay of the $\chi T(T)$ plots of **1** and **6** compounds (Figure 2.6) indicates that inclusion of the nitro-groups effectively destabilizes the compound, leading to decomposition at lower temperatures. Due to the low decomposition temperature, the quartet state is only partially populated, as we see in the lower-than-expected room-temperature $\chi T(T)$ values, even lower than **1**.

This behavior is seen to be in sharp contrast to that seen in other functionalized Co(salen) derivatives. The magnetic data for **2**, **3**, and **5**, (Figure 2.8) exhibited temperature-independent moments of 0.519, 0.797, and 0.781 emuK/mol at 300 K, respectively. These values are much larger than the expected value of 0.375 emuK/mol for isolated spins of Co^{II} with $S = 1/2$ and $g = 2.0$. Similarly, high values observed in other Co(salen) complexes, and the discrepancies, are either attributed to spin-orbit coupling of the Co^{II} centers or the effects of the planar salen ligand.[9] In all of these cases, the susceptibility is seen to remain consistent until low temperatures (< 10 K), where evidence of weak antiferromagnetic coupling is observed. The presence of weak antiferromagnetic coupling is observed for other Co(salen) systems and has been fit to linear 1-D Ising and 1-D Heisenberg chain models, as well as dimeric models, and may indicate interaction between Co^{II}(salen) complexes, though the lack of structural determination precludes accurate assignment of this behavior.[12] The presence of dimers seems unlikely as tristability has been linked to Co^{II}(salen), which possess a definite structure.[6]

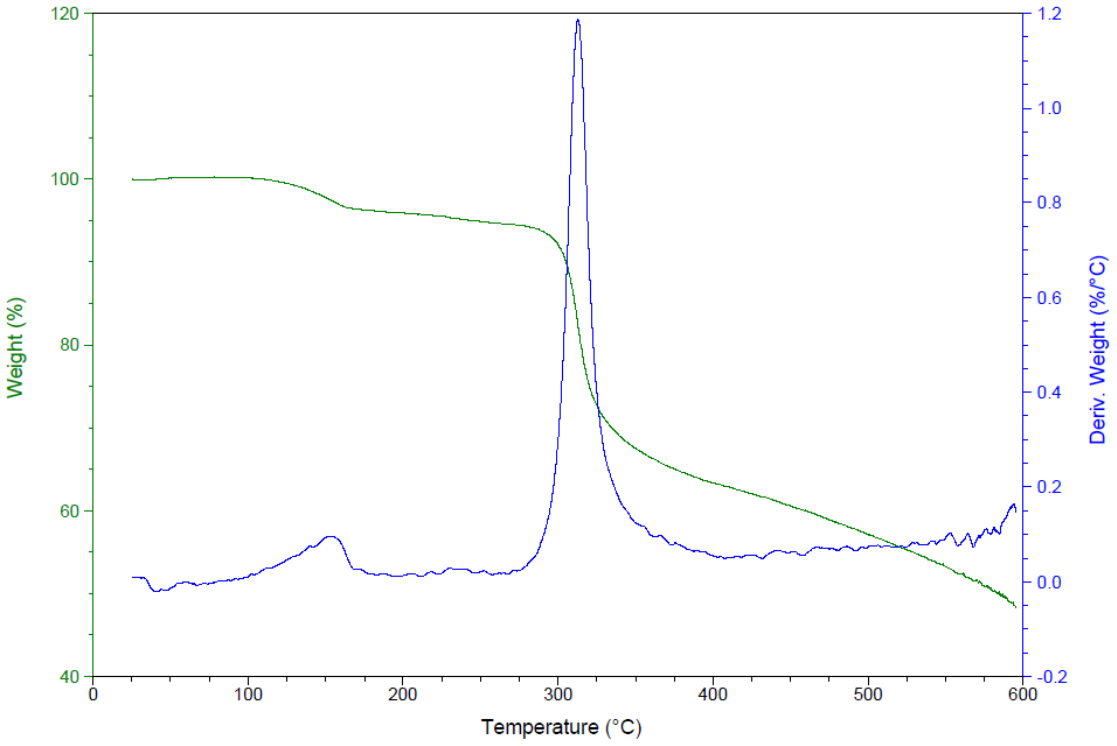

Figure 2.7. TGA of $[Co(salen\text{-}(NO_2)_4)]_2$ indicating decomposition above 250°C.

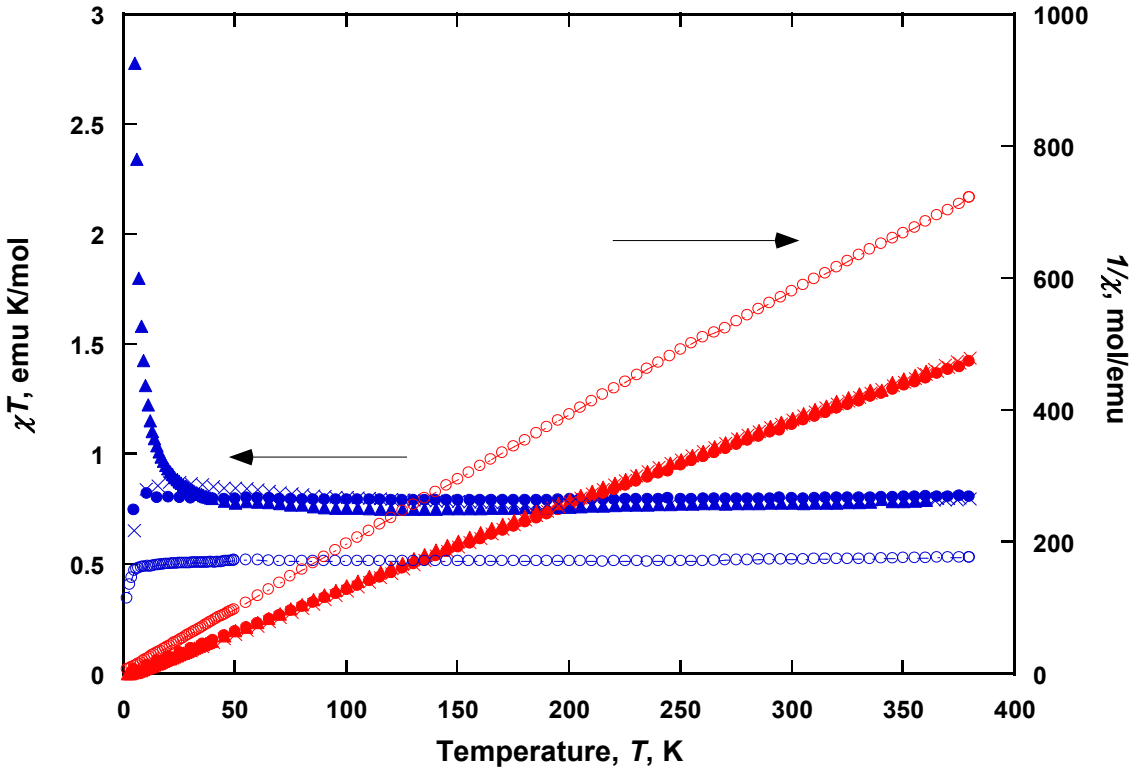

Figure 2.8. *χT(T)* and *1/χ(T)* [*N*,*N*'-bis(3,5-di-*tert*-butylsalicylidene)-1,2-cyclohexanediaminato(2-)cobalt(II)] (**2**)(○) [*N*,*N*'-bis(5-chlorosalicylidene)-1,2-cyclohexanediaminato(2-)cobalt(II) (**3**)(●), [*N*,*N*'-bis(3,5-dichlorosalicylidene)-1,2-cyclohexanediaminato(2-)cobalt(II)] (**4**)(▲), [*N*,*N*'-bis(5-nitrosalicylidene)-1,2-cyclohexanediaminato(2-)cobalt(II)] (**5**)(x).

The magnetic behavior of **4** indicates a room-temperature moment of 0.776 emuK/mol-Co, respectively. This value falls within the room-temperature moments observed for related Co(salen) systems.[9] Again, the discrepancy between the observed value and the expected room-temperature moment for a Co^{II} ion is attributed to spin-orbit coupling. However, while the magnetic response is well-behaved at higher temperatures, as the sample is measured below 35 K, $\chi T(T)$ rises sharply to a maximum of 7.92 emuK/mol for **4**, indicating the presence of ferromagnetic coupling (Figure 2.8). A similar response was noted by Murray and coworkers for oxygenated species of Co(salen).[12] A tetrameric model provided the best fit for Murray,[12] but the lack of crystal structures makes the assignment of this behavior difficult.

The appearance of tristability in **6** and its absence in **4** is attributed to the greater electron-withdrawing nature of the nitro compound. Quantification of electronegativity of functional groups has been more difficult than that of atoms. However, several studies[23] have indicated the nitro-group to have group electronegativity of 4.83 χ_G (Pauling units) 1.67 χ_G greater than the -Cl group. This combined electronegativity is thought to decrease electron density on the metal center, increasing its propensity to form dimers through association with atoms of adjacent compounds. The structure of **6** is being investigate to support this hypothesis.

In contrast to the behavior of most compounds with the cyclohexyl backbone, the magnetic response of **7** was also seen to show tristability (Figure 2.9). The room-temperature $\chi T(T)$ value is 2.25 emuK/mol, much higher than the value seen in the previous compounds, but similar to the theoretical value for $S = 3/2$ spin sites seen in related compounds.[19] The susceptibility is also in good agreement with literature values (2.21 emuK/mol) for compounds with nitrogen-bound groups,[9] which is beyond that seen

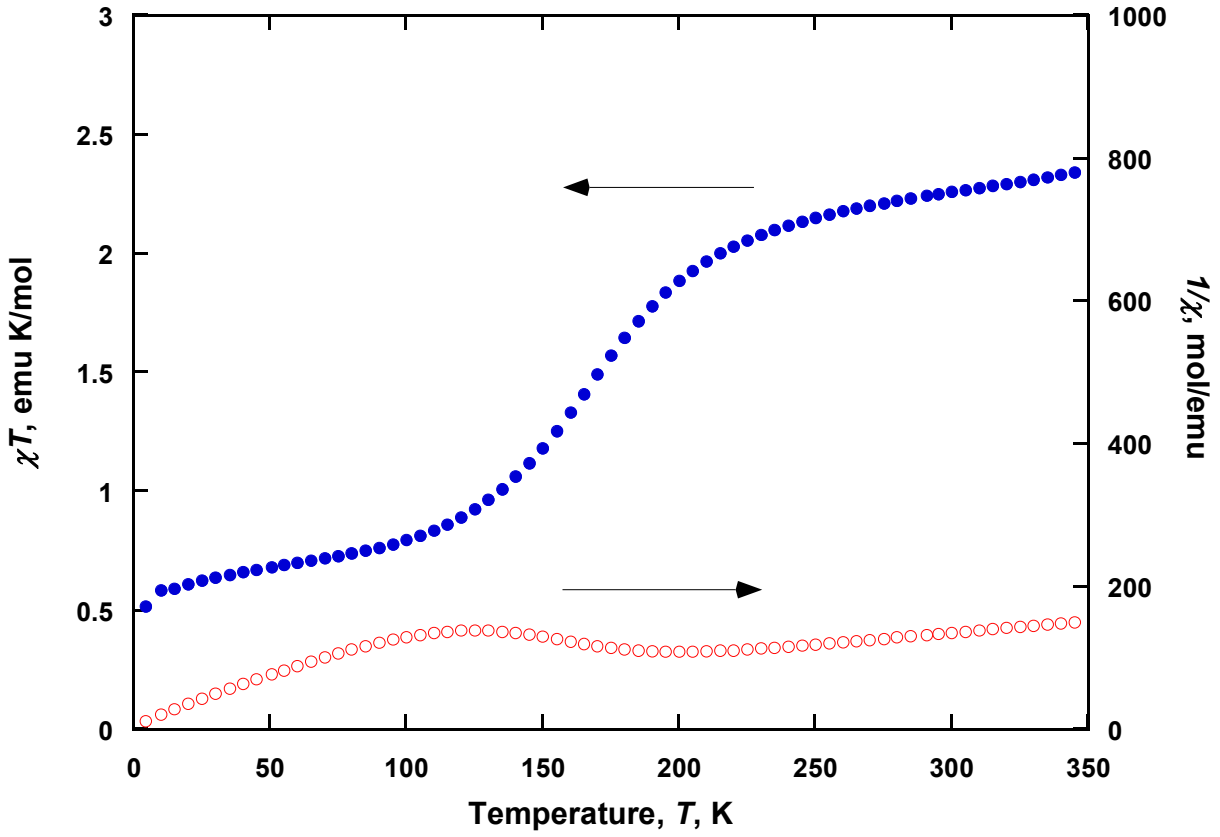

Figure 2.9. $\chi T(T)$ (●) and $1/\chi(T)$ (○) of [*N*,*N*'diaminomaleonitrilebis(salicylideniminato-(2-) cobalt(II)] (**7**).

for previous compounds and what would be anticipated from isolated spin values. The susceptibility continues to decrease with the temperature at a rate of ~0.002 emuK/mol/K until ~250 K where the value is 2.13 emuK/mol. Below 250 K, the moment rapidly decreases to 0.783 emuK/mol at 100 K. Once below 100 K, the rate of decreases lessens. The susceptibility slowly decreases to 0.564 emuK/mol at 10 K. Below 10 K, the moment appears to begin a more rapid decrease until, at 5 K, the susceptibility is measured as 0.507 emuK/mol.

The $\chi T(T)$ behavior deviated from that expected of tristable cobalt salen materials. The $\chi T(T)$ at low temperatures (20 - 100 K), arising from the excited triplet state, is roughly twice as large as that seen for **1** and **6**. It does closely correspond to the value observed for functionalized Co(salen) compounds **2** and **4**, where the large value is attributed to spin-orbit coupling of the Co^{II} sites. However, similarly large room-temperature values have been observed for *N*-substituted salen compounds, and this was attributed to interaction between the cobalt centers and the steric constraints of these complexes.[9] The increase in $\chi T(T)$ assigned to spin crossover begins to occur near 100 K, much earlier than observed for the other tristable compounds.

The appearance of tristability in **7** is also attributed to the electon-withdrawing nitrile groups on the backbone. Studies have indicated the -CN group to have an electronegativity near 3.84 χ_G. This is about 0.68 χ_G greater than the -Cl group.[24] The greater susceptibility values seen for **7** are thought to arise from the inclusion of the diaminomaleonitrile compound as the backbone. This enforces a rigid planar structure arising from the conjugated π-systems, potentially leading to elongation of the metal-Schiff base bonds and a lowering of the quartet-state energy. A study by Murray and coworkers on Co(II) Schiff base complexes noted a similar trend,[19] where higher

susceptibilities were noted for compounds with 1,2-diaminobenzene serving as the backbone over compounds with ethylenediamine backbones.

Compound **7** is thought to decompose over time, as is observed in the magnetic data (Figure 2.10). After heating **7** to 400 K, the sample was cooled and the temperature-dependent susceptibility was measured multiple times. On the second run, $\chi T(T)$ was seen to be 2.38 emuK/mol, a 5.8% increase over the original moment. The $\chi T(T)$ then decreased with temperature where the difference between the measurements continues to increase (Figure 2.10). The $\chi T(T)$ measured 2.28 emuK/mol at 250 K, 0.953 emuK/mol at 100 K, and 0.846 emuK/mol at 30 K where it was 7.0, 21.7, and 33.7% higher than the original measurement, respectively. Below 30 K, the $\chi T(T)$ is seen to begin increasing, to 1.13 emuK/mol at 5 K, indicating a ferromagnetic coupling in this region. The origin of this ferromagnetic region is not currently known, though may indicate oxygen complexation as ferromagnetic coupling has been noted by Murray in some oxygen-bound species.[12]

Conclusions

The tristability of oxygen-inactive dimer, $[Co^{II}(salen)]_2$ (**1**), was investigated and the increases in the $\chi T(T)$ measurements were assigned to singlet-triplet transitions and spin crossover behavior. In both cases, the transitions led to an increase in unpaired electrons, increasing the magnetic measurement. A series of functionalized Co^{II}salen complexes were investigated for the presence of tristability and two species, **6** and **7,** were discovered to exhibit evidence of tristability in their magnetic data. Tristability is thought to arise from close association between Co^{II} centers, as seen in the inactive form of Co^{II}salen. A correlation between the electron-withdrawing strength of the substituent

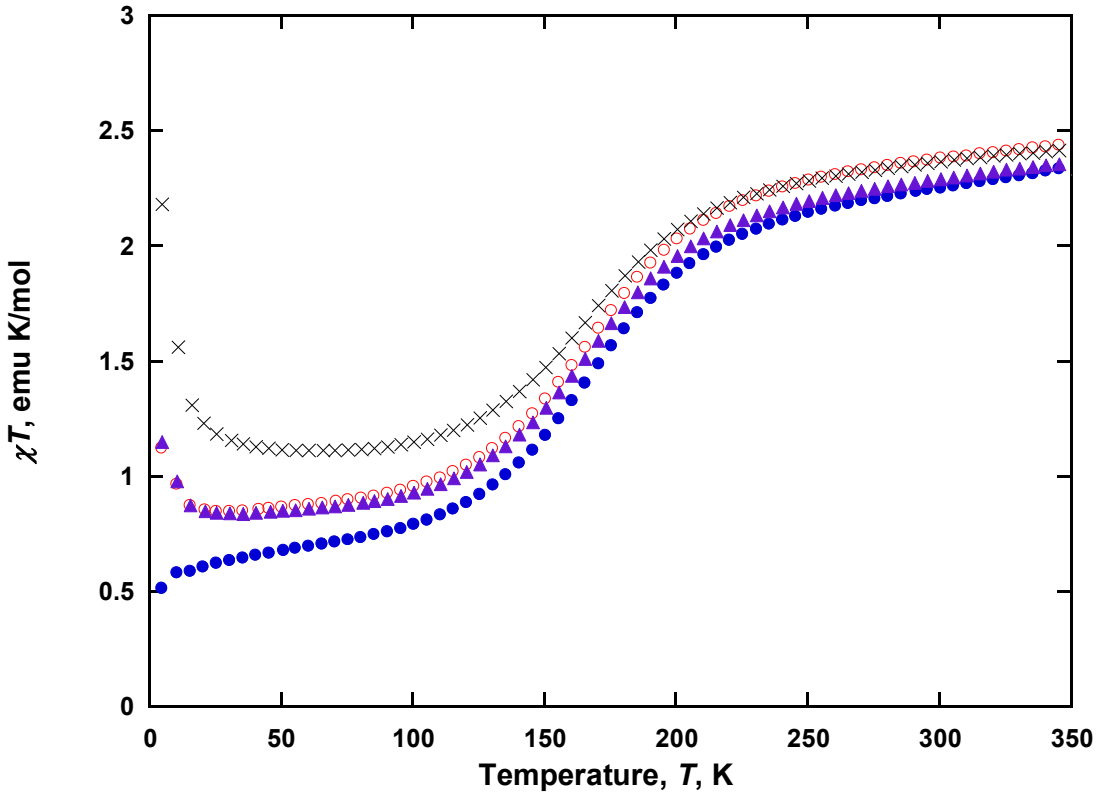

Figure 2.10. $\chi T(T)$ of [*N*,*N*'diaminomaleonitrilebis(salicylideniminato(2-) cobalt(II)], **7**, for 1st (●), 2nd (○), 3rd (▲), and 4th (x) iteration.

groups is thought to exist and may explain the magnetic behavior.

It was shown by Hitchman that axial bonding of ligands in low-spin Co(II) Schiff base complexes led to a lowering in energy of quartet states.[13] This is not directly due to the effects on the electronic structure due to introduction of electrons from the coordinating species, but results from a slight elongating of the Co-N and Co-O bond lengths from the Schiff base as the metal center leaves the coordination plane of the Schiff base.[12] It is thought that the nitro-groups may also slightly increase the metal-ligand bond lengths, as more electron density is pulled into the Schiff base.

This is supported by the results that the only cobalt salen compound with an electron donating group, **2**, showed the lowest room-temperature moment. As the electron-withdrawing groups, -Cl and -NO_2, are introduced at the 5' position on the aromatic rings for compounds **3** and **5**, the moment increases, though no evidence of tristability is noted. Further introduction of the electron-withdrawing groups at the 3' position of the aromatic ring appears to increase interaction between Co(salen) compounds. In the tetrachloro derivative **4**, there is evidence of ferromagnetic coupling at low temperatures. Also, this may explain the earlier onset of spin crossover behavior seen in **6,** when compared to **1**. The tetranitro derivative **6**, shows a reduced moment, attributed to antiferromagnetic coupling of two Co(salen) interacting as dimers. The appearance of this phenomenon in **6** and its absence in **4** is attributed to the greater electron-withdrawing nature of the nitro compound.

This may also explain the appearance of tristability in **7**, as studies have indicated the -CN group to have a higher electronegativity than the -Cl group.[24] The greater susceptibility values are attributed to longer metal-ligand bonds and a lowering of the quartet-state energy, consistent with previous studies.[19]

References

(1) Yu, B.; Meyyappan, M. *Solid-State Electronics* **2006**, *50*, 536.

(2) For example: (a) Feringa, B.L. *Molecular Switches*; Wiley-VCH: Weinheim, Germany, 2001. (b) Kahn, O.; Launary, J.P. *Chemtronics* **1988,** *3*, 140. (c) Guihery, N.; Durad, G.; Lepetit, M.-B. *Chem. Phys.* **1994,** *183*, 45. (d) Sato, O.; Zhang, Y.-Z. *Angew. Chem., Int. Ed.* **2007,** *46*, 2152. (e) Kahn, O.; Kröber, J.; Jay, C. *Adv. Mater.* **1992,** *4*, 718. (f) Guihery, N.; Durad, G.; Lepetit, M. -B.; Malrieu, J.-P. *Chem. Phys.* **1994,** *183*, 61. (g) Sato, O.; Zhang, Y.-Z.; Angew. Chem. Int. Ed. **2007**, *46*, 2152.

(3) For example: *Spin Crossover in Transition Metal Compounds*; Gütlich, P.; Goodwin, H.A., Eds.; Springer: New York, 2004; Vols 1-3.

(4) For example: (a) Shultz, D.A.; In *Magnetism-Molecules to Materials;* Miller, J.S., Drillion, M., Eds.; Wiley-VCH: Weinheim, Germany, 2001; Vol. *2*, p 281. (b) Pierpoint, G.C.; Buchanan, R. M. *Coord. Chem. Rev.* **1981**, *38*, 45. (c) Pierpoint, G.C.; Lange, C.W. *Prog. Inorg. Chem.* **1994**, *41*, 331.

(5) For example: *Photochromism: Molecules and Systems*; Dürr, H., Bouas-Laurent, H., Eds.; Elsevier: Amsterdam, The Netherlands, 1990; p 64. Organic Photochromic and Thermochromic Compounds. *Main Photochromic Families*; Crano, J. C., Guglielmetti, R., Eds.; Plenum Publishers: New York, 1999; Vol. *1*.

(6) Min, K.S.; Arthur, J.; Shum, W.W.; Bharathy, M.; zur Loye,H.-C.; Miller, J.S.; *Inorg. Chem.* **2009**, *48*, 4593.

(7) (a) Bruckner, S.; Calligaris, M.; Nardin, G.; Randaccio, L. *Acta Crystallogr., Sect. B*, **1961**, *25*, 1671. (b) Carlisle, G.O.; Simpson, G.D.; Hatfield, W.E.; Crawford, V.H.; Drake, R.F. *Inorg. Chem.* **1975**, *14*, 217.

(8) Schaefer, W.P.; Marsh, R.E. *Acta. Cryst.* **1969**, *B25*, 1675.

(9) Earnshaw, A.; Hewlett, P.C.; King, E. A.; Larkworthy, L.F. *J. Chem. Soc. A* **1968**, 241.

(10) Delasi, R.; Holt, S.L.; Post, B. *Inorg. Chem.* **1971**, *10*, 1498.

(11) Lämmle, K.; Trevethan, T.; Schwarz, A.; Watkins, M.; Schluger, A.; Wiesendanger, R. *Nano Lett.* **2010**, *10*, 2965.

(12) Murray, K.S.; van der Bergen, A.; Kennedy, B.J.; West, B. O. *Aust. J. Chem.* **1986**, *39*, 1479

(13) Hitchman, M.A. *Inorg. Chem.* **1977**, *16*, 1985.

(14) Bailes, R.H.; Calvin, M. *J. Amer. Chem. Soc.* **1947**, *69*, 1886.

(15) Takeichi, T. Arihara, M.; Ishimori, M. Tsurata, T. *Tetrahedron*, **1980**, *36*, 3391.

(16) The diamagnetic corrections of -166 and -366 x 10-6 emu/mol was used, respectively.

(17) Brandon, E.J.; Rittenburg, D.K.; Arif, A.M.; Miller, J.S. *Inorg. Chem.* **1998**, *37*, 3376.

(18) (a) Siebert, F. Mäntele, W.; Gerwert, K. *Eur. J. Biochem.* **1983,** *136*, 119. (b) Rigamonti, Demartin, F.; Forni, A.; Righetto, S.; Pasini, A. *Inorg. Chem.* **2006,** *45*, 10976.

(19) Kennedy, B.J.; Fallon, G.D.; Gatehouse, B.M.K.C.; Murray, K.S. *Inorg. Chem.* **1984**, *23*, 580.

(20) Pauling, L. (1960). *The Nature of the Chemical Bond,* 3rd Edition, p. 441. Ithaca: Cornell Univ. Press.

(21) Spin Crossover in Transition Metal Compounds; Gutlich, P.; Goodwin, H.A., Eds.; Springer: New York, 2004; Vols *1-3*.

(22) Constable, E.C.; Baum, G.; Bill, E.; Raylene, D.; van Eldik, R.; Fenske, D.; Kaderli, S.; Morris, D.; Neubrand, A.; Neuburger, M.; Smith, D.R.; Wieghardt, K.; Zehnder, M.; Zuberbühler, A.D. *Chem. Eur. J.* **1999**, *5*, 498.

(23) Garnder-O'Neale, L. D.; Bonamy, A. F.; Meek, T. L.; Patrick, B. G. *J. Mol. Struct. (Theochem)* **2003**, *639*, 151.

(24) (a) Huheey, J. E. *J. Phys. Chem.* **1965**, *69*, 3284. (b) Huheey, J. E. *J. Phys. Chem.* **1966**, 2086.

CHAPTER 3

SYNTHESIS, STRUCTURE, AND CHARACTERIZATION OF QUINONE-BASED CYANOCARBON ACCEPTORS

Introduction

Cyanocarbon acceptors are among the most studied class of organic building blocks in molecule-based magnetic systems.[1-5] TCNQ (7,7,8,8-tetracyano-*p*-quinodimethane) and TCNE (tetracyanoethylene) (Figure 3.1), in particular, have been widely studied and a large number of magnetic systems have been reported.[1,2] The origin of the popularity of these compounds is twofold. First, the nitrile groups provide coordination sites for bonding to metal centers. Second, the electron-withdrawing nature of the nitrile groups, coupled with the conjugated π-orbitals, allow for formation of persistent radical anions. The organic radicals are able to contribute an additional $S = 1/2$ spin to systems, encouraging magnetic ordering, by providing exchange pathways between metal centers.

The formation of the stable, room-temperature magnet, $V(TCNE)_2$[2b,6] has led to much interest in researching the relationship between structure and magnetic properties. The structure of $V(TCNE)_2$ has yet to be solved, due to the resulting disordered product.[7] TCNE as well as TCNQ possess four nitriles and form homoleptic complexes of $M^{II}(TCNE)_2$ stoichiometry with octahedral M^{II} ions. Thus, two acceptors have a total of

---

Reproduced in part with permission from Advanced Functional Materials, *in press*.

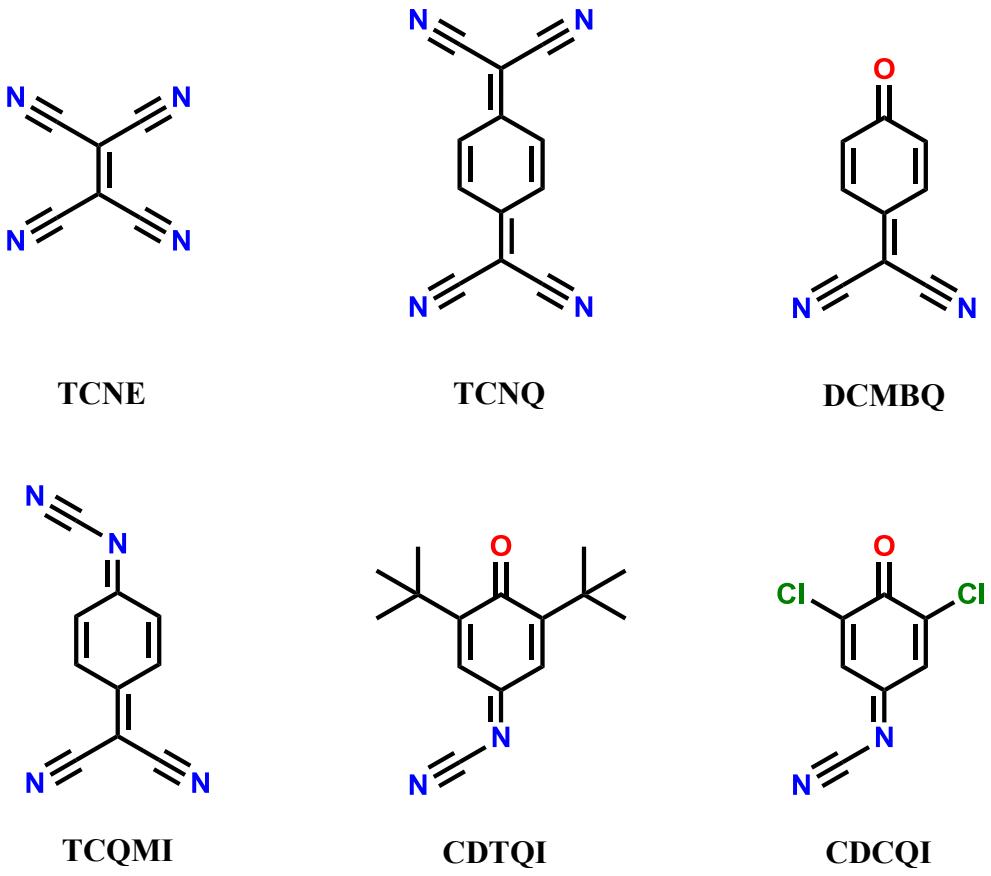

Figure 3.1. Cyanoacceptors TCNE, TCNQ, DCMBQ, TCQMI, CDTQI, and CDCQI.

eight nitriles, but only six can be accommodated. This is a possible source of disorder. *N*,7,7-Tricyanoquinomethanimine (TCQMI), previously synthesized,[8,9] was reinvestigated as a possible building block in molecule-based materials as the three nitrile groups would allow for more complete agreement of nitrile groups with metal sites possessing an octahedral coordination geometry.

Our findings for this compound have also served to expand our interest into a more general exploration of novel organic molecules. Specifically, we sought to examine asymmetric cyanocarbon acceptors, an area of research which has received very limited attention to date. Herein is reported the synthesis, structure, and characterization of cyanocarbon acceptors TCQMI, *p*-(dicyanomethylene)benzoquinone (DCMBQ), *N*-cyano-2,6-di-*tert*-butylquinonimine (CDTQI), and *N*-cyano-2,6-dichloroquinonimine (CDCQI) (Figure 3.1).

Experimental

Chemicals were procured from multiple sources. Cyclohexane-1,4-dione (Alfa Aesar), *p*-toluenesulfonic acid (Lancaster Chemical), 1,4-butanediol (Sigma), acetic acid (EMD), malononitrile (Arcos), 2,6-dichloro-*p*-benzoquinone (Sapon Laboratories), 2,6-di-*tert*-butylphenol (Aldrich), 30% hydrogen peroxide(aq) (Mallinckrödt), and bis(trimethylsilyl)carbodiimide (Petrarch Systems, Inc.) were used without further purification. Titanium(IV) tetrachloride ($TiCl_4$) (Janssen Chimica) was distilled under vacuum, and stored under a dry N_2 atmosphere. Manganese(IV) dioxide (MnO_2) was prepared freshly before use according to the methods of Attenburrow et al.,[10] with the substitution of $MnCl_2 \cdot 4H_2O$ for $MnSO_4 \cdot 4H_2O$.

***p*-(Dicyanomethylene)benzoquinone (DCMBQ).** DCMBQ was synthesized

following a modification of a route described by Hyatt and coworkers (Scheme 3.1).[11] Modifications included isolation of the monoketal from unreacted starting material by serial extraction with a 1:4 solution of acetonitrile:hexanes. The starting material dissolved easily into the acetonitrile (MeCN) layer, while the targeted oil remained in the hexane layer. Additional modifications to the preparation included repeating the deprotection of the monoketal intermediate to increase the purity of the resulting ketone. Also, the MnO_2 used in the reduction of an intermediate to DCMBQ was always prepared fresh and used after drying in an oven as done by Attenburrow et al.[10] Despite these precautions, the yield was always much lower than reported in literature.[11]

First, 10.04 g (89.3 mmol) of 1,4-cyclohexanedione was dissolved in 100 mL of toluene and 71 mg (0.41 mmol) of *p*-toluenesulfonic acid was added (Scheme 3.1). The resulting yellow solution was then heated to reflux and 8.10 g (89.9 mmol) of 1,4-butanediol was added dropwise over 4.5 hr using an automated syringe pump. After addition was complete, the reaction was refluxed for an additional 0.5 hr and then cooled to room-temperature. Once cooled, volume was reduced to 1/3 of original. The resulting yellow solution was triturated with ethyl acetate (EtOAc) and cooled in a freezer.

Bisketal side product crystallized as large white crystals, which were then filtered off and the solvent was removed under vacuum. The oily residue was separated between hexane and MeCN to remove starting material. The solvent from the hexane layer was then removed under vacuum, resulting in a colorless oil of the monoketal (**1**). [Yield: 8.1 g (49%)] IR (KBr; cm^{-1}); $\nu_{C\text{-}H}$ 2943, 2882, 2845 cm^{-1}, $\nu_{C=O}$ 1718 cm^{-1}, $\nu_{C\text{-}O}$ 1262, 1133, 1060 cm^{-1}. NMR($CDCl_3$) δ 7.69 (dd, 1H), 7.63 (dd, 1H), 7.40 (dd, 1H), 7.19 (dd, 1H).

Next, 2.10 g (11.4 mmol) of the monoketal oil (**1**) was mixed in 22 mL of ethanol (EtOH) (Scheme 3.1). To the clear, colorless solution, 0.10 mL of piperidine and 0.04 mL

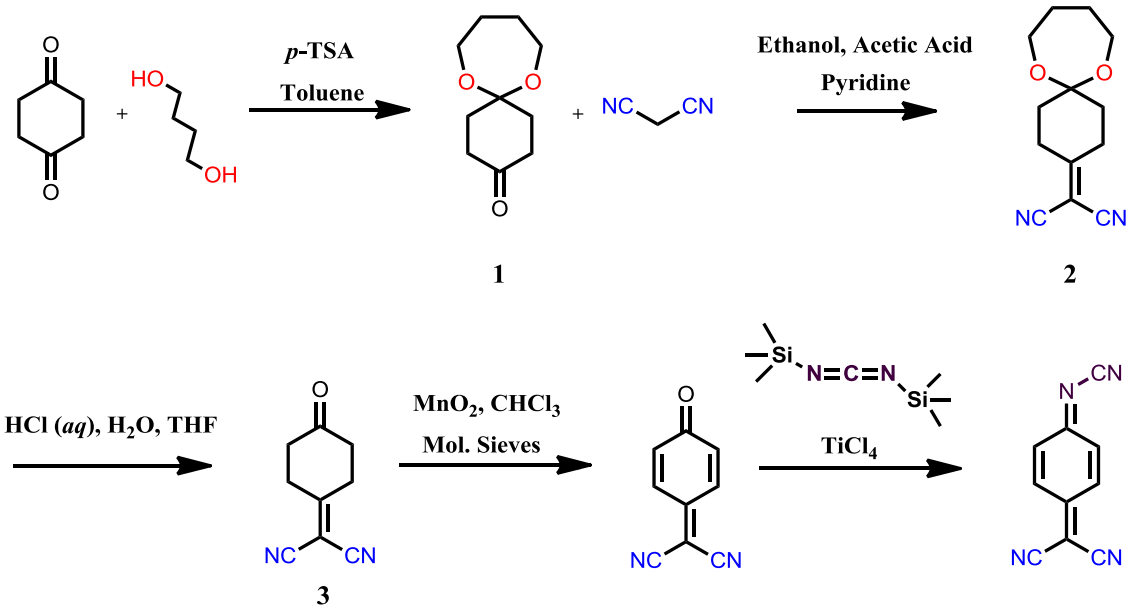

Scheme 3.1. Synthesis of DCMBQ and TCQMI.

of acetic acid were added, resulting in a slight color change to pink. Then, 0.83 g (12.6 mmol) of malononitrile was dissolved in the solution, changing the color to dark purple/maroon.

The reaction was allowed to sit at room-temperature for 3 hr. The resulting red/brown crystals were collected by filtration and washed until colorless. The colorless crystals were then dissolved, with stirring, in boiling EtOH and allowed to cool in a freezer as the white cyanomethide monoketal (**2**) recrystallized. The crystals were then collected by filtration, washed with cold EtOH, and dried under vacuum. [Yield: 2.1 g (79%)] IR (KBr; cm^{-1}); $\nu_{C\text{-}H}$ 2967, 2949, 2935 cm^{-1}, $\nu_{C=N}$ 2233 cm^{-1}, $\nu_{C=N}$ 1598 cm^{-1}, $\nu_{C\text{-}O}$ 1124, 1096 cm^{-1}. NMR($CDCl_3$) δ 7.69 (dd, 1H), 7.63 (dd, 1H), 7.40 (dd, 1H), 7.19 (dd, 1H).

The dicyanomethide (**2**) was deprotected by dissolving 980 mg (4.22 mmol) of the white crystals in 12 mL of tetrahydrofuran (THF) (Scheme 3.1). The resulting light tan solution was then heated to reflux. While at reflux, 1.25 mL of 10% hydrochloric acid (HCl) (aq) was added and the solution was stirred at reflux for 2 hr. After 2 hr, the solution was cooled and separated between EtOAc and H_2O. The organic layer was then dried with magnesium(II) sulfate ($MgSO_4$) and the solvent removed under reduced atmosphere. The procedure was repeated if thin-layer chromatography (TLC) indicated starting material. The pale-yellow oil solidified upon standing to form **3**. [Yield: 669 mg (99.0%)] IR (KBr; cm^{-1}); $\nu_{C\text{-}H}$ 2966, 2949, 2922 cm^{-1}, ν_{CN} 2233 cm^{-1}, $\nu_{C=O}$ 1723 cm^{-1}, $\nu_{C=N}$ 1598 cm^{-1}. NMR($CDCl_3$) δ 7.69 (dd, 1H), 7.63 (dd, 1H), 7.40 (dd, 1H), 7.19 (dd, 1H).

Reduction to the quinone-like structure was achieved by dissolving 840 mg (5.25 mmol) of 4-(dicyanomethy1ene)cyclohexanone (**3)** in 54 mL of chloroform ($CHCl_3$). To the solution was added 10.75 g of MnO_2 and 8.93 g of activated molecular sieves (3 Å)

(Scheme 3.1). The solution was then stirred under nitrogen, at reflux, for 40 min. The reaction was removed from heat and allowed to cool for ~10 min. It was then filtered through celite while still hot. The celite was then washed with hot $CHCl_3$ until colorless. The red filtrate and combined washings were taken to dryness under vacuum, resulting in crude red crystals, which were then recrystallized from EtOH to yield fine, red needles of DCMBQ. [Yield: 110 mg (9.2%)] IR (KBr; cm^{-1}); $\nu_{C\text{-}H}$ 3062 cm^{-1}, ν_{CN} 2229 cm^{-1}, $\nu_{C=O}$ 1638 cm^{-1}, $\nu_{C=N}$ 11619 cm^{-1}, $\nu_{C=C}$ 1570 cm^{-1}. NMR($CDCl_3$) δ 7.69 (dd, 1H), 7.63 (dd, 1H), 7.40 (dd, 1H), 7.19 (dd, 1H).

N,7,7-Tricyanoquinomethanimine (TCQMI) (5). Synthesis of TCQMI (**5**) (Scheme 3.1) was achieved through using a preparation from Itoh and coworkers.[9] While the established procedure advocated the use of column chromatography for purification, recrystallization from a 1:1 benzene/hexanes solution afforded red-orange crystals suitable for single crystal X-ray diffraction (XRD).

TCQMI was formed by dissolving 100 mg (0.624 mmol) of DCMBQ in 5.57 mL of CH_2Cl_2, forming a red solution, which was then cooled in an ice bath. Next, 552 mg (2.91 mmol) of freshly distilled $TiCl_4$ was added dropwise, resulting in the formation of an orange precipitate. The solution was stirred in the ice bath for 0.5 hr, then 0.36 mL (1.59 mmol) of bis(trimethylsilyl)carbodiimide was added dropwise. Gray vapor evolved during addition of the carbodiimide; and the solution thickened and became reddish in color. The mixture was then removed from the ice bath and stirred at room-temperature, under N_2, for 2 days. After 2 days, additional CH_2Cl_2 was added to dissolve the orange/brown precipitate.

Next, distilled H_2O was added, forming an orange organic layer and a milky aqueous layer. The organic layer was isolated, dried with $MgSO_4$, and the solvent was

removed under vacuum. The resulting orange solid was then recrystallized from a 1:1 solution of benzene:hexanes to yield bright orange crystals of TCQMI that faded to orange plates when dried. [Yield: 81.9 mg (71.0%)] IR (KBr; cm^{-1}); ν_{C-H} 3054 cm^{-1}, $\nu_{C\equiv N}$ 2230, 2169 cm^{-1}, $\nu_{C=N}$ 1548 cm^{-1}, $\nu_{C=C}$ 1475 cm^{-1}. NMR($CDCl_3$) δ 7.69 (dd, 1H), 7.63 (dd, 1H), 7.40 (dd, 1H), 7.19 (dd, 1H).

***N*-cyano-2,6-di-*tert*-butylquinonimine (CDTQI).** CDTQI was synthesized from 2,6-di-*tert*-butyl-*p*-benzoquinone (Scheme 3.2). The quinone was synthesized from a preparation published by Minisci and coworkers.[12] A solution of 5.0 mL of 30% H_2O_2, 1.5 mL of H_2SO_4, and 70 mL of MeOH was made. Next, 4.92 g of 2,6-di-*tert*-butylphenol was added and stirred until it was solvated. The solution was placed under an inert N_2 atmosphere and 0.70 mL of Br_2 was added. The solution was heated to reflux, with stirring, for 0.5 hr. The reaction was then cooled to room temperature, during which time bright yellow crystals precipitated. The crystals were collected, recrystallized from MeOH, and dried under vacuum.

CDTQI was formed by first dissolving 351 mg (1.59 mmol) of 2,6-di-*tert*-butyl-*p*-benzoquinone in 20 mL of dry CH_2Cl_2, forming a yellow solution. The solution was then cooled in an ice bath and 483 mg (2.55 mmol) of $TiCl_4$ was added dropwise, forming a red precipitate. The red slurry was mixed for 0.5 hr and then 246 mg (1.32 mol) of bis(trimethylsilyl)carbodiimide was added, evolving gray vapor and forming a dark brown solution with brown/orange precipitate. The mixture was allowed to mix at room temperature for 3 days.

After 3 days, the brown solution was poured into distilled H_2O, forming a bright orange organic layer and a yellow-tinted aqueous layer. The organic layer was collected and dried with anhydrous $MgSO_4$. The solvent was then removed under reduced pressure,

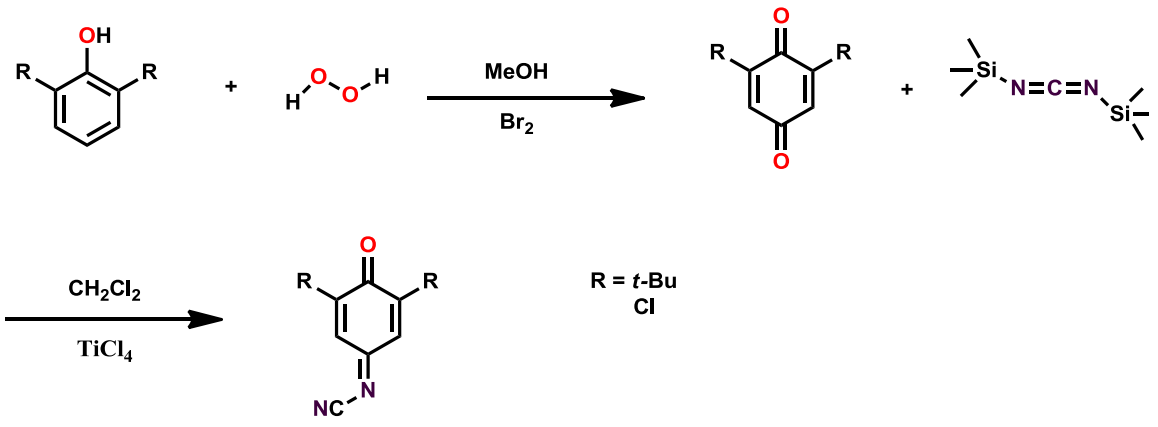

Scheme 3.2. Synthesis of CDTQI and CDCQI.

resulting in an orange solid. The solid was recrystallized from EtOH, yielding red/orange crystals suitable for PXRD. [Yield: 91.4 mg (23.5%)] IR (KBr; cm^{-1}); $\nu_{C\equiv N}$ 2177 cm^{-1}, $\nu_{C=O}$ 1656 cm^{-1}, $\nu_{C=N}$ 1636 cm^{-1}, $\nu_{C=C}$ 1691, 1537 cm^{-1}.NMR($CDCl_3$) δ 7.20 (dd, 1H), 6.88 (dd, 1H), 1.30 (m, 18 H).

***N*-cyano-2,6-dichloroquinonimine (CDCQI).** CDCQI was synthesized (Scheme 3.2) by dissolving 300 mg (1.70 mmol) of 2,6-dichlorobenzoquinone in 10 mL of CH_2Cl_2, forming a yellow solution. The solution was then cooled in a freezer and 863 mg (4.09 mmol) of cold $TiCl_4$ was added dropwise, turning the solution orange and forming a yellow/orange precipitate. The reaction was then allowed to stir at room-temperature for 0.5 hr. After 0.5 hr, 328 mg (1.76 mmol) of bis(trimethylsilyl)carbodiimide was added dropwise, changing the solution and precipitate to red. The slurry was then stirred at room temperature for 3 days, during which time the solution turned dark red/brown.

After 3 days, the solution was poured into H_2O and more CH_2Cl_2 was added, resulting in a milky aqueous layer and an orange organic layer. The organic layer was separated, dried with $MgSO_4$ and the volume reduced to yield an orange oil. The oil was dissolved in benzene and an equal volume of heptane was added. The solution was then cooled in the freezer, resulting in dark yellow crystals suitable for PXRD. [yield: 220 mg (64.4%)] IR (KBr; cm^{-1}); IR (KBr; cm^{-1}); $\nu_{C\equiv N}$ 2175 cm^{-1}, $\nu_{C=O}$ 1686 cm^{-1}, $\nu_{C=N}$ 1623 cm^{-1} $\nu_{C=C}$ 1576, 1535 cm^{-1}. NMR($CDCl_3$) δ 7.72 (dd, 1H), 7.44 (dd, 1H).

Physical methods. IR spectra were taken using a Bruker Tensor 37 spectrometer from KBr pellets (±1 cm^{-1}). NMR (^1H and ^{13}C) were conducted on a Varian Unity 300 Spectrometer equipped with a Nalorac Quad-probe ($^1H/^{19}F$, $^{13}C/^{31}P$) direct probe. UV-Vis studies were conducted using quartz cuvettes on a Hitachi u-4100 Spectrometer.

Reduction potentials were measured on a Bioanalytical Systems, Inc. Epsilon EC using a $Ag/AgNO_3$ electrode with $[NBu_4][PF_6]$ as the supporting electrolyte and ferrocene ($FeCp_2$) as the reference. Reduction potentials were corrected to reflect the voltage (V) vs. SCE. Thermogravimetric analysis (TGA) was conducted on a TA Instruments Q500 located in a Vacuum Atmospheres DriLab under inert atmosphere (N_2) to avoid O_2/H_2O degradation of the samples. Samples were loaded in an aluminum pan, heated for 10 min at 20°C before ramping from 20 - 600°C at 5.00°C/min under a continuous N_2 purge of 10 mL/min.

X-ray structure determination. The single crystal structure of TCQMI was determined by Dr. Arnold Rheingold on a Nonius KappaCCD diffractometer equipped with Mo Kα radiation. All the reflections were merged and only those for which $I_o > 2\sigma(I)$ were included in the refinement, where $\sigma(F_o)^2$ is the standard deviation based on counting statistics. The data for TCQMI were integrated using the Bruker SAINT software program.[13] The structure was solved by a combination of direct methods and heavy atom methods. Patterson methods and the refinement by full-matrix least-squares methods using SHELXL-97 were used for the structures of TCQMI. All the non-hydrogen atoms were refined with anisotropic displacement coefficients. Hydrogen atoms were assigned isotropic displacements $U(H) = 1.2U(C)$, and their coordinates were allowed to ride on their respective carbons using SHELXL97.[14]

The high-resolution powder X-ray diffraction (PXRD) measurements of DCMBQ, CDTQI, and CDCQI were collected on the X16C beamline at the National Synchrotron Light Source, Brookhaven National Laboratory by Dr. Peter Stephens and Saul Lapidus. A Si(111) channel-cut monochromator selected a parallel 0.69998-Å incident beam. The diffracted X-rays were analyzed by a Ge(111) crystal and detected

using a NaI scintillation counter. The wavelength and diffractometer zero position were calibrated by measuring a sample of NIST standard reference material 1976 (sintered plate of Al_2O_3). All measurements were done at room-temperature and the capillaries were rotated during data collection for better averaging of powder pattern.[15] Simulated annealing was used to determine the structure of DCMBQ, CDTQI, and CDCQI.[16] After obtaining an acceptable agreement between observed and calculated patterns, Rietveld refinements were performed in order to improve the structure. Hydrogens were placed in idealized positions. Bonds of similar nature (e.g., nominally single C-C bonds in the ring, separate from nominally double bonds) were restrained to be equal and individually refined.

Results and Discussion

The goal of this research, to form a tridentate cyanocarbon, was inspired by the formation of the room-temperature magnet, $V(TCNE)_2$. The compound's high T_c, > 400 K, makes the magnet of great theoretical and practical interest. Though a crystal structure has been elusive, the stoichiometry and elemental analysis data suggest that each vanadium(II) ion is coordinated to six nitrile groups, though the formula indicates two TCNE molecules per metal site, leaving one of the four nitrile groups, per TCNE molecule, uncoordinated. TCQMI was sought as a known compound which possessed a redox potential comparable to both TCNE and TCNQ.

A general inquest into the properties of asymmetrical cyanoacceptors was also desired as relatively little research has been conducted in this area. Additionally, research into the chemistry of cyanimines as ligands capable of promoting magnetic ordering and their correlation to TCQMI expanded this to a general inquest into the synthesis and

properties of asymmetrical, cyanimine bearing compounds with a quinone structure.

Spectroscopic studies. The IR, NMR, and UV-Vis spectra of the compounds were studied to better characterize them and quantitate their potential in forming stable anionic radicals. Additionally, the compounds were examined in an attempt to detect patterns that would indicate guidelines in the future synthesis of cyanocarbon acceptors. Important spectroscopic values are summarized in Table 3.1.

The spectra of DCMBQ showed one sharp ν_{CN} peak at 2230 cm^{-1}, well in accord with other vinyl nitrile stretches such as TCNQ (~2222 cm^{-1}).[1b] Another sharp peak was seen at 1638 cm^{-1}, representing the carbon-oxygen stretch of the ketone. While occurring at lower wavenumbers than prototypical ketone stretches, this value was in keeping with the stretches previously observed by Hyatt (1633cm^{-1}).[11] The shift to lower wavenumbers was attributed to conjugation of the stretch to the quinone π-system containing the electron-withdrawing dicyanomethylene group. Data, including an imine stretch at 1619 cm^{-1}, also conformed to previous values.[11] NMR studies showed a pair of doublets at δ 6.67 and δ 7.66, consistent with the expected spectrum resulting from two sets of distinct protons. The UV-VIS spectrum of the compound (35.9 μM) exhibited an intense, sharp peak at 31500 cm^{-1} and a small shoulder at 43600 cm^{-1} (Figure 3.2).

TCQMI exhibited two sharp ν_{CN} at 2230 and 2169 cm^{-1}. The peak at higher energy compared well with TCNQ while the lower energy band was attributed to a C-N triple bond stretch of the imine nitrile group and conformed to ν_{CN} stretches found in the *N,N'*-dicyano-*p*-quinone diimines (DCNQI).[17] The compound was marked by a disappearance of the C=O stretch at 1633 cm^{-1}. There was a C=N stretch in the 1600-1700 cm^{-1} region typical of imines, appearing at 1640 cm^{-1}. As with ketone stretches, the electron-withdrawing nitriles shifted the stretches to lower energy. A medium strength

Table 3.1. Selected spectroscopic data for DCMBQ, TCQMI, CDTQI, and CDCQI.

	IR Stretches	NMR Shifts	UV-Vis Peaks
DCMBQ	2230 cm^{-1} ($\nu_{C\equiv N}$) 1638 cm^{-1} ($\nu_{C=O}$) 1619 cm^{-1} ($\nu_{C=C}$)	δ 7.66 (2H) δ 6.67 (2H)	43600 cm^{-1} (sh) 31500 cm^{-1} (s)
TCQMI	2230, 2169 cm^{-1}($\nu_{C\equiv N}$) 1640 cm^{-1}($\nu_{C=O}$) 1548 cm^{-1}($\nu_{C=C}$)	δ 7.69 (dd, 1H) δ 7.63 (dd, 1H) δ 7.40 (dd, 1H) δ 7.19 (dd, 1H)	44600 cm^{-1} (w) 28700 cm^{-1} (sh) 27500 cm^{-1} (s) 25000 cm^{-1} (sh)
CDTQI	2177 cm^{-1} ($\nu_{C\equiv N}$) 1656 cm^{-1} ($\nu_{C=O}$) 1636 cm^{-1} ($\nu_{C=N}$) 1691 cm^{-1} ($\nu_{C=C}$)	δ 7.20 (dd, 1H) δ 6.88 (dd, 1H) δ 1.30 (m, 18H)	32900 cm^{-1} (s) 29000 cm^{-1} (sh)
CDCQI	2175 cm^{-1} ($\nu_{C\equiv N}$) 1686 cm^{-1} ($\nu_{C=O}$) 1652 cm^{-1} ($\nu_{C=N}$) 1576 cm^{-1} ($\nu_{C=C}$)	δ 7.72 (dd, 1H) δ 7.44 (dd, 1H)	32200 cm^{-1} (s) 30800 cm^{-1} (sh) 29000 cm^{-1} (sh)

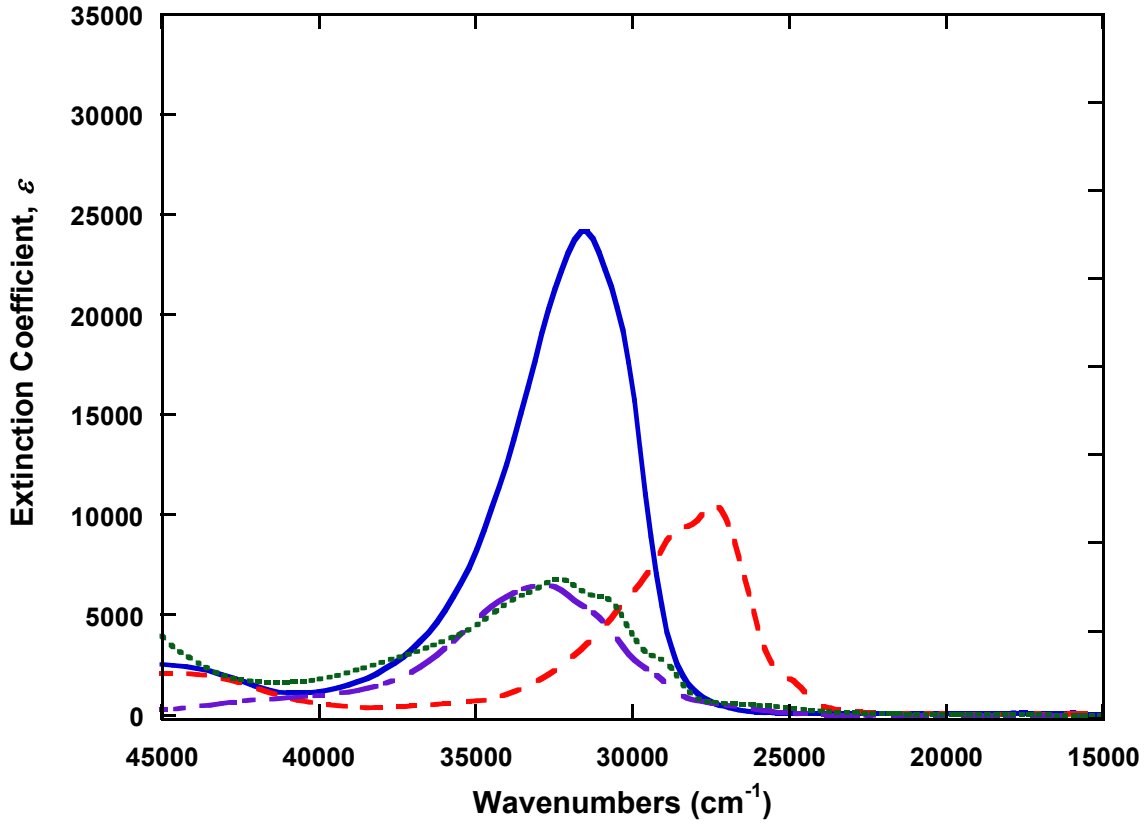

Figure 3.2. UV-Vis spectra of DCMBQ (—), TCQMI(- - - -), CDTQI (— - —), and CDCQI (••••).

band at 1548 cm^{-1} was noted, which was consistent with the spectrum reported by Itoh and coworkers,[9] and is more aptly attributed to the C=C stretch in the ring.

The ^{1}H-NMR spectra indicated shifts at δ 7.69 (dd, 1H), 7.63 (dd, 1H), 7.40 (dd, 1H), and 7.19 (dd, 1H). These findings contradicted previous works[8,9] which reported only three shifts at 7.68 (d, 2 H), 7.49 (1 H, d), and 7.16 (1 H, d).[9] The small differences in shifts are attributed to variation between instrumentation. The observation of two separate shifts at ~ δ 7.6 likely arises from increased resolution from a higher field instrument. The UV-Vis spectrum of TCQMI, taken in MeCN (44.4 μM), showed a sharp peak at 27500 with shoulders at 25000 and 28700 cm^{-1}. A small peak could be seen at 44600 cm^{-1}. The UV-Vis peaks were shifted to lower wavenumbers due to the effect of the three nitrile groups.

The IR spectrum of CDTQI showed a multitude of medium ν_{CH} stretches from 2850-3000 cm^{-1} expected from the *t*-Bu groups. A single, sharp peak in the ν_{CN} region 2177 cm^{-1} was indicative of a nitrile from a cyanimine group, which is generally lower in energy by ~60 cm^{-1} than vinyl nitrile stretches.[17,18] A ketone and an imine stretch were noted at 1656 and 1636 cm^{-1}, respectively, and indicated only one ketone had undergone imination by bis(trimethylsilyl)carbodiimide. Proton NMR showed shifts at δ 7.20 (dd, 1H), 6.88 (dd, 1H), and 1.30 (m, 18 H). This indicated a significant difference in the environment of the ring-bound protons. The UV-Vis spectrum of CDCQI (99.8 μM in MeCN) showed a strong, broad peak at 32900 cm^{-1} and a weak shoulder at 29000 cm^{-1}. The strongest UV-Vis stretch was found at nearly the same position as that observed for DCMBQ, indicating that the electron-withdrawing effects of bond dicyanomethide and cyanimine groups are responsible for the shifting of the main peak to lower wavenumbers.

CDCQI showed a ν_{CN} stretch at 2175 cm^{-1}, in close agreement with the stretches exhibited by the other monocyanoquinone imine. The compound also exhibited sharp peaks at 1686 and 1652 cm^{-1}, assigned to a ketone and imine, respectively. The imine stretch is at higher wavenumbers than seen in DCNQI compounds,[18] which is consistent with a system containing only one withdrawing *N*-cyanimine group. The NMR spectrum showed the expected pair of doublets at δ 7.72 and 7.44. As with CDTQI, the protons are seen to be readily differentiated, due to the asymmetrical geometry of the cyanimine group. They are also seen to be more deshielded, as anticipated from the inclusion of the electron-withdrawing chloride groups. The UV-Vis spectrum (39.8 μM) was very similar to that shown by CDTQI, indicating similar electronic states. The compound exhibited a strong peak at 32200 cm^{-1}, with weaker shoulders at 30800 and 29000 cm^{-1}.

Structure. Though DCMBQ and TCQMI were known compounds, previously synthesized, these are the first reports of their crystal structures. This work also contains the first reported structures of CDTQI and CDCQI. Compounds of this type have previously been reported as nonisolated, uncharacterized side-products in the synthesis of DCNQI by Aumüller and Hünig.[18] The structures of DCMBQ and the monocyanoquinone imines were solved by powder X-ray diffraction in the lab of Dr. Peter Stephens in Stony Brook University.

The structure of TCQMI was solved by single crystal diffraction in the lab of Dr. Arnold Rheingold at the University of California, San Diego. Important crystallographic parameters are tabulated in Table 3.2. Select bond lengths of the compounds are detailed in Table 3.3. Comparison of the bond lengths indicate the general effects of electron-donating and -withdrawing groups as the former led to longer bonds in the quinone-ring and the latter favors shorter bond lengths.

Table 3.2. Important crystallographic parameters of cyanocarbon acceptors.

	DCMBQ	TCQMI•½ Benzene	CDTQI	CDCQI
mol formula	$C_9H_4N_2O$	$C_{13}H_7N_4$	$C_{15}H_{20}N_2O_1$	$C_7H_2Cl_2N_2O$
mol wt, daltons	156.14	219.23	244.33	201.01
crystal system	monoclinic	monoclinic	monoclinic	monoclinic
space group	$P2_1/n$	$P2_1/n$	$P2_1/n$	$P2_1/c$
Z	4	4	4	4
temp, K	300	150(2)	300	300
a, Å	13.3407(4)	12.2600(17)	6.44511(19)	6.54496(7)
b, Å	7.39973(22)	6.2948(9)	12.3416(37)	10.52548(37)
c, Å	7.84798(23)	14.290(2)	18.44876(55)	12.17402(37)
α, deg	90	90	90	90
β, deg	92.6556(28)	100.726(2)	94.2811(28)	106.1777(32)
γ, deg	90	90	90	90
V, Å^3	773.899(39)	1083.6(3)	1463.24(8)	805.4454(38)
calcd density, g/cm^3	1.3401	1.344	1.1091	1.6576
R_p, %	6.676	5.07	5.849	6.002
R_{wp}, %[a,b]	8.958	9.05	7.852	8.151
GOF (R_{wp}/R_{exp})[b,c]	2.307	1.069	2.323	3.390

[a] $$R_{wp} = \sqrt{\frac{\sum_i w_i (y_i^{calc} - y_i^{obs})^2}{\sum_i w_i (y_i^{obs})^2}}$$

[b] y_i^{calc} and y_i^{obs} are the calculated and observed intensities at the i^{th} point in the profile, normalized to monitor intensity. The weight w_i is $1/\sigma^2$ from the counting statistics, with the same normalization factor. N is the number of points in the measured profile minus number of parameters.

[c] $$R_{exp} = \sqrt{\frac{N}{\sum_i w_i (y_i^{obs})^2}}$$

Table 3.3. Select bond lengths of DCMBQ, TCQMI, Me_3TCQMI,[8a] Me_4TCQMI,[8a] CDTQI, and CDCQI.

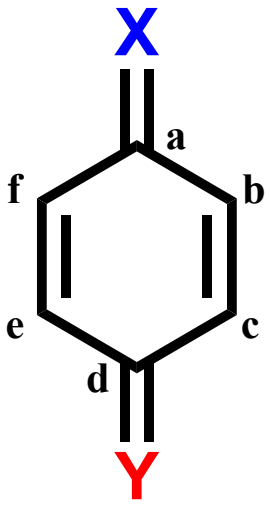

X = O, N-C≡N

Y = O, C-(C≡N)$_2$

	DCMBQ	**TCQMI**	**Me_3TCQMI[8a]**	**Me_4TCQMI[8a]**	**CDTQI**	**CDCQI**
X	O	N-C≡N	N-C≡N	N-C≡N	N-C≡N	N-C≡N
Y	C-(C≡N)$_2$	C-(C≡N)$_2$	C-(C≡N)$_2$	C-(C≡N)$_2$	O	O
C_a-C_b	1.472(4)	1.452(2)	1.466(4)	1.47(1)	1.431(5)	1.4684(9)
C_b-C_c	1.304(6)	1.345(2)	1.360(7)	1.354(4)	1.366(7)	1.352(13)
C_c-C_d	1.473(5)	1.451(2)	1.457(6)	1.48(1)	1.431(5)	1.468(22)
C_d-C_e	1.473(5)	1.450(2)	1.451(4)	1.47(2)	1.431(4)	1.4684(9)
C_e-C_f	1.305(8)	1.343(2)	1.338(7)	1.351(4)	1.367(7)	1.352(13)
C_f-C_a	1.472(5)	1.453(3)	1.462(6)	1.463(3)	1.431(6)	1.4684(9)
C=C	1.383(8)	1.372(2)	1.373(8)	1.360(3)	-	-
C=O	1.205(5)	-	-	-	1.230(7)	1.266(11)
C-N	-	1.345(2)	1.326(4)	1.331(4)	1.37(1)	1.328(19)
C=N	-	1.312(2)	1.304(8)	1.299(4)	1.269(8)	1.327(13)
C≡N	1.142(6)	1.156(2)	1.151(5)	1.151(4)	1.11(1)	1.150(16)

The structure of DCMBQ (Figure 3.3) showed similarities to related cyanocarbon acceptors TCNQ[19] and DCNQI.[20] The six-membered-ring possessed an alternating single bond/double bond motif with lengths of 1.472(4) and 1.305(8) Å, respectively. While the length of the single bond is in good agreement with those of *p*-benzoquinone (1.481(2) Å), the C=C, was significantly shorter than the analogues bond in *p*-benzoquinone (1.344(3) Å).[21] The shorter length is attributed to the electron-withdrawing effects of the nitrile groups of the dicyanomethide functionality. This effect was also noted in the ketone bond length of DCMBQ (1.205(5) Å), as it was significantly shorter than the ketone bond lengths of *p*-benzoquinone (1.225(2) Å).[21]

The structure of TCQMI (Figure 3.4) was similar to DCMBQ, though the effects of the cyanimine functional group led to shorter C-C bonds and longer C=C. The structure is consistent with expectations; within ring C-C bonds lengths of 1.452 Å and C=C bond lengths of 1.344 Å observed. The C=N imine bond length is 1.313 Å, within limits of similar compounds.[20b] The compound is seen to be largely planar, as noted for trimethyl substituted TCQMI, Me_3TCQMI.[8] Interestingly, both the tetramethyl, Me_4TCQMI, and tetramethyl substituted TCNQ, Me_4TCNQ were deformed into a boat-like structure.[8]

The structure of CDTQI (Figure 3.5) was obtained through PXRD. The *t*-Bu groups were chosen to favor single cyanimination of the unobstructed ketone and were observed to be successful in that regard. Only a single cyanimine group was noted. Other important characteristics included the six-membered-ring, which exhibited a quinone-like structure, with single bonds measuring an average of 1.431 Å and the double bonds measuring an average of 1.367 Å. The compound corresponds closely to that of TCQMI, though the ring C=C bonds are slightly longer (0.021 Å , 1.4%) and the ring C-C bonds

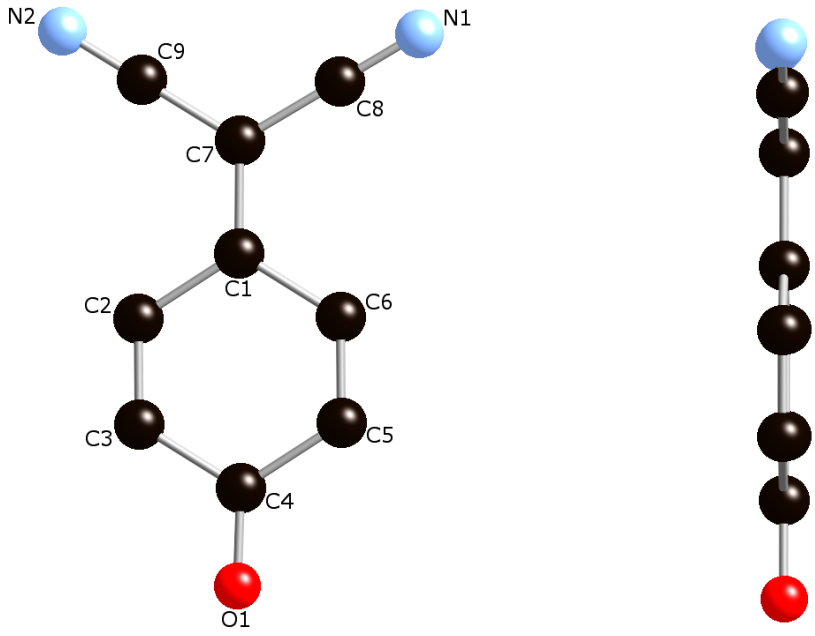

Figure 3.3. Crystal structure of DCMBQ with labeling (a), and side view (b).

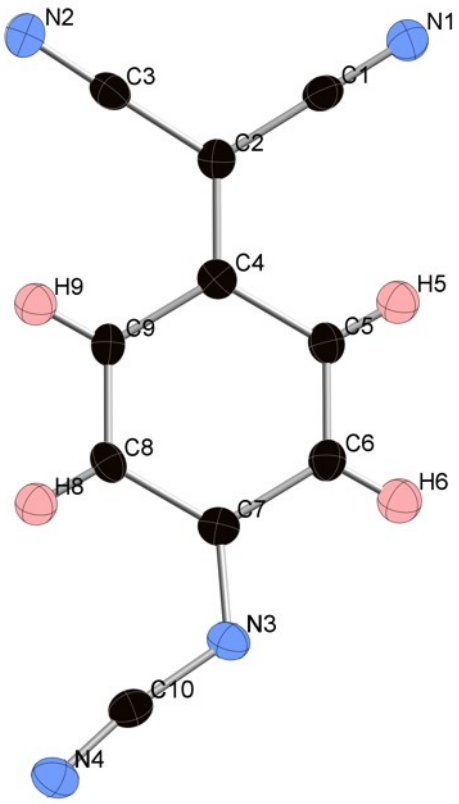

(a) **(b)**

Figure 3.4. Ortep diagram (50% electron density) of the structure of TCMQI with atom labels (a), and its side view (b), showing the slight deviation from planarity.

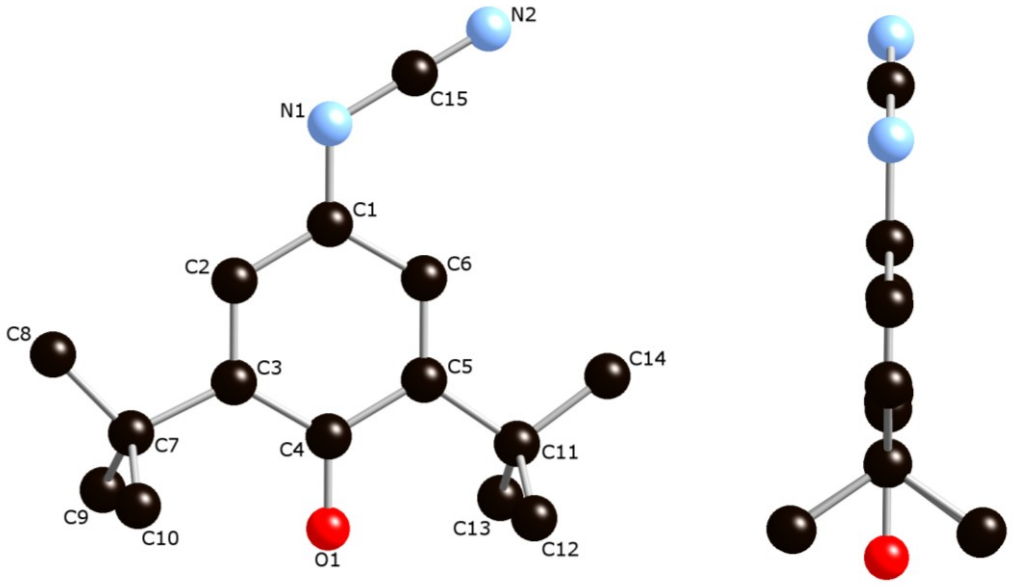

(a) **(b)**

Figure 3.5. Crystal structure of CDTQI with atom labeling (a), and side view (b).

are slightly shorter (0.021 Å, 1.5%), possibly due to the electron-donating and steric effects of the *t*-butyl groups. The C-N bond also showed effects of the electron-donating *t*-butyl groups as it was elongated to 1.37(1) Å, the longest in the series and 0.025 Å (1.9%) longer than that seen in TCQMI. In contrast, the nitrile bond was the shortest, measuring 1.11(1) Å, or 0.046 Å (4.0%) shorter than in TCQMI, also indicative of the effects of the bulky alkyl-groups. The C=O ketone bond measured 1.230(7) Å, in keeping with typical ketone bond lengths.

CDCQI's crystal structure (Figure 3.6) was also obtained by PXRD and compares to the previous compounds very well. It is important to note that while monocyanimination of CDTQI was accomplished through the bulky *t*-Bu groups, the chlorine atoms are expected to have accomplished the same result through electronic effects, as their bulk is not significantly greater than that of hydrogen atoms.

As with CDTQI, CDCQI's six-membered-ring shows the expected quinone structure with alternating single and double bonds, averaging 1.468 and 1.352 Å, respectively. The double bonds were somewhat shorter (0.014 Å, 1.0%) than the double bonds of the analogous CDTQI and TCQMI. This effect was attributed to electron-withdrawing chlorine atoms. The C=O and C=N bond distances were recorded as 1.266(11) Å and 1.327(13) Å, respectively. Interestingly, the C-N bond measured 1.328(19), very similar to the C=N bond. This was in contrast to the structure seen in CDTQI, indicating that the hybridization between the C-N and C=N bonds are not observed in all cyanimine quinones.

Electrochemical studies. The reduction potentials of DCMBQ, TCQMI, CDTQI, and CDCQI were studied by cyclic voltammetry (Figure 3.7). The results are tabulated in Table 3.4 and reported alongside reduction potentials of common cyanocarbon

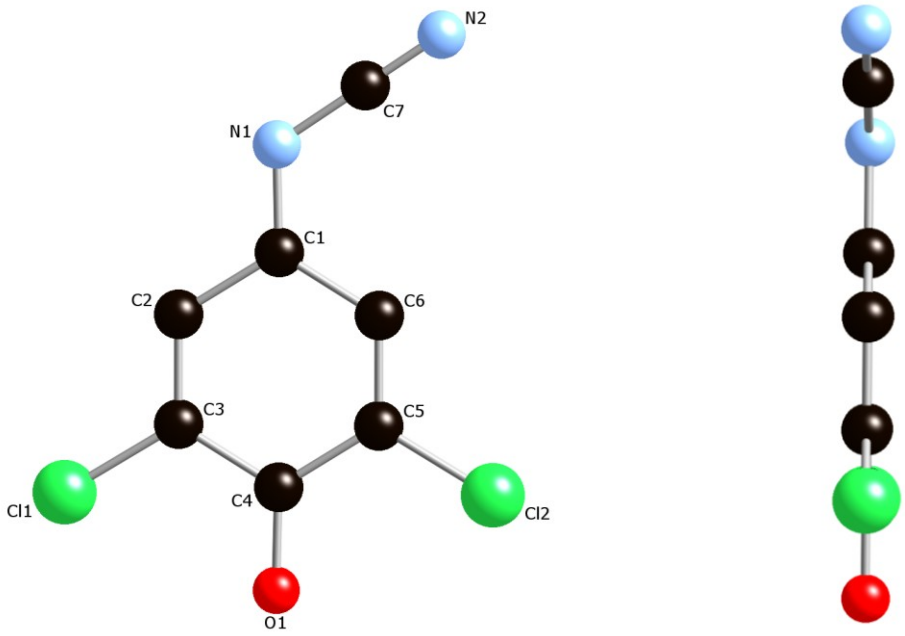

(a) **(b)**

Figure 3.6. Crystal structure of CDTQI with atom labeling (a), and side view (b).

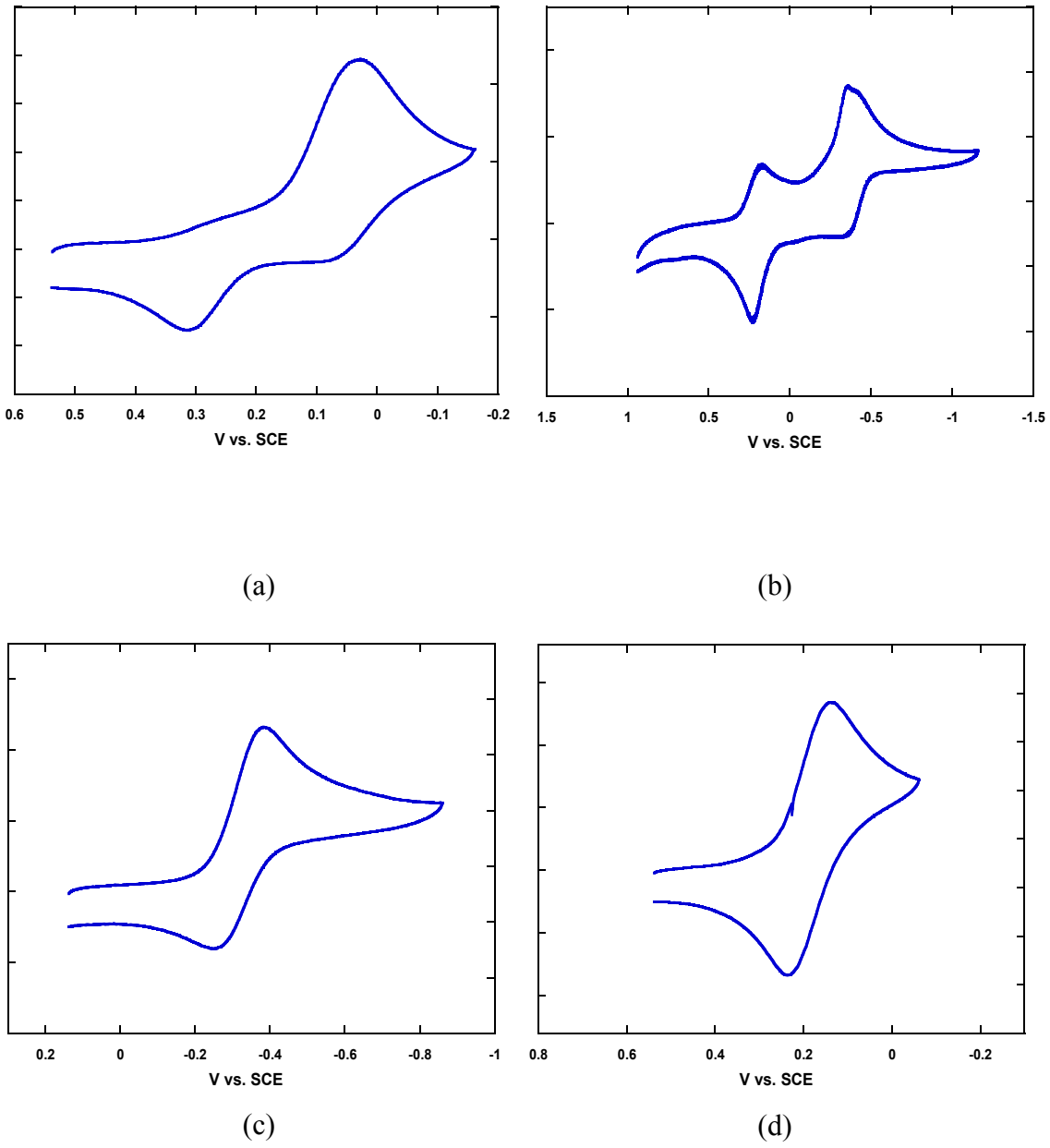

Figure 3.7. Cyclic voltamogram of DCMQB (a), TCQMI (b), CDTQI (c), and CDCQI (d) in MeCN with $[Bu_4N][PF_6]$ (0.1 M) as the supporting electrolyte; scan rate = 100 mV/s using a $Ag/AgNO_3$ electrode.

Table 3.4. Reduction potentials of selected cyanocarbon acceptors.[a]

Compound	1st Reduction Potential	2nd Reduction Potential
TCNE[23]	0.24	-0.77
TCNQ[23]	0.22	-0.37
2,5-DMeDCNQI[23]	0.05	-
DCMBQ	0.054*	-
TCQMI	0.20	-0.47
CDTQI	-0.32	-
CDCQI	0.19	-0.32*

[a] In acetonitrile/0.1 M $[Et_4N][BF_4]$; potentials in V vs. SCE. Scan rate 100 mV/s.* Quasi-reversible reduction potentials.

acceptors.

DCMBQ exhibits one reversible and one quasi-reversible one-electron reduction. The potentials are not in agreement with those reported by Itoh and coworkers, but are within reason given the structure and electron-withdrawing groups on the quinone base.[9] The reversible reduction potential is observed at 0.054 V vs. SCE and the quasi-reversible reduction potential occurs at 0.297 V vs. SCE. Itoh and coworkers[9] reported reduction potentials at -0.07 V and -0.52 V. However, the cyclic voltammogram of this study was not provided, making comparison between the two compounds difficult. The irreversible potential may result from dimerization of DCMBQ at the dicyanomethide carbon as this has been observed in similar compounds.[22]

The electrochemistry of TCQMI indicated the compound exhibited two reversible, one-electron reductions with potentials at 0.21 and -0.43 V vs. SCE. These values are in good agreement with previous literature values.[8,9] The position and number of reduction potentials highlighted the similarity of compound to both TCNE and TCNQ.[23] It also indicates TCQMI is an appropriate candidate for use as a building block in magnetic systems.

The cyclic voltamagram of CDTQI (Figure 3.7) shows a reversible, one-electron reduction at -0.32 V vs. SCE. This potential is much more negative than the values seen for substituents of TCNQ,[24] TCQMI,[8] and DCNQI[25] compounds. The value is more negative than would be expected from *tert*-butyl groups, though there are few examples of *tert*-butyl groups as substituents on cyanocarbon acceptors.

CDCQI was shown to possess two reduction potentials. The first is a fully reversible, one-electron reduction observed at 0.19 V vs. SCE. The second reduction occurs at -0.32 V vs. SCE and is quasi-reversible. The first reduction potential is slightly

lower than the value observed in TCQMI, TCNE, and TCNQ; but near enough to indicate this compound would serve as a useful cyanocarbon accepter when paired with suitable electron donors.

.

Conclusions

The goal of this research project was met. The target compound, TCQMI, was successfully synthesized and the first reported crystal structure of this compound was isolated. Additionally, the precursor to TCQMI, DCMBQ, was successfully isolated and the structure was solved. Also, the general inquest into formation of asymmetric cyanocarbons was successful. Two novel cyanocarbons, CDTQI and CDCQI, were synthesized and their structural and electrochemical characteristics were investigated.

Of the four compounds studied, TCQMI and CDCQI show the greatest potential for inclusion in molecule-based systems. These compounds exhibit nitrile groups for coordination to metal sites as well as reversible reduction potentials (TCQMI: 0.20 V; CDCQI: 0.19 V) that indicate they form stable radicals. The other two compounds do not form radicals until greater negative voltage is applied, indicating a stronger oxidizing agent may be required.

References

(1) (a) Miller, J. S.; Calabrese, J. C.; Harlow, R. L.; Dixon, D. A.; Zhang, J. H.; Reiff, W. M.; Chittipeddi, S.; Mark, C.; Selover, A.; Epstein, A. J. *J. Am. Chem. Soc.***1990**, *112,* 5496. (b) Vickers, E. B.; Selby, T. D.; Thorum, M. S.; Taliaferro, M .L.; Miller, J. S. *Inorg. Chem.* **2004**, *43*, 6414.

(2) (a) Miller, J. S. *Inorg. Chem.* **2000**, *39,* 4392. (b) Zhang, J.; Zhou, P.; Brinckerhoff, W. B.; Epstein, A. J.; Vazquez, C.; McLean, R. S.; Miller, J. S. *ACS Symp. Ser.* **1996**, *644*, 311. (c) Zhang, J.; Ensling, J.; Ksenofontov, V.; Gütlich, P.; Epstein, A. J.; Miller, J. S. *Angew. Chem., Int. Ed.* **1998**, *37*, 657.

(3) (a) Sugiura, K. -i.; Mikami, S.; Johnson, M. T.; Raebiger, J. W.; Miller, J. S.; Iwasaki, K.; Okada, Y.; Hino, S.; Sakata, Y. *J. Mater. Chem.* **2001**, *11*, 2152. (b) Werner, H. -P.; Von Schütz, J. U.; Wolf, H. C.; Kremer, R.; Gehrke, M.; Aumüller, A.; Erk, P.; Hünig, S. *Solid State Comm.* **1988**, *65*, 809.

(4) Tanaka, J.; Katayama, C.; Kumagai, H.; Saito, G.; Enoki, T.; Inokuchi, H. *Mol. Cryst. Liq. Cryst.* **1985**, *125*, 223.

(5) O'Hare, D.; Rai-Chaudhuri, A.; Murphy, V. *J. Chem. Soc., Dalton Trans.* **1993**, *20*, 3071.

(6) (a) Manriquez, J. M.; Yee, G. T.; McLean, R.; Epstein, A. J.; Miller, J. S. *Science* **1991**, *252*, 1415. (b) Zhou, P. Long, S. M.; Miller, J. S.; Epstein, A. J. *Phys. Lett. A* **1993**, *181*, 71. (c) Pokhodnya, K. I., Epstein, A. J.; Miller, J. S. *Adv. Mater.* **2000**, *12*, 410.

(7) Matsuura, H.; Miyake, K.; Fukuyama, H. *J. Phys. Soc. Jpn* **2010**, *79*, 034712.

(8) Bryce, M. R.; Davies, S. R.; Grainger, A. M.; Hellberg. J.; Hursthouse, M. B.; Mazid, M. Bachmann, R.; Gerson, F. *J. Org. Chem.* **1991**, *57*, 1690.

(9) Iwatsuki, S.; Itoh, T.; Itoh, H. *Chem. Lett.* **1988**, *17*, 1187.

(10) Attenburrow, J.; Cameron, A. F. B.; Chapman, J. H.; Evans, R. M.; Hems, B. A.; Jansen, A. B. A.; Walker, T. *J. Chem. Soc.* **1952**, 1094.

(11) Hyatt, J. A. *J. Org. Chem*. **1983**, *48*, 129.

(12) Minisci, F.; Attilio, C.; Vismara, E.; Fontana, F.; De Bernardinis, S. *J. Org. Chem.* **1989**, *54*, 728.

(13) (a) Saint Plus, v. 6.02; Bruker Analytical X-ray: Madison, WI 1999. (b) Sheldrick G. M. SADABS; University of Göttingen: Göttingen, Germany, 1996.

(14) (a) Goldberg, I.; Krupitsky, H.; Stein, Z.; Hsiou, Y.; Strouse, C. E. *Supramol. Chem* **1995**, *4*, 203. (b) Krupitsky, H.; Stein, Z.; Goldberg, I. *J. Inclusion Phenom. Mol. Recognit. Chem.* **1995**, *20*, 211. (c) Goldberg, I. *Mol. Cryst. Liq. Cryst*. **1996**, *278*, 767. (d) Byrn, M. P.; Curtis, C. J.; Hsiou, Y.; Kahn, S. I.; Sawin, P. A.;

Tendick, S. K.; Terzis, A.; Strouse, C. E. *J. Am. Chem. Soc*. **1993**, *115*, 9480. Byrn, M. P.; Curtis, C. J.; Hsiou, Y.; Khan, S. I.; Sawin, P. A.; Terzis, A.; Strouse, C. E. in *Comprehensive Supramolecular Chemistry*; Atwood, J. L., Davies, J. E. D., MacNicol, D. D., Vogtle, F., Eds.; 1996; Vol. 6, p 715.

(15) Coelho, A.A. *J. Appl. Cryst.* **2003**, *36*, 86.

(16) Coelho, A.A. TOPAS Academic, available at www.topas-academic.net.

(17) Lunardi, G.; Pecile, C. *J. Chem. Phys.***1991**, *95*, 6911.

(18) Aumüller, A. H.; Hünig, S. *Liebigs Ann. Chem.* **1986**, 142.

(19) Long, R. E.; Sparks, R. A.; Trueblood, K. N. *Acta Crystallog.* **1965**, *18*, 932.

(20) (a) Suigiura, K. Mikami, S. Johnson, M. T.; Raebiger, J. W.; Miller, J. S.; Iwasaki, K.; Okada, Y.; Hino, S.; Sakata, Y. *J. Mater. Chem.* **2001**, *11*, 2152. (b) Aumüller, A.; Erk, P.; Hünig, S.; von Schnering, H. G. Chem. Ber. 1991, 124, 2001.

(21) Pou-Amèrigo, R.; Merchàn, M. Ortì, E. *J. Chem. Phys.* **1999**, *110*, 9536.

(22) (a) Wang, G.; Slebodnick, C.; Yee, G. T. *Inorg. Chem.* **2007**, *46*, 9641. (b) Miller, J. S.; Pokhodnya, K. I. *J. Mater. Chem.* **2007**, *17*, 3585. (c) Jakowski, J. Simons, J. *J. Am. Chem. Soc.* **2003**, *125*, 16089. (d) Shimomura, S.; Horike, S.; Matsuda, R.; Kitagawa, S. *J. Am. Chem. Soc.* **2007**, *129*, 10990. (e) Ballester, L.; Gutiérrez, A.; Perpiñán, M. F.; Azcondo, M. T.; Sánchez, A. E. *Synth. Metals* **2001**, *120*, 965.

(23) Olbrich-Deussner, B.; Kaim, W.; Gross-Lannert, R. *Inorg. Chem.* **1989**, 3113.

(24) Zhang, J. Z.; Ellis, A. B. *J. Phys. Chem.* **1992**, *96*, 2700.

(25) Aumüller, A.; Hünig, S. *Liebigs. Ann. Chem.* **1986**, 165**.**

CHAPTER 4

N,7,7-TRICYANOQUINOMETHANIMINE-BASED MAGNETIC MATERIALS

Introduction

Molecule-based electronics have been of increasing interest since the discovery of organic-based materials, particularly with the discovery of [TTF][TCNQ] (TTF = tetrathiafulvalene; TCNQ = 7,7,8,8-tetracyano-*p*-quinodimethane), which forms segregated chains of alternating cationic TTF and anionic TCNQ.[1] The first magnetically ordered organic-based material was observed for $[FeCp^*_2]^{\bullet+}[TCNQ]^{\bullet-}$ (Cp* = pentamethylcyclopentadienide), which exhibited metamagnetic behavior.[2] Above a 1300 Oe applied critical field, H_c, it exhibited ferromagnetic-like behavior with a magnetic ordering temperature, T_c, of 2.5 K.[2a,3] The structure of $[FeCp^*_2]^{\bullet+}[TCNQ]^{\bullet-}$ consists of alternating chains of $[FeCp^*_2]^{\bullet+}$ cations and $[TCNQ]^{\bullet-}$ anions. This discovery led to the design and synthesis of $[FeCp^*_2]^{\bullet+}[TCNE]^{\bullet-}$ (TCNE = tetracyanoethylene), which is a bulk ferromagnet (T_c = 4.8 K), and extended the use of organic radical carriers in forming magnetically ordered materials.[4]

Many organic-based magnets possess cyanocarbon acceptors, including functionalized TCNQ derivatives,[5] TCNE,[6] *N,N'*-dicyanoquinone diimine (DCNQI) derivatives,[7] hexacyanobutadiene (HCBD),[8] and hexacyanotrimethylenecyclopropane

---

Reproduced in part with permission from Advanced Functional Materials, *in press*.

(HCTMCP).[9] Each of these acceptors (Figure 4.1) is readily reduced to a stable radical anion. In addition, the ability of the nitrile groups to coordinate to metal ions has enabled the formation of extended network structures. Lattices with extended 1-, 2-, and 3-D networks have been reported that display interesting and important magnetic behaviors.[4,10,11]

Several magnetic coordination compounds based on reduced TCNE and TCNQ have been structurally characterized. An octahedrally coordinated metal ion bonds to six nitriles in a 2:3 M:$[TCNE]^{\bullet-}$ ratio for the 171-K ferrimagnet $Mn^{II}[TCNE]_{3/2}(I_3)_{1/2}\bullet z$THF.[12] Several materials based on 2-D networks of octahedral metals equatorially bonded to μ_4-$[TCNE]^{\bullet-}$, with two axial bonds of magnetically inert moieties to the metal ion, have been described, with magnetic ordering temperatures in the range 68 to 171 K.[13] Materials of composition $M(TCNQ)_2$ (M = Mn, Fe, Co, Ni) have been described with ordering temperatures between 7 and 44 K, but they have not been structurally characterized.[14] Tetrahedrally coordinated Ag(TCNQ) and Cu(TCNQ) do not magnetically order; however, this is due to the lack of spin on the M^I sites.[15]

Of the metal/cyanocarbon materials, $vanadium^{II}(TCNE)_2$ has exhibited the highest T_c (~400 K),[6] however, the structure has yet to be solved. To date, all of the cyanocarbons used in magnetic materials have been symmetric, possessing an even number of nitrile groups. This leads to poor agreement between coordination sites on the metal and the number of nitrile groups, possibly leading to disorder. This has led us to study the asymmetric *N*,7,7-tricyanoquinodimethanimine (TCQMI)[16] and its ability to form new organic-based magnetic materials. Unlike both TCNE and TCNQ, TCQMI has three nitriles; thus, in principle, two TCQMIs could fully satisfy the coordination environment in a 1:2 ratio of M^{II}:TCQMI. Additionally, due to the presence of the

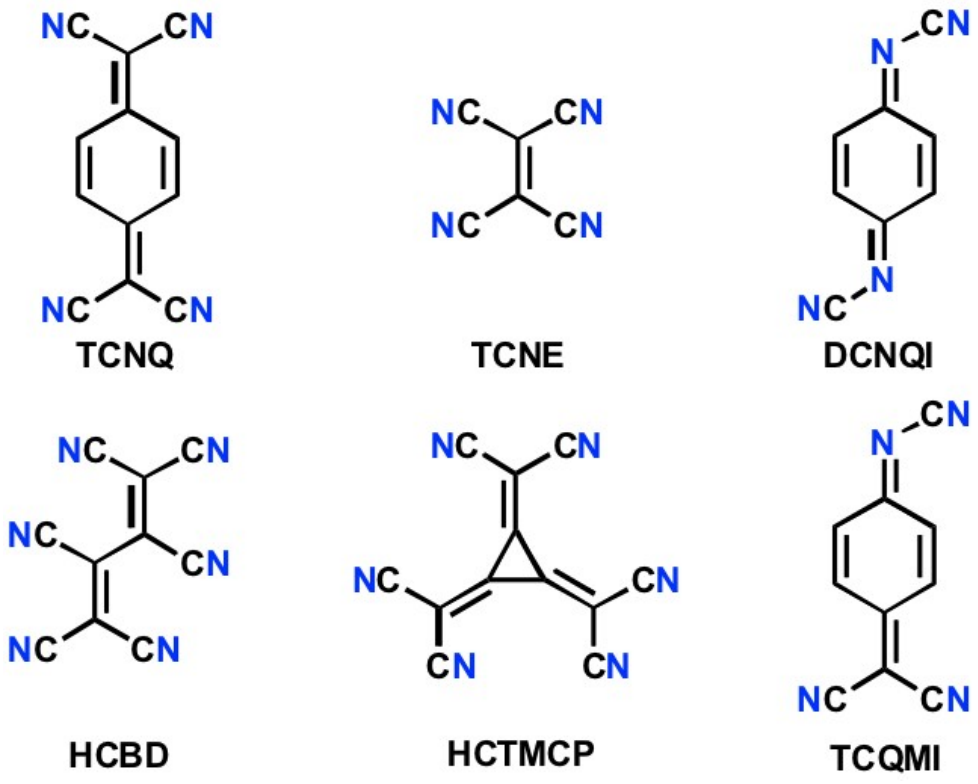

Figure 4.1. Cyanocarbon acceptors used in forming molecule-based magnetic systems.

-NCN- moiety, a shorter 3-atom M-NCN-M linkage, with respect to the more prevalent five atom M-NCCCN-M, could provide a stronger coupling. This might lead to a higher T_c, as observed for M[N(CN)$_2$] magnetic materials.[17]

TCQMI has been previously reported[16a,c] and has two reversible one-electron reductions at 0.20 and -0.47 V vs. SCE, in good agreement with literature values.[16a] The former is comparable to the first reduction potentials of both TCNE (0.24 V vs. SCE)[18] and TCNQ (0.22 V vs. SCE).[18] This indicates that [TCQMI]$^{\bullet-}$ should be isolatable and suitable for forming molecule-based magnetic materials. Hence, the reaction of TCQMI with FeCp*$_2$, Fe(CO)$_5$, and V(CO)$_6$ was pursued to identify new organic-based magnets. Herein, we report the structure of [FeCp*2]$^{+}$[TCQMI]$^{\bullet-}$ as well as the magnetic behavior of this compound and the materials incorporating Fe and V with TCQMI as the ligand.

Experimental

Synthesis. The solvents used in the generation of organic radicals were dried, distilled, and deoxygenated prior to use. Steps generating organic radicals were conducted under an inert N_2 atmosphere in a DriLab glove box (<1 ppm O_2). TCQMI was synthesized as detailed previously.[19] Decamethylferrocene (Arcos Organics) was used without further purification. Fe(CO)$_5$ was purchased from Fisher Scientific and freeze-pump-thawed over several cycles to deoxygenate the compound. V(CO)$_6$ was synthesized from [NEt$_4$][V(CO)$_6$] following a literature procedure.[19]

[Fe^{III}Cp*$_2$]$^{\bullet+}$[TCQMI]$^{\bullet-}$. [Fe^{III}Cp*$_2$]$^{\bullet+}$[TCQMI]$^{\bullet-}$ was synthesized by adding one equivalent of TCQMI, (16.6 mg, 0.92 mmol) dissolved in 20 mL MeCN, dropwise to an equivalent of Fe^{II}Cp*$_2$ (25.3 mg, 0.0774 mmol) dissolved in 20 mL MeCN in a glove box. This resulted in an immediate color change to a dark green/blue. The reaction was

stirred for 2 days in the glove box and no further color change or precipitate was observed. The solution was then placed in a freezer in a glove box for 4 days, during which time clusters of a dark green clay-like powder precipitated [Yield: 31 mg (79%)]. Crystals suitable for single crystal X-ray diffraction could not be obtained, and the structure was determined with the use of synchrotron powder X-ray diffraction data. IR (KBr; cm^{-1}): ν_{CN}, 2185 m, 2169 m, 2150 m, 2131 m, 2098 m.

Attempts were made to grow crystals in order to provide a purer sample. The reaction was repeated in CH_2Cl_2 and solid was seen to precipitate out of the solution upon standing in a freezer for 4 days. The solid appeared somewhat clay-like and was the same color as the solid taken from the previous reaction. When the solid was collected and dried, the resulting IR spectrum proved to be nearly identical to that seen in the MeCN reaction.

$Fe[TCQMI]_2 \bullet zCH_2Cl_2$. $Fe[TCQMI]_2 \bullet zCH_2Cl_2$ was prepared by dissolving $Fe(CO)_5$ (53 mg, 0.271 mmol) and TCQMI (96.5 mg, 0.536 mmol) each in 15 mL CH_2Cl_2. The $Fe(CO)_5$ solution (pale yellow) was added dropwise to the orange TCQMI solution with no immediate color change. The color slowly darkened to green/black over the course of 4 hr with a precipitate forming after several hours. The solution was left to stir for 5 days in a glove box at room-temperature, after which time a dark green precipitate was collected by filtration, washed with hexanes until the filtrate was colorless, and then placed in a drying tube for 4 hr. [Yield: 102 mg (91%)]. IR (KBr; cm^{-1}): ν_{CN} 2245 w, 2173 s, 2116 s. Anal. Calcd (obsd) for $Fe[TCQMI]_2 \bullet zCH_2Cl_2$, z = 0.38: C 54.58 (54.43), H 1.97 (1.97), N 24.99 (24.89), Cl 6.01 (6.30), Fe 12.45 (12.41). The loss of CH_2Cl_2 is facile and thus there is poor baseline; nonetheless, a 6.8% weight loss occurs below 242°C in the TGA trace that is attributed to the CH_2Cl_2 loss and corresponds

to z = 0.36.

V[TCQMI]$_2$•zCH$_2$Cl$_2$. V[TCQMI]$_2$•zCH$_2$Cl$_2$ was prepared by the procedure outlined for the synthesis of V[TCNQ]$_2$.[22] TCQMI (82.3 mg, 0.457 mmol) was dissolved in 15 ml of CH_2Cl_2 and $V(CO)_6$ (51.3 g, 0.228 mmol) was dissolved in 5 mL of CH_2Cl_2. After filtering each solution, the solution of $V(CO)_6$ was dropwise added to the solution of TCQMI, with stirring. Immediately, the TCQMI solution turned black and a black precipitate formed. After the addition of a few drops, the solution bubbled due to carbon monoxide liberation. After the addition was completed, the reaction was stirred for 15 min with occasional venting and then stirred overnight. The next day, the dark precipitate was filtered off, washed with CH_2Cl_2, and dried under vacuum at room-temperature, yielding a dark black solid. [Yield: 95 mg (99%)]. IR (KBr; cm^{-1}): ν_{CN} 2250 sh, 2086 s. Anal. Calcd (obsd) for V(TCQMI)$_2$•zCH$_2$Cl$_2$, z = 0.10 calculated from the TGA data.

Physical methods. IR spectra were taken using a Bruker Tensor 37 spectrometer from KBr pellets (±1 cm^{-1}). UV-Vis studies were conducted using quartz cuvettes on a Hitachi u-4100 spectrometer. Magnetic susceptibility data were measured at 1 kOe between 2 and 300 K on a Quantum Design MPMS-5XL 50 kOe SQUID magnetometer equipped with a reciprocating sample measurement system as previously described.[23] The samples were placed in the magnetometer and the magnetic field was removed by oscillating the field until it had reached zero. The magnetometer was then cooled, the field was applied, and data were recorded upon warming. Magnetic studies were conducted in a gelatin capsule. Ac susceptibilities were recorded at 33, 100, and 1000 Hz.

In addition to correcting for the diamagnetic contribution from the sample holder, the core diamagnetic corrections of -270, -181, and -167 x 10^{-6} emu/mol was used for [FeCp*$_2$][TCQMI], Fe[TCQMI]$_2$, and V[TCQMI]$_2$, respectively. Instrumental oxygen

contamination is responsible for an interruption of the data from 30 - 60 K, though an attempt to minimize the disruption has been made by subtracting out the oxygen moment. Iron impurities of 39 and 20 ppm were estimated for $[FeCp^*_2][TCQMI]$ and $Fe[TCQMI]_2$, respectively, from fits to Honda plots. Reduction potentials were measured on a Bioanalytical Systems, Inc. Epsilon EC using a $Ag/AgNO_3$ electrode with $[NBu_4][PF_6]$ as the supporting electrolyte and ferrocene ($FeCp_2$) as the reference. Reduction potentials were corrected to reflect the V vs. SCE. Thermogravimetric analysis (TGA) was conducted on a TA Instruments Q500 located in a Vacuum Atmospheres DriLab under inert atmosphere (N_2) to avoid O_2/H_2O degradation of the samples. Samples were loaded in an aluminum pan, heated for 10 min at 20°C before ramping from 20 to 600°C at 5.00°C/min under a continuous N_2 purge of 10 mL/min. Elemental analysis (EA) was performed by Desert Analytics, Tucson, AZ.

X-ray structure determination. High-resolution powder X-ray diffraction (PXRD) measurements of $[FeCp^*_2][TCQMI]$ were collected on the X16C beam line at the National Synchrotron Light Source, Brookhaven National Laboratory. A Si(111) channel-cut monochromator selected a parallel 0.699975-Å incident beam. The diffracted X-rays were analyzed by a Ge(111) crystal and detected using a NaI scintillation counter. The capillary was spun at several Hz during data collection to improve particle statistics. The powder diffraction pattern was indexed and a tentative space group of $P2_1$ was assigned.[24] Simulated annealing was used to determine the structure of $[FeCp^*_2][TCQMI]$.[25] After obtaining an acceptable agreement between observed and calculated patterns, Rietveld refinements were performed in order to improve the structure. Hydrogens were placed in idealized positions. Bonds of similar nature (e.g., nominally single C-C bonds in the TCQMI ring, separate from nominally double

bonds) were restrained to be equal and individually refined. Likewise, angles of a similar nature (e.g., C-C-C and C-C=C angles in the TCQMI ring) were restrained to be equal and refined. The Cp* rings were restrained to be parallel with one another, but allowed to rotate about their common axis.

Results and Discussion

Spectroscopic data. TCQMI exhibited two sharp ν_{CN} at 2230 and 2169 cm^{-1}. The higher energy peak compares well with TCNQ with ν_{CN} bands at around 2220 cm^{-1},[22] while the lower energy band is attributed to the C≡N cyanimine stretch. Interestingly, there was no C=N stretch in the ~1700 cm^{-1} region, typical of imines. The peak at 1548 cm^{-1}, consistent with the spectrum reported by Itoh and coworkers,[16c] was attributed to the ring C=C stretch.

Reduction of TCQMI was sought through reaction with $Fe^{II}Cp^*_2$, $Fe(CO)_5$, and $V(CO)_6$, with the goal of forming new organic-based magnets, and determining the structure and behavior of reduced TCQMI. Reaction of TCQMI with $Fe^{II}Cp^*_2$ in MeCN formed a dark green powder that exhibited a weak ν_{CN} absorption at 2241 cm^{-1}, and several medium ν_{CN} bands at 2185, 2169, 2150, 2131, and 2098 cm^{-1} and a shoulder at 2106 cm^{-1}. The bands were generally shifted to lower wavenumbers, consistent with a change in ν_{CN} stretch seen upon reduction of TCNQ[2c] and TCNE.[4] The number of peaks, six in total, stands in contrast to the three inequivalent nitriles in the crystal structure (*vide infra*). Evidence of additional phases or unreacted starting material is not observed; thus, the origin of the extra IR lines is not currently understood. Hence, based on the IR spectrum, the reaction of TCQMI with $Fe^{II}Cp^*_2$ forms $[Fe^{III}Cp^*_2]^+[TCQMI]^-$.

The reactions of $Fe(CO)_5$ and $V(CO)_6$ with TCQMI in CH_2Cl_2 led to precipitates

with IR ν_{CN} peaks at 2245, 2173, and 2116 cm^{-1} for the former, and 2250 (sh) and 2086 (s) cm^{-1} for the latter. The two lower frequency peaks, like those observed for the reaction with $FeCp^*_2$, were consistent with a radical anion as they were shifted to lower energy in comparison to $TCQMI^o$. The peak at 2245 cm^{-1} was unexpected from radical formation, as it was higher in wavenumbers than the neutral peaks. A possible explanation could be that the higher ν_{CN} band may result from a nitrile bridging between metal centers as this has been seen to cause a comparable shift in nitrile stretches in Prussian Blue analogues.[26] High-energy peaks are also observed in the spectra of $Fe[TCNQ]_2 \bullet zCH_2Cl_2$ (2194 cm^{-1}).[27] Both dark green materials were analyzed by powder diffraction in hopes of determining the structure, but did not produce usable patterns.

The IR spectra of the products from the reaction of $V(CO)_6$ and $Fe(CO)_5$ with TCQMI are similar to that seen from the reaction of TCQMI with Mn(TPP)(py).[28] Evidence for the reduction of $TCQMI^o$ by MnTPP could be seen by the ν_{CN} IR (KBr) absorptions red-shifting from 2230 and 2169 cm^{-1} for $TCQMI^o$ to 2188 and 2106 cm^{-1}.[28]

In all compounds, the ν_{CN} absorptions were much broader than those of the neutral TCQMI. This lends further support to the characterization of the compound as $[TCQMI]^{\bullet -}$ bound to M^{II} centers, as it has been observed that coordinating cyano-acceptors, specifically *N,N'*-dicyanoquinone diimines, typically showed wide ν_{CN} stretches.[29] It is worth noting that despite the large number of ν_{CN} stretches, the stretches from $[Fe^{III}Cp^*_2]^{\bullet +}[TCQMI]^{\bullet -}$ remain relatively sharp in comparison to $Fe[TCQMI]_2$. This is consistent with $[TCQMI]^{\bullet -}$ forming nonbonding chains with $[FeCp^*_2]^+$, but not coordinating to the Fe^{II} center.

Structure. The reaction of $Fe^{II}Cp^*_2$ and TCQMI produced microcrystals which, while unsuitable for a single crystal structural determination, provided a usable powder

pattern. Selected parameters are listed in Table 4.1. The crystals were used to obtain high-resolution powder X-ray diffraction data (Figure 4.2). This enabled its structural determination via simulated annealing and Rietveld refinement of the data, and to assign the composition as $[Fe^{III}Cp^*_2][TCQMI]$ (Figure 4.3). $FeCp^*_2$ was restrained to have identical Fe-C distances that refined to a distance of 2.11(1) Å. The Fe-C_5-ring centroid is 1.744(4) Å. These data are insufficient to distinguish between $Fe^{II}Cp^*_2$ and $[Fe^{III}Cp^*_2]^+$.[30] Since the IR spectrum indicates that TCQMI is reduced, the composition is $[Fe^{III}Cp^*_2]^+[TCQMI]^{\bullet-}$.

In accord with the IR data indicating that TCQMI is reduced, the structure of TCQMI differs from the aforementioned neutral TCQMI (Table 4.2) due to the elongation of C2-C4 by 0.098 Å (7.1)% and of C7-N3 by 0.068 Å (5.2%), and a contraction of C10-N3 by 0.033 (2.5%). Additionally, while the neutral compound exhibited variation in bond length for the six-membered-ring with alternating bonds of single bond [1.451(12) Å] and double bond [1.344(2) Å] character; this $[TCQMI]^{\bullet-}$ exhibits a loss of distinct character with C-C ring bonds measuring 1.363(11) and 1.350(17) Å, respectively.

Similar behavior can be seen in the TCNQ analogue, though the contraction (1.433 to 1.424 Å) and elongation (1.355 to 1.362 Å) are not as dramatic.[31] The same trend is observed for $[TCQMI]_2^{2-}$, with loss of distinct single bond/double bond character in the ring, the bonds being much more similar in length.[28] The C-C ring bonds of the dimer are not as uniform as the bonds of the radical anion. This is due to warping of the six-membered-ring, attributed to steric constants of the dimerization as well as the mode of coordination to the metal centers.[28]

The solid-state motif of $[Fe^{III}Cp^*_2][TCQMI]$ consists of alternating $[Fe^{III}Cp^*_2]^{\bullet+}$

Table 4.1. Selected crystallographic parameters for TCQMI and [FeCp*$_2$][TCQMI].

	[FeCp*$_2$][TCQMI]
mol formula	$C_{30}H_{34}FeN_4$
mol mass, daltons	506.46
crystal system	Monoclinic
space group	$P2_1$
Z	2
temp, K	300
a, Å	10.5880 (3)
b, Å	13.7831 (4)
c, Å	10.7078 (3)
α, deg	90
β, deg	119.644 (4)
γ, deg	90
V, Å^3	1358.13 (8)
calcd density, g/cm^3	1.238
wavelength, Å	0.699975
absorpn coeff, mm^{-1}	0.55
F(000)	536
min 2θ; deg	4.00
max 2θ; deg	30.5
reflections collected	5301
GoF	2.005
R_{wp}[a,b]	0.0580
R_{exp}[b,c]	0.0314

[a] $$R_{\mathrm{wp}} = \sqrt{\frac{\sum_i w_i (y_i^{calc} - y_i^{obs})^2}{\sum_i w_i (y_i^{obs})^2}}$$

[b] y_i^{calc} and y_i^{obs} are the calculated and observed intensities at the i^{th} point in the profile, normalized to monitor intensity. The weight w_i is $1/\sigma^2$ from the counting statistics, with the same normalization factor. N is the number of points in the measured profile minus number of parameters.

[c] $$R_{\mathrm{exp}} = \sqrt{\frac{N}{\sum_i w_i (y_i^{obs})^2}}$$

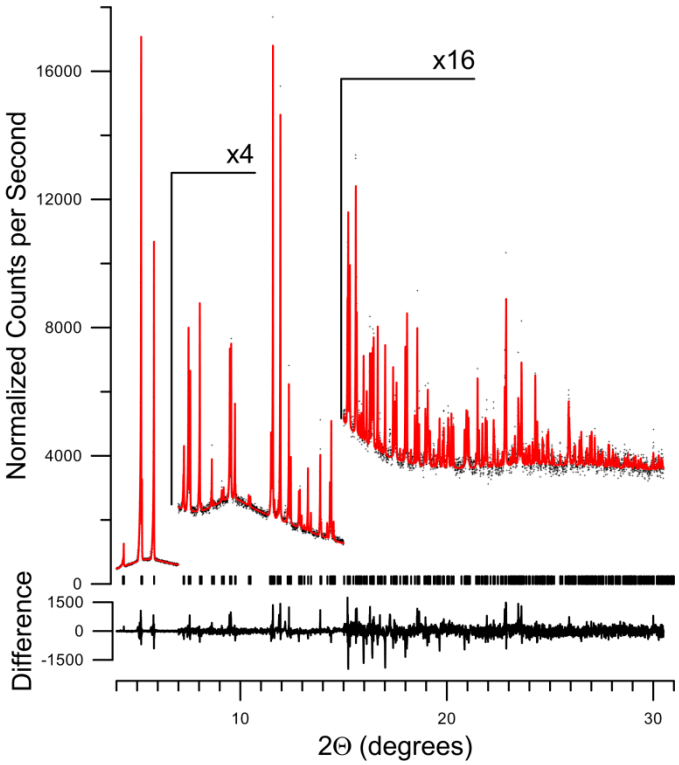

Figure 4.2. High-resolution synchrotron powder diffraction data (dots) and Rietveld fit of the data for [$Fe^{III}Cp^*_2$][TCQMI] (line). The lower trace is the difference, measured minus calculated, plotted to the same vertical scale.

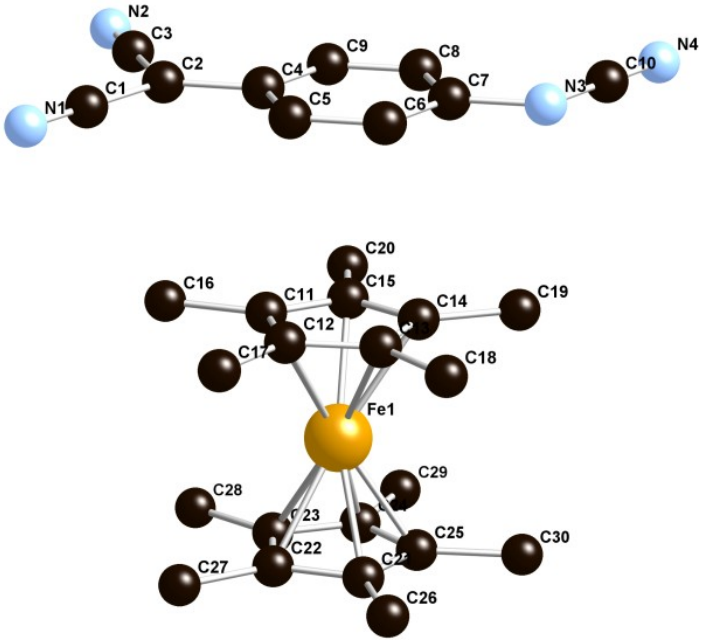

Figure 4.3. Atom labeling diagram for [FeCp*$_2$][TCQMI] (hydrogen atoms not shown for clarity).

Table 4.2. Comparison of the TCQMI bond distances (Å) with esds observed for TCQMI, Me_3TCQMI,[16 a] Me_4TCQMI,[16 a] and [$Fe^{III}Cp^*_2$][TCQMI]. Distances marked (a), (b), and (c) were constrained to be equal.

	TCQMI	Me_3TCQMI[16a]	Me_4TCQMI[16a]	[$FeCp^*_2$][TCQMI]
C2-C4	1.372(2)	1.373(8)	1.360(3)	1.470(25)
C1-N1	1.149(2)	1.147(5)	1.14(1)	1.142(18) (a)
C3-N2	1.152(2)	1.144(6)	1.14(2)	1.142(18) (a)
C4-C5	1.450(2)	1.457(6)	1.47(2)	1.363(11) (b)
C4-C9	1.451(2)	1.451(4)	1.48(1)	1.363(11) (b)
C5-C6	1.343(2)	1.360(7)	1.351(4)	1.350(17) (c)
C8-C9	1.345(2)	1.338(7)	1.354(4)	1.350(17) (c)
C6-C7	1.452(3)	1.466(4)	1.463(3)	1.363(11) (b)
C7-C8	1.452(2)	1.462(6)	1.47(1)	1.363(11) (b)
C7-N3	1.313(2)	1.304(8)	1.299(3)	1.381(23)
C10-N3	1.345(2)	1.326(4)	1.331(4)	1.312(28)

and $[TCQMI]^{\bullet-}$ in parallel chains, as observed for both $[Fe^{III}Cp^*_2][TCNE]$[4] and $[Fe^{III}Cp^*_2][TCNQ]$.[2] As occurs for $[Fe^{III}Cp^*_2][TCNQ]$, the unit cell contains distinct chains with 10.588-Å intrachain Fe•••Fe separations. This motif has three unique pairs of chains (Figure 4.4): out-of-registry **I-III**, **I-IV**, and in-registry **I-II**. Their key interatomic separations are noted in Figure 4.5.

The interchain distances for **I-II**, **I-III**, and **I-IV** are 8.52, 9.31, and 8.12 Å, respectively, and have interchain Fe•••Fe separations of 8.524 (**I-II**), 10.707 (**I-III**), and 9.660(**I-IV**) and 9.723 (**I-IV**). These distances are comparable to those observed for $[Fe^{III}Cp^*_2][TCNQ]$[2c] and $[Fe^{III}Cp^*_2][TCNE]$.[32] The intrachain Fe•••N distances measure from 5.849 to 7.121 Å with the shortest distance arising from the imine nitrogen. The interchain Fe•••N distances range from 5.286 to 8.50 Å, with the shorter distances from the imine nitrogen. The interchain N•••N distances range from 3.893 to 7.744 Å. The $[Fe^{III}Cp^*_2][TCQMI]$ chain interactions are intermediate to those observed in the $[Fe^{III}Cp^*_2][TCNE]$ and $[Fe^{III}Cp^*_2][TCNQ]$ structures, but span wider ranges due to the cyanimine group.

The $[TCQMI]^{\bullet-}$ is parallel to, and 3.47 Å away from, the Cp* rings (Figure 4.3). This structure is very similar to the $FeCp^*_2$ analogues formed from TCNQ[2c] and TCNE[10] where the distance between the alternating species are 3.56 and 3.52 Å, respectively.

The reactions of TCQMI with $Fe(CO)_5$ or $V(CO)_6$ formed powders that were unsuitable for diffraction analysis. The reaction of TCNQ with $Fe(CO)_5$ and $V(CO)_6$ also resulted in powders that did not diffract.[22,27] TCQMI compounds $M(TCQMI)_2 \bullet zCH_2Cl_2$ (M = Fe, V) likewise formed. The ν_{CN} absorptions at 2245, 2173, and 2116 cm^{-1} and 2250 and 2086 cm^{-1}, respectively, for M = Fe and V, indicating formation of reduced TCQMI. These stretches are in accord with the ν_{CN} stretches seen in the TCNQ analogues with the

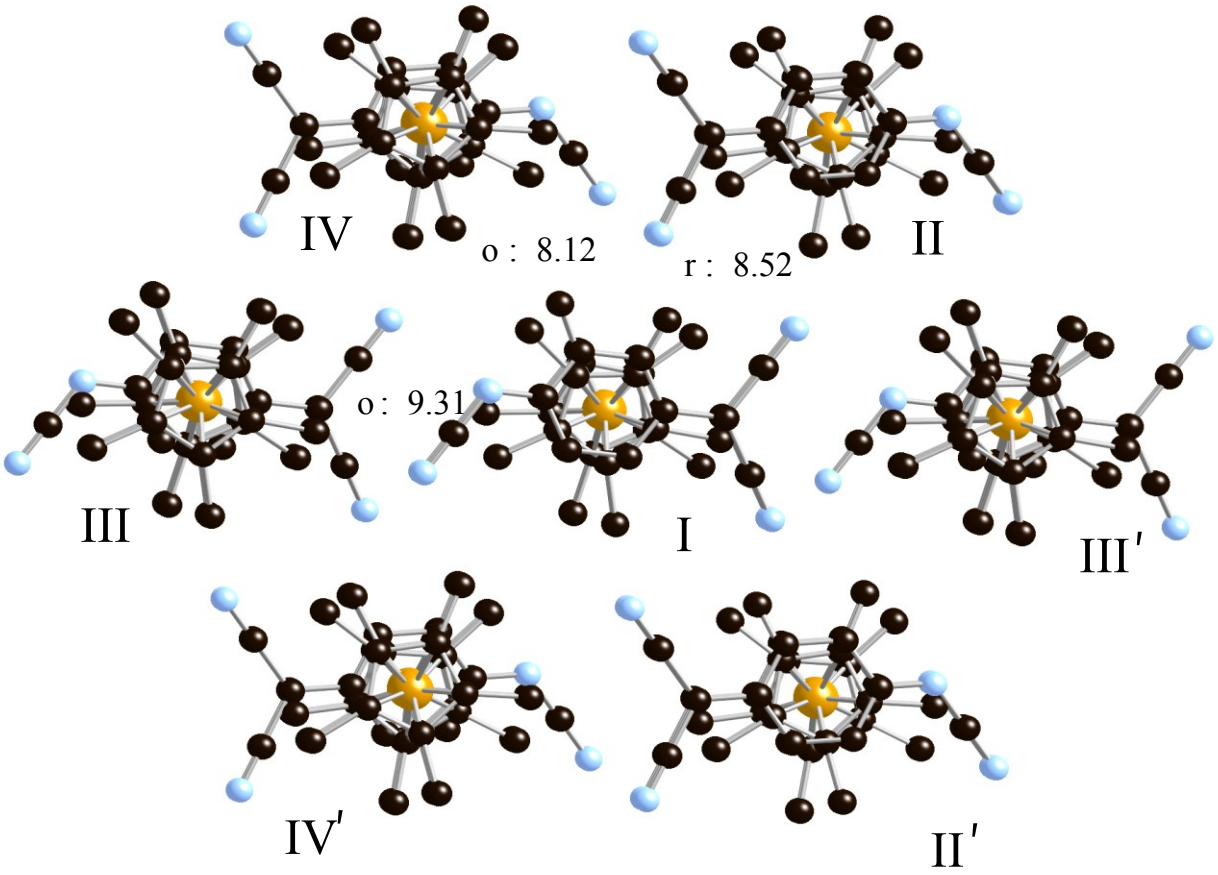

Figure 4.4. Top-view showing the unique adjacent parallel chains of $[Fe^{III}Cp^*_2][TCQMI]$ and their interchain separations (r: in-registry chains; o: out-of-registry chains). Hydrogen atoms not shown for clarity.

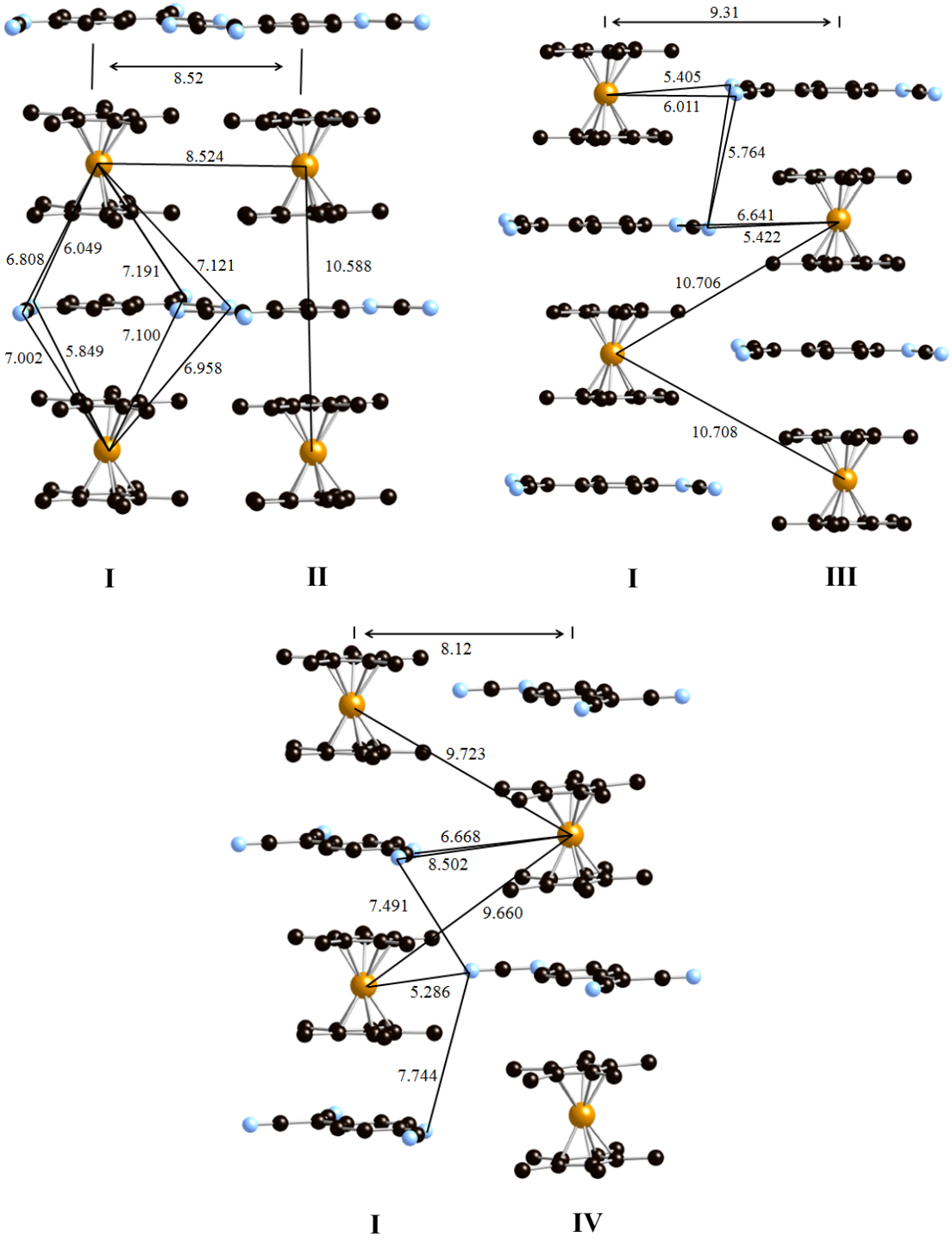

Figure 4.5. Adjacent in-registry (r) **I-II** and out-of-registry (o) **I-III**, **I-IV** parallel chains of $[Fe^{III}Cp^*_2][TCQMI]$ and their interchain separations. Hydrogen atoms are not shown for clarity.

same metals.

UV-Vis. The UV-Vis spectra of TCQMI and $[TCQMI]^{\bullet-}$ in MeCN was obtained. TCQMI exhibited a peak at 27500 and shoulders at 25000 and 28700 cm^{-1} with a smaller peak at 44600 cm^{-1} (Figure 4.6). The TCQMI radical displayed absorption bands at lower energies than the neutral compound. Major absorptions occur at 13300; 14800; 26900; and 32600 cm^{-1}, with shoulders at 13500; 14500; and 16100 cm^{-1}. The general shape and shift seen from the neutral compound to the radical anion are consistent with TCNQ/$[TCNQ]^{\bullet-}$ spectra.[33] The radical absorptions around 13000 cm^{-1} covered the $[FeCp^*_2]^+$ band that appears in the region, but bands at 32450 and 36100 cm^{-1} identify the cation.

Magnetic studies. The temperature-dependent magnetic susceptibility, χ, data were measured from 2 to 300 K, and are plotted as $\chi T(T)$ and $\chi^{-1}(T)$ for $[FeCp^*_2][TCQMI]$ and $M[TCQMI]_2 \bullet zCH_2Cl_2$ (M = Fe, V) (Figure 4.7).

$[FeCp^*_2][TCQMI]$. The room-temperature χT value for $[FeCp^*_2][TCQMI]$ is 0.995 emu K/mol, and exceeds the calculated spin-only value of 0.75 emu K/mol for a system of two $S = 1/2$ ions (Figure 4.7). This is expected due to the anisotropic nature of $[Fe^{III}Cp^*_2]^+$, as has been observed for other $[Fe^{III}Cp^*_2]^+$ salts including $[FeCp^*_2][TCNE]$[30c] and $[FeCp^*_2][TCNQ]$.[4c] The $\chi T(T)$ data can be fit to the Curie-Weiss expression, $\chi \propto (T - \theta)^{-1}$, with θ = 1.5 K, and g = 2.98. The θ value indicates weak ferromagnetic coupling. The $\chi T(T)$ and $1/\chi(T)$ data show a jump in the data at ~120 K. This jump occurs in all samples. A closer examination of the region indicates this is not an instrumental artifact, but is innate to the system. This jump possibly arises from a phase transition inherent to the compound.

To further investigate the genesis of the small positive θ -value, the in-phase

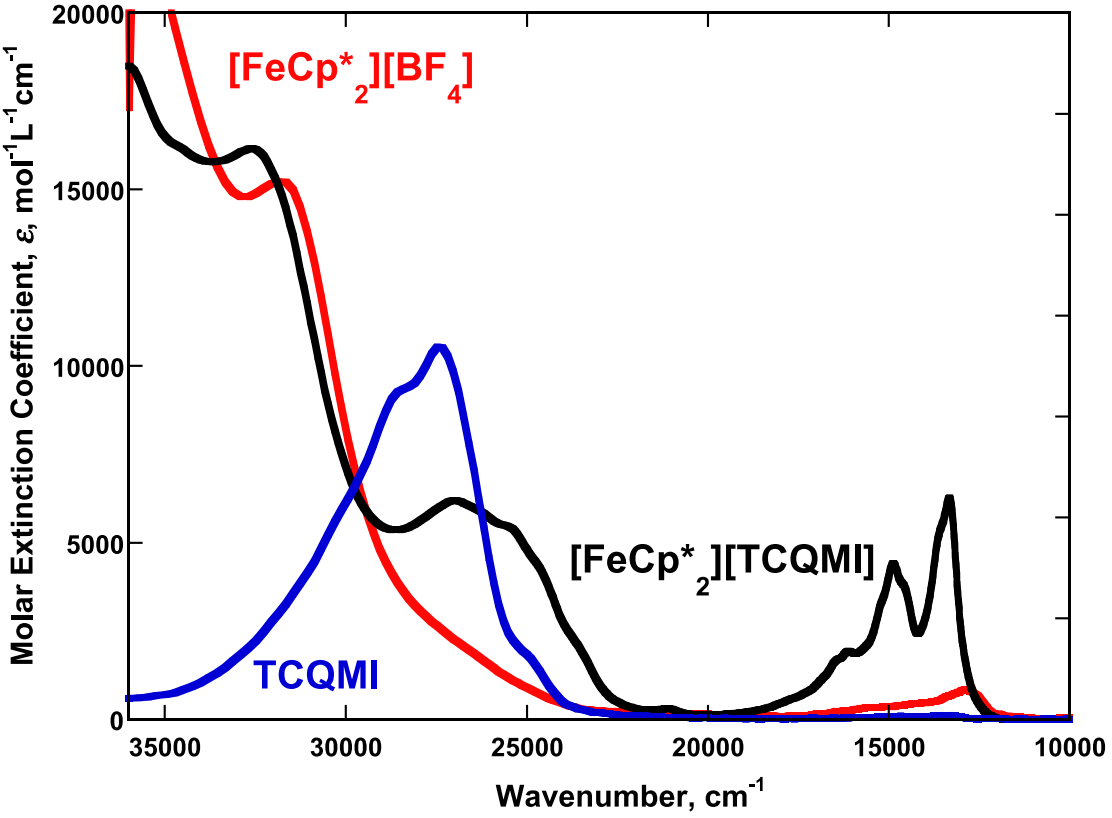

Figure 4.6. UV-Vis spectra of TCQMI, $[Fe^{III}Cp^*_2][TCQMI]$, and $[Fe^{III}Cp^*_2][BF_4]$ in MeCN.

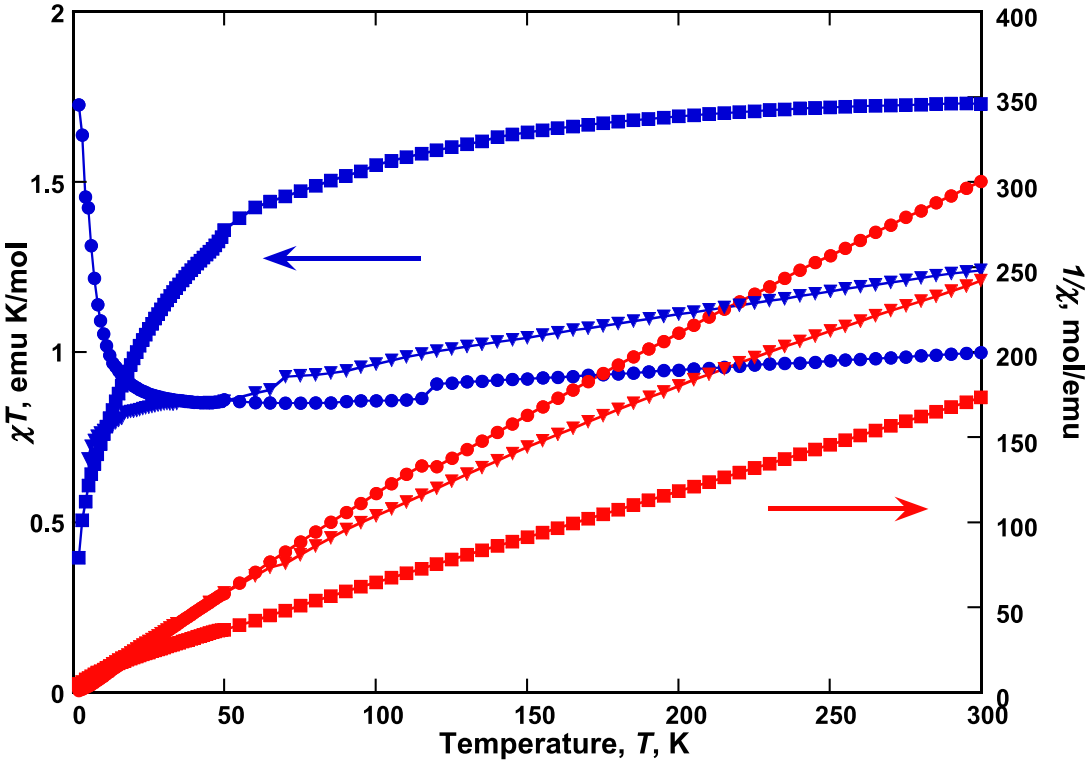

Figure 4.7. $\chi T(T)$ and $1/\chi(T)$ for [FeCp*$_2$][TCQMI] (●), Fe[TCQMI]$_2$ (■), and V[TCQMI]$_2$(▼).

(real) and out-of-phase (complex) ac susceptibilities, $\chi'(T)$ and $\chi''(T)$, respectively, were measured between 2 and 10 K (Figure 4.8). $\chi'(T)$ exhibits a frequency-independent peak at 3.4 K in $\chi'(T)$, and a frequency-dependent upturn in $\chi''(T)$ with decreasing temperature. This is indicative of more complicated magnetic ordering occurring with a T_c of 3.4 K. Interestingly, the ac susceptibility data were seen to be identical whether the solution was taken to dryness or precipitated in a freezer.

Saturation of the magnetization, M_S, is achieved at ~50 kOe at 2 K, and is 2700 emuK/mol. This value is much lower than that seen for the TCNE and TCNQ analogues[4c] and the calculated M_S value expected for a ferromagnetically ordered system, i.e., 13900 emuOe/mol assuming the aforementioned g = 2.98. The value is consistent with an antiferromagnetically coupled, ferrimagnetically ordered system, i.e., 2736 emuOe/mol as calculated from $M_S = N\Delta gS\mu_B$ where N = Avogadro's number, and μ_B is the Bohr magneton. Ferrimagnets arise from antiferromagnetic coupling whereby the antiparallel spins cannot cancel due to different g-values. The behavior is still anomalous as hysteresis was not evident from a 2-K (± 90 kOe) $M(H)$ study.

$Fe^{II}[TCQMI]_2 \bullet zCH_2Cl_2$. The room-temperature χT value for $Fe^{II}[TCQMI]_2 \bullet zCH_2Cl_2$ is 1.62 emuK/mol, and it substantially reduced from the calculated spin-only value of 2.75 emuK/mol for a system of two S = 1/2 ions plus an S = 2 high-spin Fe^{II} ion (Figure 4.7). This must arise for antiferromagnetic coupling. The $\chi T(T)$ data can be fit to the Curie-Weiss expression with θ = -14 K, indicating antiferromagnetic coupling.

The 2 to 10 K $\chi'(T)$ and $\chi''(T)$ ac susceptibility exhibits a frequency-dependent peak in $\chi'(T)$ at 3.7 K at 1000 Hz, and onset at 4.4 K upon cooling for $\chi''(T)$ (Figure 4.9). Hence, magnetic ordering occurs ~4 K; this is substantially less than that observed for

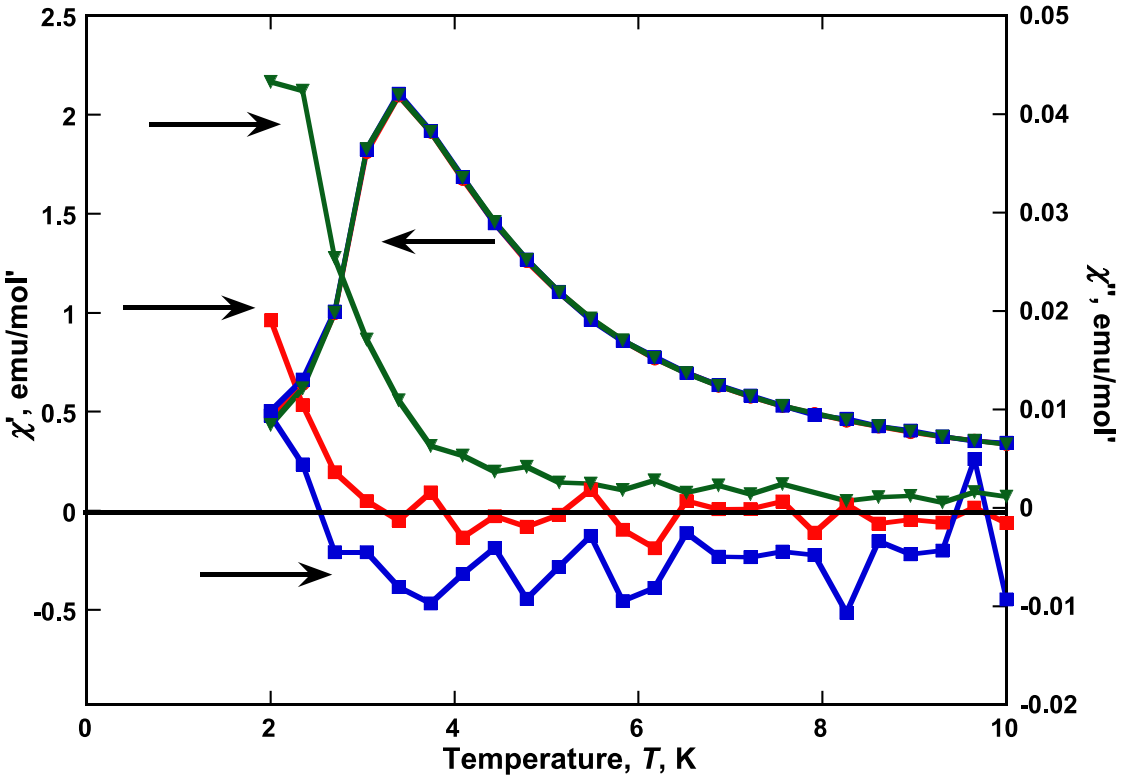

Figure 4.8. Frequency dependency of $\chi'(T)$ and $\chi''(T)$ for [FeCp*$_2$][TCQMI] (33 Hz: ●, 100 Hz: ■, 1000 Hz: ▼).

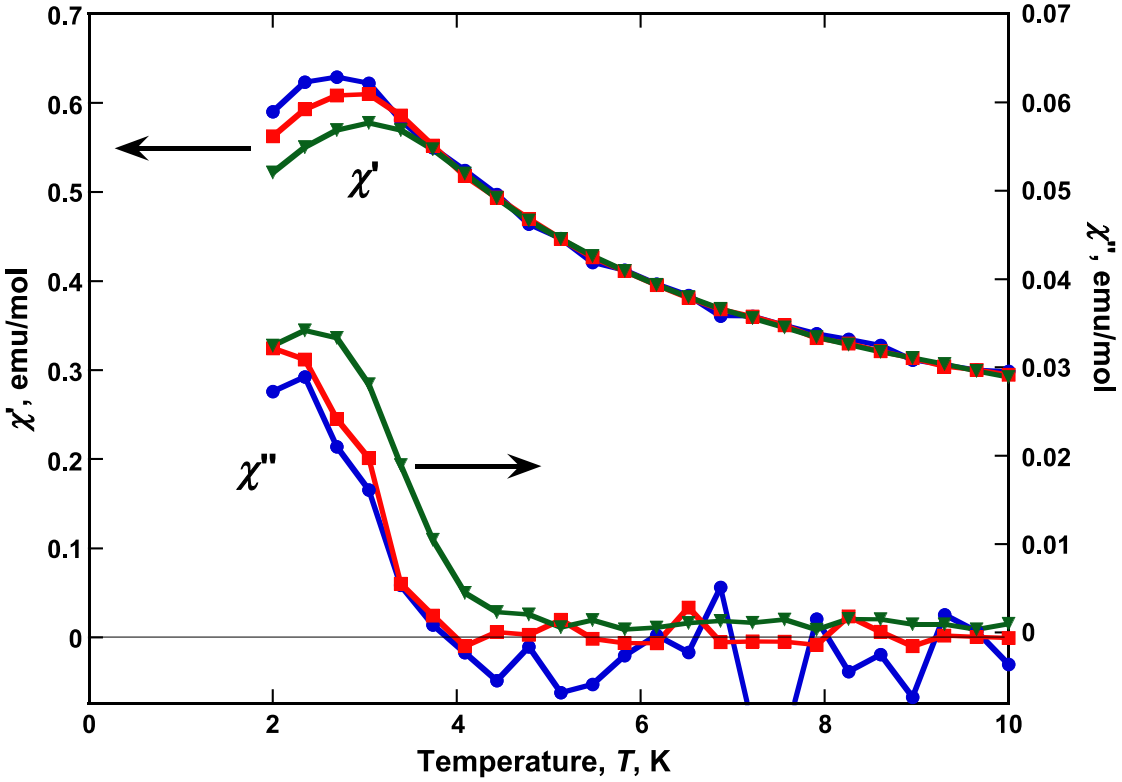

Figure 4.9. Frequency dependency of $\chi'(T)$ and $\chi''(T)$ for $Fe[TCQMI]_2 \bullet 0.40CH_2Cl_2$ (33 Hz: ●, 100 Hz: ■, 1000 Hz: ▼).

$Fe[TCNE]_2$ (T_c ~ 100 K), and $Fe[TCNQ]_2$ (T_c ~ 35 K).[27] The frequency-dependent data suggest spin-glass behavior. Similar behavior is observed in the heat-annealed $Fe[TCNQ]_2$, which is also classified as a spin-glass. However, $Fe[TCNQ]_2$ exhibits a bifurcation in the zero-field-cooled and field-cooled (ZFC/FC) data, while $Fe^{II}[TCQMI]_2 \bullet zCH_2Cl_2$ does not indicate bifurcation.[27] The magnetization is 5800 emuOe/mol at 90 kOe at 2 K, but it is still increasing with increasing applied field, and thus is not saturated. The low value suggests a weak ferromagnetic behavior. Hysteresis was not evident from a 2-K (± 90 kOe) $M(H)$ study.

$V^{II}[TCQMI]_2 \bullet zCH_2Cl_2$. The room-temperature χT value for $V[TCQMI]_2$ is 0.88 emuK/mol (Figure 4.7), well below the value of 1.59 emuK/mol seen for $V[TCNQ]_2 \bullet zCH_2Cl_2$ with S = 3/2 V^{II} and two S = 1/2 radical anions. $\chi T(T)$ linearly decreases with decreasing temperature and has no evidence of magnetic ordering. The $1/\chi(T)$ data indicated antiferromagnetic coupling with a θ = -1.8 K. This is also noted from 1000-Hz 2 to 10 K ac susceptibility studies that did not have absorptions in either the real $\chi'(T)$ or imaginary $\chi''(T)$ data (Figure 4.10). The reason for the lack of ordering in the magnetic phase is not currently understood, as TCQMI forms magnetically ordered compounds in the reaction with other metal systems.[19] A possible source of the lack of ordering may be dimerization of TCQMI, as this has been previously observed.[28]

Conclusion

The structures and electron-accepting properties of cyanocarbon *N,*7,7-tricyanoquinomethanimine, TCQMI, and its radical anion $[TCQMI]^{\bullet -}$, are reported. The close similarity between the reduction potential of TCQMI (0.20 V vs. SCE), TCNE, and TCNQ, as well as their structures, highlighted TCQMI as a candidate in forming new

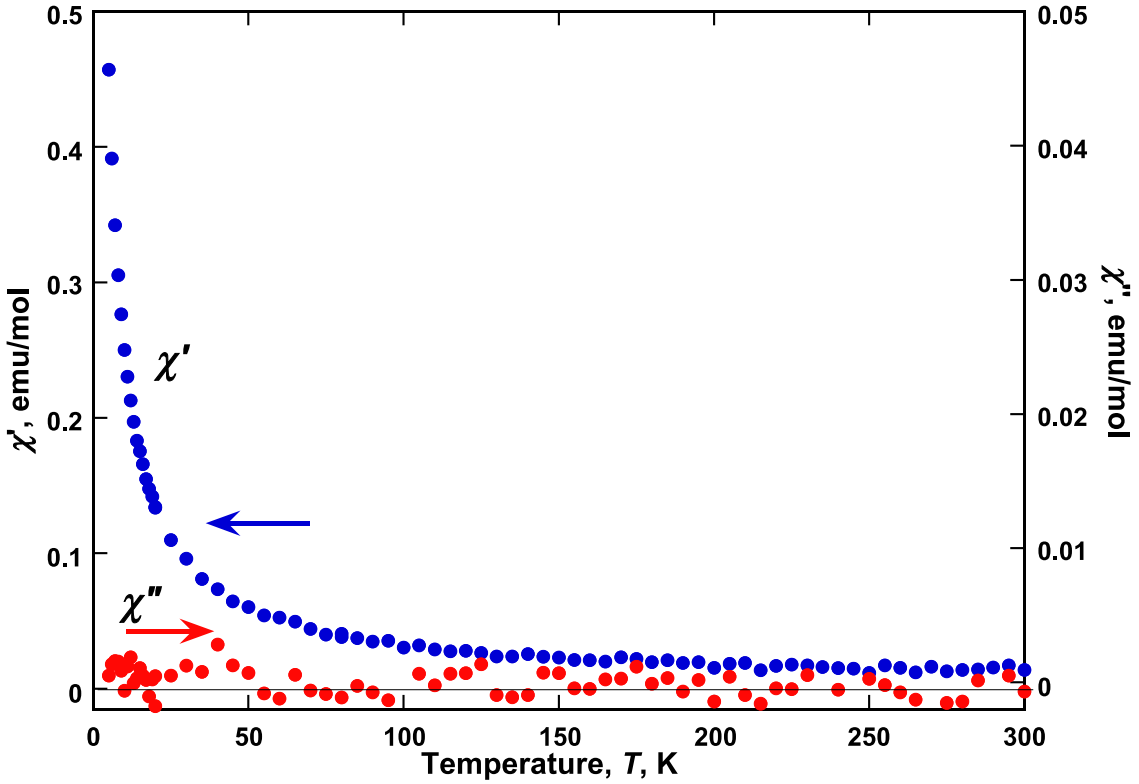

Figure 4.10. 1000-Hz $\chi'(T)$ and $\chi''(T)$ for $V(TCQMI)_2 \bullet 0.10CH_2Cl_2$.

molecule-based materials. Additionally, it was expected to form compounds of $M^{II}[TCQMI]_2$ stoichiometry with all nitriles bonded, resulting in less disordered structures. This was studied through the synthesis and characterization of a new series of TCQMI-based magnetic materials from reactions of TCQMI with decamethylferrocene ($FeCp^*_2$), iron pentacarbonyl, and vanadium hexacarbonyl.

The reaction of $[FeCp^*_2]^+[TCQMI]^{\bullet-}$ showed a close correlation with other cyanocarbon acceptors, e.g., TCNE and TCNQ, as it formed a motif composed of 1-D, parallel chains of alternating $[Fe^{III}Cp^*_2]^{\bullet+}$ and $[TCQMI]^{\bullet-}$ ions. The inter- and intrachain separations are comparable to those reported for $[FeCp^*_2][TCNE]$ and $[FeCp^*_2][TCNQ]$. $[Fe^{III}Cp^*_2]^{\bullet+}$ and [TCQMI] magnetically orders with a T_c of 3.4 K, intermediate of that reported for $[FeCp^*_2][TCNE]$ and $[FeCp^*_2][TCNQ]$.

$M[TCQMI]_2 \bullet zCH_2Cl_2$ does not order for M = V, and for M = Fe orders at a low temperature of 3.7 K, in contrast to the significantly higher ordering temperatures of compounds of apparent stoichiometry $M[TCNE]_2 \bullet zCH_2Cl_2$ and $M[TCNQ]_2 \bullet zCH_2Cl_2$ (M = V, Fe). The source of the low ordering in $Fe[TCQMI]_2$ and lack of ordering in $V[TCQMI]_2$ is not currently understood. It does indicate that TCQMI is well-suited to forming charge transfer salts in cases where direct coordination to metal sites is not encountered.

References

(1) (a) Ferraris, J.; Cowan, D.O.; Walatka, V.; Perlstein, J.H. *J. Am. Chem. Soc.* **1973**, *95*, 948. (b) Bright, A.; Garito, A.F. Heeger, A.J. *Solid State Commun*. **1973**, *13*, 943. (c) Cohen, M.J.; Coleman, L.B.; Garito, A.F.; Heeler, A.J. *Phys. Rev. B* **1974**, *10*, 1298.

(2) (a) Candela, G.A.; Swartzendruber, L.J.; Miller, J.S.; Rice, M.J. *J. Am. Chem. Soc.* **1979**, *101*, 2755. (b) Miller, J.S.; Reis Jr., A.H.; Gerbert, E.; Ritsko, J.J.; Saleneck, W.R.; Kovnat, L.; Cape, T.W.; Van Duyne, R.P. *J. Am. Chem. Soc.* **1979**, *101*, 7111. (c) Miller, J.S.; Zhang, J.H.; Reiff, W.M.; Preston, L.D.; Reis, Jr., A.H.; Gerbert, E.; Extine, M.; Troup, J.; Ward, M.D. *J. Phys. Chem.* **1987**, *91*, 4344.

(3) Taliaferro, M.L.; Palacio, F.; Miller, J.S. *J. Mater. Chem.* **2006**, *16,* 2677.

(4) (a) Miller, J.S.; Calabrese, J.C.; Epstein, A.J.; Bigelow, R.W.; Zhang, J.H.; Reiff, W.M.; *J. Chem. Soc. Chem. Commun.* **1986**, 1026. (b) Miller, J.S.; Epstein, A.J.; Reiff, W.M. *Science*, **1988**, *240*, 40. (c) Miller, J.S.; Epstein, A.J.; Reiff, W.M.; *Chem. Rev*. **1988**, *88*, 201. (d) Miller, J.S.; Epstein, A.J.; Reiff, W.M. *Acc. Chem. Res*. **1988**, *21*, 114.

(5) Miller, J.S.; Calabrese, J.C.; Harlow, R.L.; Dixon, D.A.; Zhang, J.H.; Reiff, W.M.; Chittipeddi, S.; Mark, C.; Selover, A.; Epstein, A.J. *J. Am. Chem. Soc.***1990**, *112,* 5496.

(6) (a) Miller, J.S. *Inorg. Chem.* **2000**, *39,* 4392. (b) Zhang, J.; Zhou, P.; Brinckerhoff, W.B.; Epstein, A.J.; Vazquez, C.; McLean, R.S.; Miller, J.S. *ACS Symp. Ser.* **1996**, *644*, 311. (c) Zhang, J.; Ensling, J.; Ksenofontov, V.; Gütlich, P.; Epstein, A.J.; Miller, J.S. *Angew. Chem., Int. Ed.* **1998**, *37*, 657. (d) Matsuura, H.; Miyake, K.; Fukuyama, H. *J. Phys. Soc. Jpn* **2010**, *79*, 034712.

(7) (a) Sugiura, K.-i.; Mikami, S.; Johnson, M.T.; Raebiger, J.W.; Miller, J.S.; Iwasaki, K.; Okada, Y.; Hino, S.; Sakata, Y. *J. Mater. Chem.* **2001**, *11*, 2152. (b) Werner, H.-P.; Von Schütz, J.U.; Wolf, H.C.; Kremer, R.; Gehrke, M.; Aumüller, A.; Erk, P.; Hünig, S. *Solid State Comm.* **1988**, *65*, 809.

(8) Tanaka, J.; Katayama, C.; Kumagai, H.; Saito, G.; Enoki, T.; Inokuchi, H. *Mol. Cryst. Liq. Cryst.* **1985**, *125*, 223.

(9) O'Hare, D.; Rai-Chaudhuri, A.; Murphy, V. *J. Chem. Soc., Dalton Trans.* **1993**, *20*, 3071.

(10) Miller, J.S. *J. Mater. Chem.* **2010**, *20*, 184

(11) (a) Blundell, S.J.; Pratt, F.L. *J. Phys.: Condens. Matter*, **2004**, *16*, R771. (b) Ovcharenko, V.I.; Sagdeev, R.Z. *Russ. Chem. Rev.* **1999**, *68*, 345. (c) Miller, J.S.; Epstein, A.J. *Chem. Commun.* **1998**, 1319. (d) Miller, J.S.; Epstein, A.J. *Angew. Chem. Int. Ed. Engl.* **1994**, *33*, 385.

(12) Stone, K.H.; Stephens, P.W.; McConnell, A.C.; Shurdha, E.; Pokhodnya, K.I.; Miller, J.S. *Adv. Mater.* **2010**, *22*, 2514.

(13) (a) Pokhodnya, K.I.; Bonner, M.; Her, J.H.; Stephens, P.W.; Miller, J.S. *J. Am. Chem. Soc.* **2006**, *128*, 15592. (b) Her, J.H.; Stephens, P.W.; Pokhodnya, K.I.; Bonner, M.; Miller, J.S.; *Angew. Chem., Int. Ed*. **2007**, *46*, 1521. (c) Lapidus, S.H.; McConnell, A.C.; Stephens, P.W.; Miller, J.S. *Chem. Commun.* **2011**, *47*, 7602.

(14) Clerac, R.; O'Kane, S.; Cowen, J.; Ouyang, X.; Heintz, R.; Zhao, H.; Bazile, Jr., J.J.; Dunbar, K.R. *Chem. Mater* **2003**, *15*, 1840.

(15) (a) Shields, L. *J. Chem. Soc., Faraday Trans. 2* **1985**, *81*, 1. (b) Heintz, R.A.; Zhao, H.; Ouyang, X.; Grandinetti, G.; Cowen, J.; Dunbar, K.R. *Inorg. Chem.* **1999**, *38*, 144.

(16) (a) Bryce, M.R.; Davies, S.R.; Grainger, A.M.; Hursthouse, M.B.; Mazid, M.; Bachmann, R.; Gerson, F.; Hellberg, J. *J. Org. Chem.* **1992**, *57*, 1690. (b) Hyatt, J.A. *J. Org. Chem*. **1983**, *48*, 129. (c) Iwatsuki, S.; Itoh, T.; Itoh, H. *Chem. Lett.* **1988**, *17*, 1187.

(17) Miller, J.S.; Manson, J.L.; *Acc. Chem. Res.* **2001**, *34*, 563.

(18) Olbrich-Deussner, B.; Kaim, W.; Gross-Lannert, R.; *Inorg. Chem.* **1989**, *28*, 3113.

(19) This work, Chapter 3.

(20) Liu, X.; Ellis, J.E.; Selby, T.D.; Ghalsasi, P.; Miller, J.S. *Inorg. Synth.* **2004**, *34*, 68.

(21) Attenburrow, J.; Cameron, A.F.B.; Chapman, J.H.; Evans, R.M.; Hems, B.A.; Jansen, A.B.A.; Walker, T. *J. Chem. Soc.* **1952**, 1094.

(22) Vickers, E.B.; Selby, T.D.; Thorum, M.S.; Taliaferro, M.L.; Miller, J.S. *Inorg. Chem.* **2004**, *43*, 6414.

(23) Brandon, E.J.; Rittenberg, D.K.; Arif, A.M.; Miller, J.S. *Inorg. Chem.* **1998**, *37*, 3376.

(24) Coelho, A.A. *J. Appl. Cryst.* **2003**, *36*, 86.

(25) Coelho, A.A. TOPAS Academic, available at www.topas-academic.net.

(26) Nakamoto, K. *Infrared and Raman Spectra of Inorganic and Coordination Compounds*, Wiley-Interscience, New York, **1997**, 111.

(27) Pokhodnya, K.I.; Petersen, N.; Miller, J.S. *Inorg. Chem.* **2002**, *41*, 1996.

(28) Arthur, J.L.; Moore, C.E.; Rheingold, A.L.; Miller, J.S. *Inorg. Chem.* **2011**, *50*, 2735.

(29) Aumüller, A.; Peter, E.; Hünig, S.; Meixner, H.; von Schütz, J.-U.; Werner, H.-P. *Liebigs Ann. Chem.* **1987**, 997.

(30) (a) Miller, J.S.; Glatzhofer, D.T.; Vazquez, C.; McLean, R.S.; Calabrese, J.C.; Marshall, W.J.; Raebiger, J.W. *Inorg. Chem.* **2001**, *40*, 2058. (b) Bildstein, B.; Hradsky, A.; Kopacka, H.; Malleier, R.; Ongania, K.-H. *J. Organomet. Chem.* **1997**, *540*, 127. (c) Miller, J.S.; Calabrese, J.C.; Rommelmann, H.; Chittipeddi, S.; Epstein, A.J.; Zhang, J.H.; Reiff, W.M. *J. Am. Chem. Soc.* **1987**, *109,* 769. (d) Freyberg, D.P.; Robbins, J.L.; Raymond, K.N.; Smart, J.C. *J. Am. Chem. Soc.* **1979**, *101,* 892.

(31) Nadtochenko, V.A.; Denisov, N.N.; Rubtsov, I.V.; Lobach, A.S.; Moravskii, A.P. *Chem. Phys. Lett.* **1993**, *208*, 431.

(32) (a) Her, J.-H.; Stephens, P.W.; Ribas-Ariño, J.; Novoa, J.J.; Shum, W.W.; Miller, J.S. *Inorg. Chem.* **2009**, *48*, 3296. (b) Miller, J.S.; Gantzel, P.K.; Rheingold, A.L.; Taliaferro, M.L. *Inorg. Chem.* **2009**, *48*, 4201.

(33) Melby, L.R.; Harder, R.J.; Hertler, W.R.; Mahler, W.; Benson, R.E.; Mochel, W.E. *J. Am. Chem. Soc.* **1962**, *84*, 3374.

CHAPTER 5

STABILIZATION OF MAGNETIC ORDERING OBSERVED FOR THE BRIDGING NCN GROUP

Introduction

Manganese(III) compounds bridged by cyanocarbon compounds form unique molecule-based magnetic materials. Two general types have been observed in this family (Figure 5.1). The first, and most studied, features organics ligands bearing radical anions as the bridging agent in porphinatomanganese (III).[1-6] Typically, these systems are structurally characterized as linear chains and magnetically characterized as ferrimagnets which exhibit a range of ordering temperatures (T_C) up to 28 K,[1] and possess complex history- and temperature-dependent magnetizations that include extraordinarily high coercivities (~27 kOe) at low temperatures.[2] These values are of particular interest as they fall in the range of those recorded in rare earth magnets.[2] The most studied radical anion of this type is $[TCNE]^{\bullet-}$ (TCNE = tetracyanoethylene),[3] although substituted 7,7,8,8-tetra-cyano-*p*-quinodimethanes (TCNQ),[4] substituted *N*,*N*'-dicyano-*p*-quinone diimines (DCNQI)[5] and chloranil[6] etc. have also been observed to produce materials with interesting magnetic properties.

Reproduced in part with permission from Arthur, J. L.; Moore, C. E.; Rheingold, A. L.; Miller, J. S. *Inorg. Chem.* **2011**, *50*, 2735.

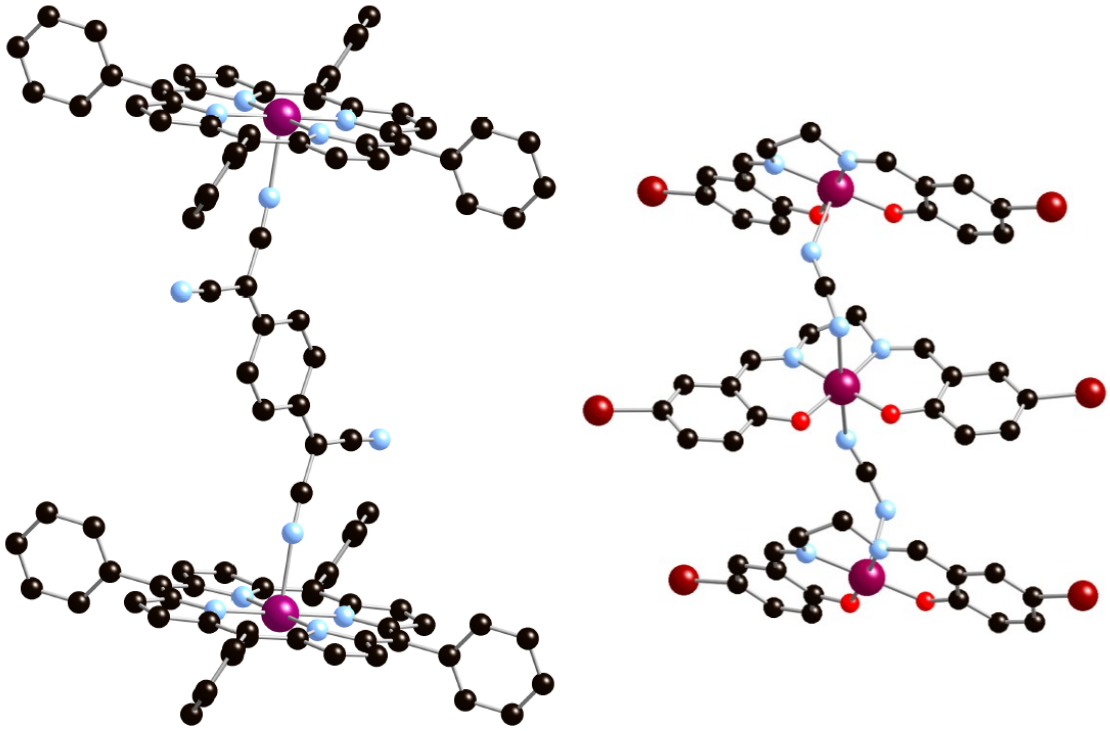

(a) (b)

Figure 5.1. Examples of manganese (III) coordination compounds bridged by cyanocarbon acceptor TCNQ[4] (a) and hydrogen cyanimine[7a] (b).

The second type consists of hydrogencyanimide and analogous compounds serving as the bridging ligand in manganese (III) centers coordinated to Schiff bases.[7] These compounds lack a radical, spin-bearing organic linker. Coordination occurs through a single cyanimine functionality where the nitrile nitrogen and the imine nitrogen each bind a separate Mn^{III} metal site. Despite the lack of an organic radical, ordering for these compounds is observed with T_cs from 2 to 5.1 K and is attributed to long-range coupling between the manganese sites.[7]

To extend this family of materials, we have investigated the reaction of *meso*-tetraphenylporphinatomanganese(II), MnTPP, with *N*,7,7-tricyanoquinomethanimine (TCQMI) (Figure 5.2). While this reaction was anticipated to form a product that corresponded closely to those of cyanocarbon acceptors such as TCNE and TCNQ, dimerization of TCQMI at the dicyanomethide carbon of the molecule leads to a unique honey-combed structure that exhibited ordering at low temperatures. Spectroscopic, structural, and magnetic data of this compound are reported.

Experimental

Synthesis. The solvents used in the generation of organic radicals were dried, distilled, and deoxygenated prior to use. Steps generating organic radicals were conducted under an inert N_2 atmosphere DriLab glovebox (<1 ppm O_2). TCQMI was synthesized through the combination of two methods,[8] as outlined earlier in this work. Tetraphenylporphyrin was prepared from the procedure developed by Basolo and Summerville.[9]

$[Mn^{III}(TPP)]^{+}[TCQMI]^{\bullet-}$. The compound was formed by dissolving TCQMI (12.8 mg, 0.071 mmol) and Mn^{II}(TPP)(py) (62.0 mg, 0.0731 mmol) in 20 mL of CH_2Cl_2

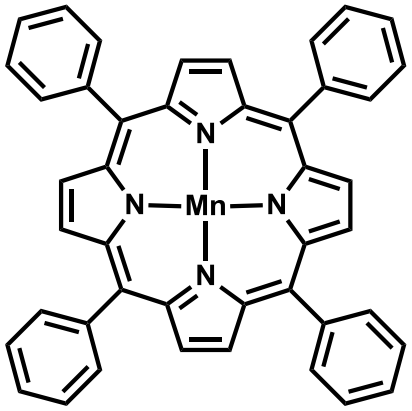

MnTPP

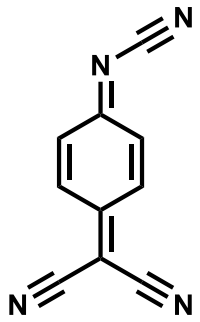

TCQMI

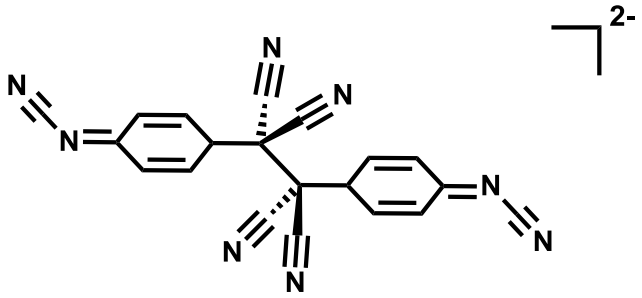

$[TCQMI]_2^{2-}$

Figure 5.2. MnTPP, TCQMI, and $[TCQMI]_2^{2-}$.

each, the porphyrin solution being dark green/black. The solutions were then filtered and combined, but no color change could be discerned due to the dark coloring of the manganese solution. After the solution had stirred for 4 hr at room-temperature, the mixture was layered with an equal volume of hexanes (40 mL) and left to stand for 3 days in an inert-gas glove box. This solution was filtered, capturing dark green/black crystals which were washed with two 5 mL portions of CH_2Cl_2. The largest of the crystals was about 2 mm in length. The crystals were sent for single-crystal X-ray diffraction. Magnetic studies were conducted in a gel cap. [yield: 6.9 mg (11%)]. IR (KBr; cm^{-1}): ν_{CN} 2188 w, 2140 sh, 2106 br.

Physical methods. IR spectra were taken using a Bruker Tensor 37 spectrometer from KBr pellets (±1 cm^{-1}). Magnetic susceptibility data were measured at 1 kOe between 2 and 300 K on a Quantum Design MPMS-5XL 50 kOe SQUID magnetometer equipped with a reciprocating sample measurement system as previously described.[10] Magnetic studies were conducted in a gelatin capsule. Ac susceptibilities were recorded at 33, 100, and 1000 Hz. In addition to correcting for the diamagnetic contribution from the sample holder, the core diamagnetic corrections of -322 x 10^{-6} emu/mol of Mn was used for $[Mn^{III}(TPP)]^{+}[TCQMI]^{\bullet-}$. Instrumental oxygen contamination is responsible for an interruption of the data from 30 - 60 K, though an attempt has been made to minimize the disruption by subtracting out the oxygen moment.

X-ray structure determination. The single crystal structure of $[Mn^{III}(TPP)]^{+}[TCQMI]^{\bullet-}$ was determined on a Nonius KappaCCD diffractometer equipped with Mo Kα radiation in the lab of Dr. Arnold Rheingold at the University of California, San Diego campus. All the reflections were merged and only those for which $I_o > 2\sigma(I)$ were included in the refinement, where $\sigma(F_o)^2$ is the standard deviation based

on counting statistics. The data for $[Mn^{III}(TPP)]^{+}[TCQMI]^{\bullet-}$ were integrated using the Bruker SAINT software program.[11] The structure was solved by a combination of direct methods and heavy atom methods. Patterson methods and the refinement by full-matrix least-squares methods using SHELXL-97 were used for the structures of $[Mn^{III}(TPP)]^{+}[TCQMI]^{\bullet-}$. All the nonhydrogen atoms were refined with anisotropic displacement coefficients. Hydrogen atoms were assigned isotropic displacements U(H) = 1.2U(C), and their coordinates were allowed to ride on their respective carbons using SHELXL97.[12]

Results and Discussion

Spectroscopic studies. The reaction of Mn^{III}(TPP)(py) and TCQMI forms nonsolvated $[Mn^{III}TPP][TCQMI]$. TCQMI was reduced, as evidenced by the ν_{CN} IR (KBr) absorptions being shifted from 2230 and 2169 cm^{-1} for $TCQMI^{o}$ to 2188 and 2106 cm^{-1} in the anion, $TCQMI^{2-}$. This is consistent with shifts seen in this compound and other cyano-acceptors upon reduction.[13] It is interesting to note this shift is consistent with radical formation, even though the compound dimerized. Additionally, the ν_{CN} at 2188 cm^{-1} is seen to be much broader than that of the neutral TCQMI. Similar broadening is seen in nitrile groups upon coordination to metal centers.[14]

Structure. The structure of $[Mn^{III}(TPP)]^{+}[TCQMI]^{\bullet-}$ was determined from single crystal X-ray diffraction, and consists of a warped MnTPP with an average Mn-N distance of 2.023 Å, and a σ-$[TCQMI]_2^{2-}$ dimer. $[TCQMI]_2^{2-}$ dimerizes with a $(NC)_2C$-$C(CN)_2$ linkage with a long 1.60(1) Å central C-C bond (Figure 5.3). Selected crystallographic parameters for {$[Mn^{III}TPP]_2[TCQMI]2$} are reported in Table 5.1. This bond length is in accord with bond lengths exhibited by the related σ-dimers of $[TCNQ]^{\bullet-}$

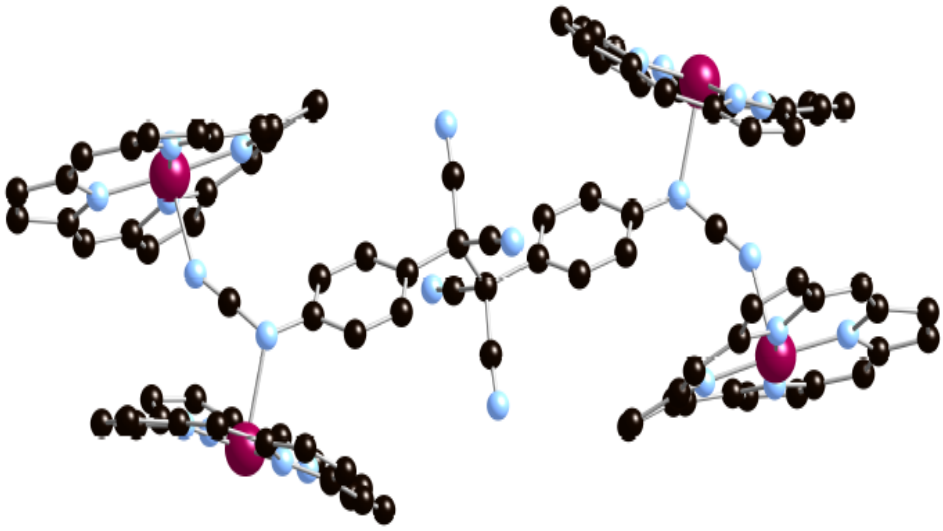

(a)

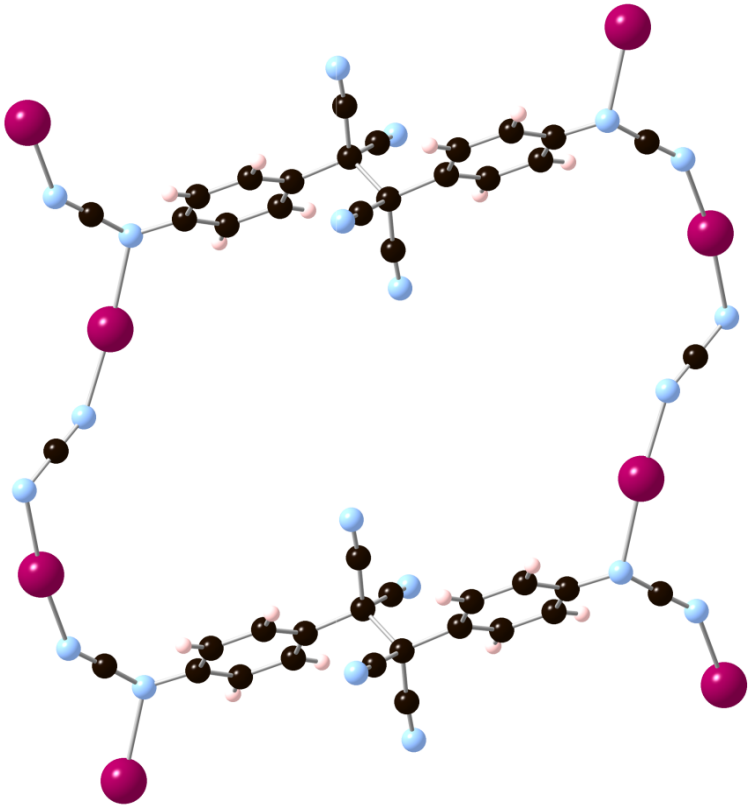

(b)

Figure 5.3. Structure of {[Mn^{III}TPP]$_2$[TCQMI]$_2$} showing linking of chains for formation of honeycombed structure.

Table 5.1. Selected crystallographic parameters for {[$Mn^{III}TPP$]$_2$[TCQMI]$_2$}.

	{[$Mn^{III}TPP$]$_2$[TCQMI]$_2$}
mol formula	$C_{54}H_{32}MnN_8$
mol wt, daltons	847.82
crystal system	Monoclinic
space group	$P2_1/c$
Z	4
temp, K	100(2)
a, Å	17.6731(15)
b, Å	22.610(2)
c, Å	11.5115(9)
α, deg	90
β, deg	107.230(6)
γ, deg	90
V, Å^3	4393.5(6)
calcd density, g/cm^3	1.282
wavelength, Å	1.54178
absorpn coeff, mm^{-1}	2.810
F(000)	1748
min 2θ; deg	3.91
max 2θ; deg	63.81
reflections collected	19749
unique reflections	7074
GoF	1.048
R_1	0.0578
wR_2	0.1430

(~1.6 Å)[15] and $[TCNE]^{\bullet-}$ [1.59(2) Å].[16-20]

Structural comparison of σ-$[TCQMI]_2^{2-}$ and neutral TCQMI[21] (Table 5.2) indicated a general pattern of contraction of the nitrile C-N bonds (C1-N1, C3-N2, C10-N4) and C-C bonds (C4-C5, C4-C9, C6-C7, C7-C8) in the six-membered-ring. The nitrile bonds shortened by an average of 0.022 Å (1.9%) while the six-membered-ring single bonds contracted by an average of 0.055 Å (3.8%). This was accompanied by elongation of exocyclic C2-C4 (0.175 Å, 12.8%) and C7-N3 (0.087, 6.6%) bonds as well as the ring double bonds, C5-C6 and C8-C9. The double bonds lengthened by an average of 0.033 Å (2.5 %), though these bonds were not equivalent to each other in the dimer, possibly due to steric constraints. The same general trend in change of bond lengths is observed in the radical anion of TCQMI seen in $[FeCp^*_2][TCQMI]$.[22] The exception to this trend are the dicyanomethylene nitrile bonds (C1-N1, C3-N2), which showed increases in bond length in the radical.[21] The change in bond lengths was attributed to the addition of electrons into antibonding π-orbitals of the compound.

The linear NCN moiety bonds to two Mn^{III} ions in a $\mu_{1,3}$-bridging manner with 2.382 and 2.241 Å separations. The bond lengths of the NCN segment (1.318 Å and 1.161 Å) indicate a resonance structure more similar to a cyanimine (N-C≡N) than a carbodiimide (N=C=N) moiety. This is an interesting result as previous findings have shown that $Mn^{II}NCN$ compounds contain a NCN^{2-} carbodiimide moiety with two equivalent C-N bonds 1.23 Å long.[7] However, a series of Mn^{III}(salen) compounds bridged by hydrogencyanamide (HNCN) are consistent with our structure as they exhibit the cyanamide form with two different C-N bonds of 1.294(4) and 1.171(4) Å.[7a,b] The factor in determining the resonance structure of the NCN moiety may be the oxidation state of the metal site.

Table 5.2. Bond length comparison of neutral TCQMI, $TCQMI^{\bullet-}$, and $TCQMI^{2-}$.

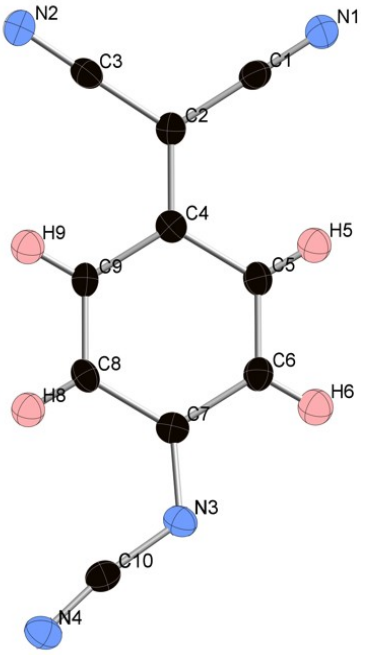

	TCQMI[21]	$[Fe^{III}Cp^*_2][TCQMI]$[22]	[MnTPP][TCQMI]
C2-C4	1.372(2)	1.410(3)	1.547(6)
C1-N1	1.149(2)	1.1828(9)	1.122(5)
C3-N2	1.152(2)	1.1828(5)	1.135(5)
C4-C5	1.450(2)	1.3900(6)	1.384(7)
C4-C9	1.451(2)	1.390(1)	1.399(5)
C5-C6	1.343(2)	1.390(3)	1.382(5)
C8-C9	1.345(2)	1.390(3)	1.372(5)
C6-C7	1.452(3)	1.390(1)	1.403(5)
C7-C8	1.452(2)	1.3900(6)	1.398(7)
C7-N3	1.313(2)	1.271(3)	1.400(5)
C10-N3	1.345(2)	1.312(1)	1.318(4)
C2-C2'	-	-	1.612(6)

The warped porphyrin rings adopt a staggered orientation, with alternating planes canted. Warping of porphyrins, particularly of TPP, has been ascribed to the porphyrin shifting to allow more favorable overlap between its orbitals and those of the central metal.[24] This is most likely due to the steric constraints of the dimer. Hence, $Mn^{III}NCNMn^{III}$ linkages with 6.204-Å Mn•••Mn separations are present, and the $S = 2$ Mn^{III}'s are not bonded to a radical and $[Mn^{III}TPP][TCQMI]$ is best formulated as $\{[Mn^{III}TPP]^{+}\}_2$-$[TCQMI]_2^{2-}$.

The MnNCNMn linkages lead to 1-D chains that are cross-linked by the σ-$[TCQMI]_2^{2-}$ dimer. This leads to a honeycomb, 2-D layered structure with 24-membered rings (Figure 5.3). This motif is similar to that reported for tetrakis(2,4,6-triphenylmethyl)porphinato-manganese(III) $[TCNQ]^{\bullet-}$ that possesses $[TCNQ]_2^{2-}$;[15a] however, the porphyrin ring is planar in that compound. The porphyrin plane warping observed for $[Mn^{III}TPP][TCQMI]$ is attributed to greater steric interactions for the shorter MnNCNMn (vs. MnNCCCNMn).

Magnetic studies. The $\chi T(T)$ of $[Mn^{III}TPP]_2[TCQMI]_2$ is 3.13 emuK/mol at 300 K in accord with the spin-only expectation of 3.00 emuK/mol for $S = 2$ Mn^{III}, and diamagnetic $[TCQMI]_2^{2-}$ (Figure 5.4). This is comparable to that reported for tetrakis(2,4,6-triphenylmethyl)porphinato-manganese(III) $[TCNQ]^{\bullet-}$.[15a] Unlike tetrakis(2,4,6-triphenylmethyl)porphinato-manganese(III) $[TCNQ]^{\bullet-}$, however, upon cooling the $\chi T(T)$ decreases, and fitting $\chi T(T)$ above 20 K to the Curie-Weiss expression, $\chi \propto (T - \theta)^{-1}$, gives θ = -19.2 K indicative of significant antiferromagnetic coupling. This deviates from the $[Mn^{III}TPP][TCNE]$ family of ferrimagnets,[2,3] as they have effective θ''s that are significantly positive. Above 15 K, the $\chi T(T)$ data were fit to the 1-D chain

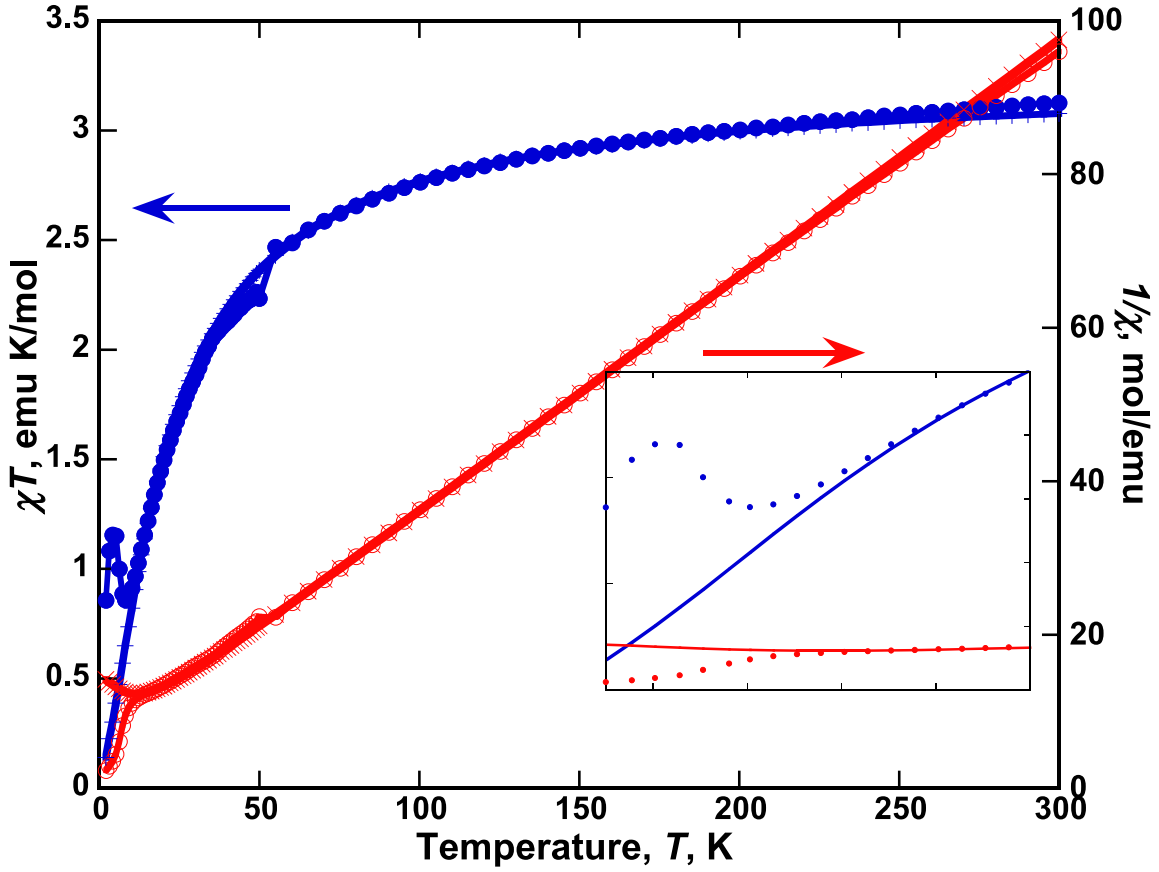

Figure 5.4. $\chi T(T)$ and $1/\chi(T)$ of $\{[Mn^{III}TPP]_2[TCQMI]_2\}$ from 2-300 K. Oxygen contamination was subtracted from the measurement.

model, eq 5.1, developed by Fisher and later modified by Smith and Friedberg,[25] with g = 2.08 and J/k_B = -2.00 K (-1.39 cm^{-1}; -4.00 cal/mol).

$$\chi T = \frac{N g^2 \mu_B{}^2 S(S+1)(1-u)}{3k_B T(1+u)}$$
$$u = \frac{T}{T_0} - \coth\frac{T_0}{T} \quad \text{and} \quad T_0 = \frac{2JS(S+1)}{3k_B T} \tag{5.1}$$

$\chi T(T)$ continues to decrease with decreasing temperature until ~8 K, where it begins to rise to a maximum of 1.19 emuK/mol at 4 K before decreasing again. The low magnetization is thought to arise from the spin canting of the Mn^{III} spin sites.

Evidence of magnetic ordering can be seen from the in-phase, $\chi'(T)$, and out-of-phase, $\chi''(T)$ components of the ac susceptibility (Figure 5.5). The peak of the 33 Hz component occurs at 3.65 K, while the rise in $\chi''(T)$ upon cooling at 3.76 K provides another value of T_c, which averages 3.7 K. Both $\chi'(T)$ and $\chi''(T)$ are frequency-dependent below 4 K, indicating either a spin-glass or superparamagnetic state.[26]

This ordering temperature is in close agreement with the bifurcation temperature (T_b) observed below ~3.2 K observed from the zero-field-cooled (ZFC) and field-cooled (FC) magnetization data (Figure 5.6). The origin of the canted antiferromagnetic/weak ferromagnetic ordering is attributed to the close proximity of the of the Mn^{III} sites. Similar behavior is seen in Mn^{III}(salen) sites bridged by hydrogencyanamide in a $\mu_{1,3}$-mode with ordering temperatures observed below 2.5 K.[23] However, in contrast to these hydrogen cyanamide-bridged Mn^{III} compounds, no hysteresis loop is evident for $[Mn^{III}TPP]_2[TCQMI]_2$ and saturation magnetization is not

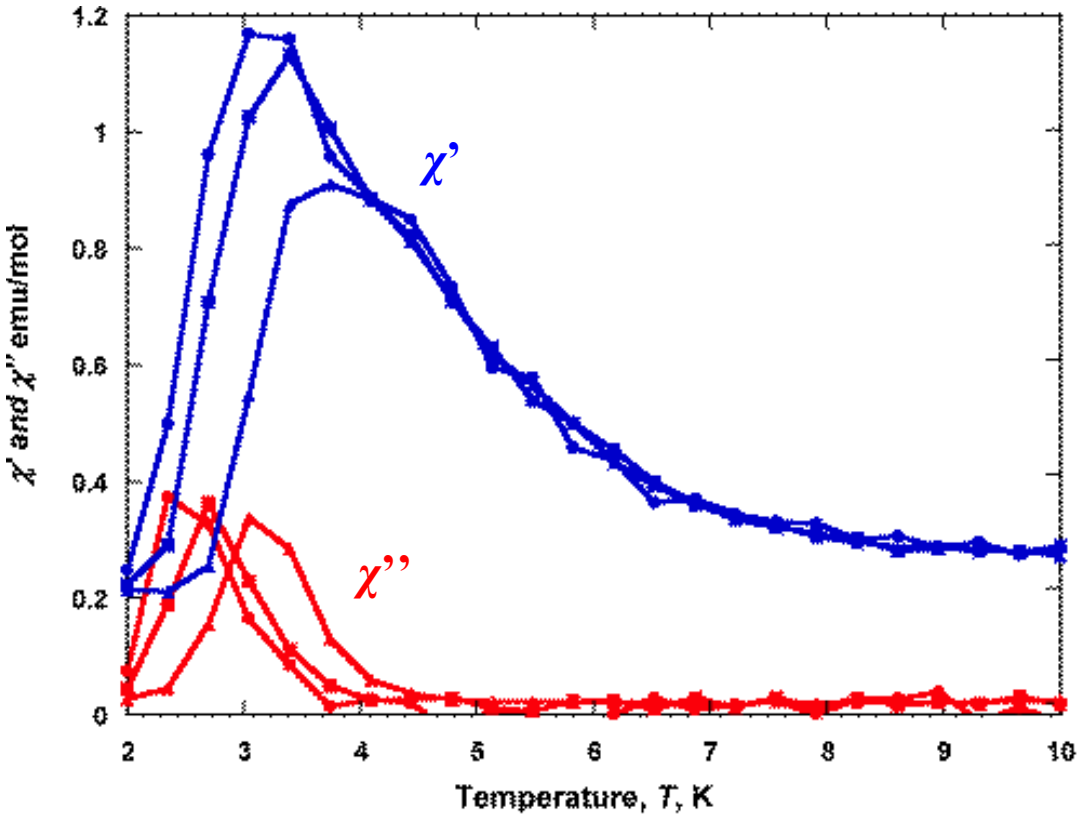

Figure 5.5. Ac susceptibility of {[$Mn^{III}TPP]_2[TCQMI]_2$} at 33(●) , 100 (■), and 1000 (▲) Hz.

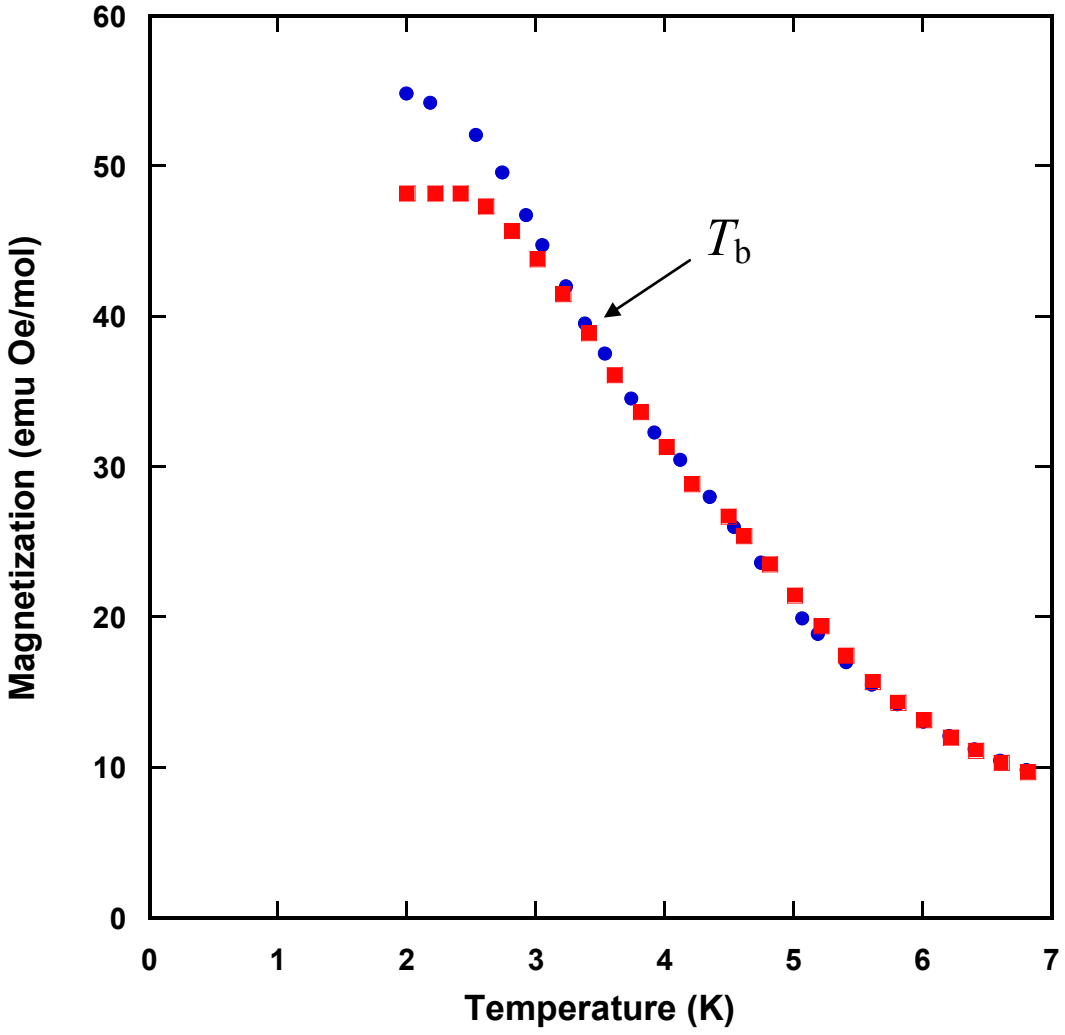

Figure 5.6. ZFC (■)/FC(●) of {[$Mn^{III}TPP]_2[TCQMI]_2$} from 2-7 K indicating the bifurcation temperature, T_b.

achieved at 90 kOe.

Conclusions

The reaction of $Mn^{II}TPP$ and TCQMI forms reduced TCQMI. Rather than 1-D chains of alternating $[Mn^{III}TPP]^{+}$ and $[TCQMI]^{\bullet-}$, μ_4-σ-$[TCQMI]_2^{2-}$ form with a $(NC)_2C$-$C(CN)_2$ linkage with a long 1.60(1) Å central C-C bond. A similar dimerization has been noted for TCNE and TCNQ and the bond length was in accord with those exhibited by related σ-dimers. Mn^{III} ions were bonded by the N-C-N functionality in a $\mu_{1,3}$-bridging manner with Mn-N bond lengths of 2.382 and 2.241 Å. The carbon-nitrogen bond lengths within the NCN fragment (1.318 Å and 1.161 Å) suggest the structure is best described as a cyanimine (N-C≡N) rather than a carbodiimide (N=C=N) moiety. Considerable warping of porphyrin plane was noted, the shifting most likely allowing a more favorable overlap between the plane orbitals and those of the central metal. The rings are seen to adopt a staggered orientation, with alternating planes canted, forming a 2-D honeycomb layered structure with 24-membered rings.

The low magnetic ordering temperature is attributed to the lack of a spin-bearing organic bridge due to the dimerization. These results indicate that increased magnetic properties (higher T_c, hystereses) might be possible if the compound could be modified to inhibit dimerization. Since it appears that dimerization is typically observed at the -$C(CN)_2$ carbon of TCQMI, TCNE, and TCNQ, it is envisioned that replacing that functionality with an oxygen or nitrogen might be a feasible route. This line of research is currently being pursued through the synthesis of new asymmetric cyanocarbon acceptors.

References

(1) Rittenberg, D.K.; Miller, J.S. *Inorg. Chem.* **1999**, *38*, 4838.

(2) Rittenburg, D.K.; Sugiura, K.-i.; Sakata, Y.; Mikami, S.; Epstein, A.J.; Miller, J. S. *Adv. Mater.* **2000**, *12*, 126.

(3) Miller, J.S.; Epstein, A. *J. Chem. Commun.* **1998**, 1319.

(4) Johnson, M.T.; Arif, A.M.; Miller, J.S.; *Eur. J. Inorg. Chem.* **2000**, *6*, 1781.

(5) Sugiura, K.-i.; Mikami, S.; Johnson, M.T.; Raebiger, J.W.; Miller, J.S.; Iwasaki, K.; Okada, Y.; Hino, S.; Sakata, Y. *J. Mater. Chem.* **2001**, *11*, 2151.

(6) Brandon, E.J.; Burkhart, B.M.; Rogers, R.D.; Miller, J.S. *Chem. -Eur. J.* **1988**, *8*, 1938.

(7) (a) Yuan, M.; Gao, S.; Sun, H.-l.; Su, G.; *Inorg. Chem.* **2004**, *43*, 8221. b) Yuan, M.; Zhao, F.; Zhang, W.; Pan, F.; Wang, Z.-m.; Gao, S. *Chem. Eur. J.* **2007**, *13,* 2937. c) Wang, T.-t.; Xie, J.-m.; Xia, C.-k.; Wu, Y.-l.; Jing, J.-j. *Z. Anorg. Allg. Chem.* **2010**, *636*, 1580.

(8) (a) Bryce, M.R.; Davies, S.R.; Grainger, A.M.; Hellberg. J.; Hursthouse, M.B.; Mazid, M. Bachmann, R.; Gerson, F. *J. Org. Chem.* **1991**, *57*, 1690. (b) Iwatsuki, S.; Itoh, T.; Itoh, H. *Chem. Lett.* **1988**, *17*, 1187.

(9) Jones, R.D.; Summerville, D.A.; Basolo, F. *J. Am. Chem. Soc.* **1978**, *100*, 4416.

(10) Brandon, E. J.; Rittenberg, D.K.; Arif, A.M.; Miller, J.S. *Inorg. Chem.* **1998**, *37*, 3376.

(11) (a) Saint Plus, v. 6.02; Bruker Analytical X-ray: Madison, WI 1999. (b) Sheldrick G. M. SADABS; University of Göttingen: Göttingen, Germany, 1996.

(12) (a) Goldberg, I.; Krupitsky, H.; Stein, Z.; Hsiou, Y.; Strouse, C.E. *Supramol. Chem* **1995**, *4*, 203. (b) Krupitsky, H.; Stein, Z.; Goldberg, I. *J. Inclusion Phenom. Mol. Recognit. Chem.* **1995**, *20*, 211. (c) Goldberg, I. *Mol. Cryst. Liq. Cryst*. **1996**, *278*, 767. (d) Byrn, M.P.; Curtis, C.J.; Hsiou, Y.; Kahn, S.I.; Sawin, P.A.; Tendick, S.K.; Terzis, A.; Strouse, C.E. *J. Am. Chem. Soc*. **1993**, *115*, 9480. Byrn, M.P.; Curtis, C. J.; Hsiou, Y.; Khan, S.I.; Sawin, P.A.; Terzis, A.; Strouse, C.E. in *Comprehensive Supramolecular Chemistry*; Atwood, J.L., Davies, J.E.D., MacNicol, D.D., Vogtle, F., Eds.; 1996; Vol. 6, p 715.

(13) (a) Miller, J.S.; Zhang, J.H.; Reiff, W.M.; Preston, L.D.; Reis, Jr., A.H.; Gerbert, E.; Extine, M.; Troup, J.; Ward, M.D. *J. Phys. Chem.* **1987**, *91*, 4344. (b) Miller, J.S.; Calabrese, J.C.; Epstein, A. J.; Bigelow, R.W.; Zhang, J.H.; Reiff, W.M.; *J. Chem. Soc. Chem. Commun.* **1986**, 1026. (c) Miller, J.S.; Epstein, A.J.; Reiff, W.M. *Science*, **1988**, *240*, 40.

(14) Aumüller, A.; Peter, E.; Hünig, S.; Meixner, H.; von Schütz, J.-U.; Werner, H-P. *Liebigs Ann. Chem.* **1987**, 997.

(15) (a) Mikami, S.; Sugiura, K.-i.; Miller, J.S.; Sakata, Y. *Chem. Lett.* **1999**, *28*, 413. (b) Zhao, H.; Heinz, R.A.; Dunbar, K.R.; Rogers, R.D. *J. Am. Chem. Soc.* **1996**, *118*, 12844. (c) Harms, R.H.; Keller, H.J.; Nöthe, D.; Werner, M.; Grundel, D.; Sixl, H.; Soos, Z.G.; Metzger, R.M. *Mol. Cryst. Liq. Cryst.* **1981**, *65*, 179. (d) Hoffman, S.K.; Corvan, P.J.; Singh, P.; Sethuklekshmi, C.N.; Metzger, R.M.; Hatfield, W.E. *J. Am. Chem. Soc.* **1983**, *105*, 4608. (e) Dong, V.; Endres, H.; Keller, H.J.; Moroni, W.; Nöthe, D. *Acta Crystallogr.* **1977**, *B33*, 2428.

(16) Zhang, J.; Liable-Sands, L.M.; Rheingold, A.R.; Del Sesto, R.E.; Gordon, D.C.; Burkhart, B.M.; Miller, J. S. *Chem. Commun.* **1998**, *13*, 1385.

(17) Miller, J.S. *Angew. Chem., Int. Ed.* **2006,** *45*, 2508; *Angew. Chem.* **2006**, *118*, 2570.

(18) Pokhodnya, K.I.; Bonner, M.; DiPasquale, A.G.; Rheingold, A.L.; Miller, J.S. *Chem. -Eur. J.* **2008**, *14*, 714.; *Angew. Chem.* **2007**, *119*, 1543.

(19) Her, J.-h.; Stephens, P.W.; Pokhodnya, K.I.; Bonner, M.; Miller, J.S. *Angew. Chem., Int. Ed.* **2007**, *46*, 1521.

(20) Stone, K.H.; Stephens, P.W.; McConnell, A.C.; Shurdha, E.; Pokhodnya, K.I.; Miller, J.S.; *Adv. Mater.* **2010**, *22*, 2514.

(21) This work, chapter 3.

(22) This work, chapter 4.

(23) Liu, X. Krott, M.; Müller, P.; Hu, C.; Lueken, H.; Dronkskowski, R. *Inorg. Chem.* **2005**, *44*, 3001.

(24) (a) Scheidt, W.R.; Reed, C.A. *Chem. Rev.* **1981**, *81*, 543. (b) Scheidt, W.R. *J. Porphyrins Phthalocyanines* **2008**, *12*, 979.

(25) Smith, T.; Friedberg, S.A. *Phys. Rev.* **1968**, *176*, 660.

(26) Mydosh, J. *Spin Glasses*; Taylor and Francis: Washington, DC, 1993; pp 66-67.

CHAPTER 6

STRUCTURE AND MAGNETOSTRUCTURALCORRELATION OF FERRIMAGNETIC *MESO*-TETRAPHENYLPORPHINATO MANGANESE(III)DIMETHYL,*N*,*N*'-DICYANOQUINONE DIIMINIDE,$[MNTPP]^{+}[ME_2DCNQI]^{\bullet -}$

Introduction

$[Mn^{III}(porphyrin)]^{+}[TCNE]^{\bullet -}$ (TCNE = tetracyanoethylene) organic-based ferrimagnets[1,2] are a large, well-studied family, as many members have been both structurally and magnetically characterized. In all cases the structures have parallel 1-D chains of alternating $S = 2$ $[Mn^{III}TPP]^{+}$ [TPP = *meso*-tetraphenylporphinato] cations, and bridging $S = 1/2$ μ-$[TCNE]^{\bullet -}$ anions. Members differ in their solvate (Sol) of the parent [MnTPP][TCNE], e.g., [MnTPP][TCNE]•xSol, or the substitution in the phenyl groups of the $[MnTPP]^{+}$. In addition, the TCNE electron acceptor has been substituted with other acceptors that can oxidize Mn^{II}(porphyrin) (= Mpor), as well as μ-bridge to two $[Mn^{III}(porphyrin)]^{+}$s to form a 1-D chain. Examples include hexacyanobutadiene,[3] chloranil,[4] 2,5-dimethyl-7,7,8,8-tetracyano-*p*-quinodimethane (Me_2TCNQ),[5] and perfluro-7,7,8,8-tetracyano-*p*-quinodimethane ($TCNQF_4$).[6] In contrast, use of tetracyano-p-quinodimethane (TCNQ) forms a honeycomb structure possessing μ_4-$[TCNQ]_2^{2-}$ bridges.[7] With a substituted porphyrin, 2,5-dimethoxy- ($(MeO)_2DCNQI$) and 2,5-dimethyl-*N*,*N*'-dicyanoquinonediimine (Me_2DCNQI) were reported.[8] All compounds

possess a radial anion, magnetically order as ferrimagnets ($T_c \leq 28$ K),[9] exhibit spin-glass behavior, and have coercive fields as great as 27 kOe at 2 K.[10]

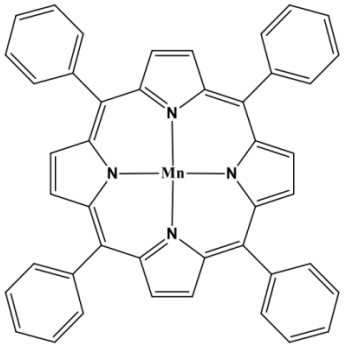

$Mn^{II}TPP$

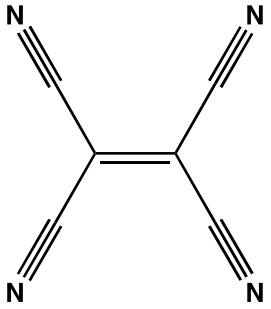

TCNE

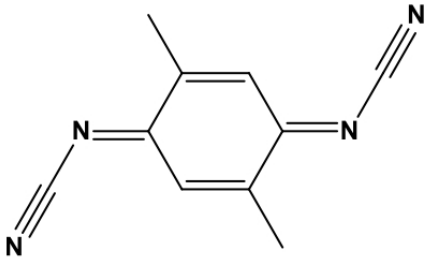

Me_2DCNQI

The dominant spin coupling for members of the $[Mn^{III}(porphyrin)]^{+}[TCNE]^{\bullet-}$ family of ferrimagnets is the intrachain antiferromagnetic coupling (J_{intra}) between the $S = 2$ and $S = 1/2$ sites.[11] A fit of temperature dependence of the magnetic susceptibility, $\chi(T)$, as $\chi^{-1}(T)$, to the Curie-Weiss expression, $\chi \propto (T - \theta)^{-1}$, where θ is the temperature at which the extrapolated linear fit intercepts the abscissa and $\theta > 0$ reflects ferromagnetic coupling while $\theta < 0$ reflects antiferromagnetic coupling. While the latter is sometimes observed at higher temperatures, the former, θ', is observed at reduced temperatures, and indicates short-range, ferromagnetic-like interactions. Higher values of θ' suggest stronger intrachain coupling, J_{intra}.[11]

Another approach to obtain J_{intra} is from a fit of the $\chi T(T)$ data to the Seiden model[12] for isolated chains ($J_{inter} = 0$) of alternating quantum $S = 1/2$ and classical $S = 2$ spins. As the model assumes the chains are isolated, a fit cannot account for the interchain (2- and 3-D) interactions. At higher temperatures, the $\chi T(T)$ data for the [Mn(porphyrin)][TCNE] family can be fit to the Seiden expression, indicating that J_{intra} is

sufficient (i.e., $J_{inter} = 0$) to model the data. In contrast, $\chi T(T)$ deviates from the fit to the Seiden expression at low temperatures, as growing magnetic correlations along the chains amplify the effect of a weak J_{inter}. The $\chi T(T)$ data have a minimum, indicative of antiferromagnetic coupling leading to ferrimagnetic behavior.[13]

An inverse linear correlation between θ' and (a) the dihedral angle between the $[Mn(porphyrin)]^+$ and the $[TCNE]^{\cdot-}$ mean planes, and (b) the $\angle$Mn-(N-C)$_{TCNE}$ has been previously reported for a series of substituted [MnTPP][TCNE]•2PhMe.[11,14] Attempts to obtain meaningful correlations with the Mn-N_{TCNE} and Mn•••Mn distances, or the $\angle$Mn-Mn-N_{TCNE} etc. were unsuccessful.[14] This correlation works well for TCNE-based examples, but insufficient data are available to extend it to electron acceptors other than TCNE. Herein we add another example of an aromatic-based electron acceptor to extend the model.

Experimental

Synthesis. All manipulations involving reduced [Me_2DCNQI] were carried out under N_2 using standard Schlenk techniques or in a Vacuum Atmospheres DriLab ($\leq$1 ppm O_2). Solvents used for the preparation of the radical [TCNE] salts were predried and distilled from appropriate drying agents. H_2TPP was prepared by the Alder-Longo method,[15] and [MnTPP][OAc] was prepared from H_2TPP and $Mn(OAc)_2$•$4H_2O$; the $Mn(OAc)_2$•$4H_2O$ was dissolved in *N*,*N*-dimethylformamide and filtered to remove paramagnetic impurities prior to the addition of H_2TPP. The [MnTPP][OAc] was subsequently reduced to MnTPP as the pyridine adduct, MnTPP(py), by $NaBH_4$, utilizing a literature method.[16] Me_2DCNQI was made via Aumüller and Hünig's method[17] from 2,5-dimethyl-*p*-benzoquinone and bis(trimethylsilyl)carbodiimide.

[MnTPP][Me_2DCNQI]. [MnTPP][Me_2DCNQI] was prepared by the reaction of filtered solutions of MnTPP(py) (58.1 mg, 0.062 mmol) dissolved in 10 mL of CH_2Cl_2 and Me_2DCNQI (14.8 mg, 0.080 mmol) dissolved in 12 mL of CH_2Cl_2. Subsequently, the filtered dark green porphyrin solution was added dropwise to the yellow diimine-containing solution. Due to the intense color of the porphyrin solution, a color change indicating redox chemistry could not be observed. The combined solution was stirred at room-temperature for 3.5 h before being poured into a glass container. An equal volume of hexanes (~20 mL) was layered over the dark green solution. The solution was allowed to sit in an inert atmosphere glove box (<1 ppm O_2) for 5 days before the resulting black/green powder was collected by filtration. The filtrate was washed several times with hexanes and dried under strong vacuum. [Yield: 7.0 mg (13%)]. IR (KBr; cm^{-1}): ν_{CN} 2101 s.

Physical methods. Infrared spectra were recorded from 400 to 4000 cm^{-1} on a Bruker Tensor 37 infrared spectrophotometer (±1 cm^{-1}) with a KBr pellet. Magnetic susceptibility measurements were made between 5 to 300 K using a Quantum Design (QD) MPMS-5 50-kOe SQUID magnetometer with a sensitivity of 10^{-8} emu or 10^{-12} emu/Oe at 10 kOe and equipped with the ultra-low field (~2 mOe), reciprocating sample measurement system, and continuous low-temperature control with enhanced thermometry features, as previously reported.[18] The temperature dependence of the dc magnetization was obtained by cooling in zero-field, and the data were collected on warming in a 5 Oe applied field. Ac susceptibilities were measured on a QD Physical Properties Measurement System (PPMS). Data were collected from 2 to 300 K and samples at 10, 100, and 1000 Hz. Samples were prepared in the same manner as the MPMS magnetization samples and in most cases the same sample was used. The

diamagnetic contribution from the sample holder was corrected for as well as the core diamagnetic corrections noted below. The diamagnetic correction for the sample was -755 x 10^{-6} emu/mol and was calculated using Pascal's constants.

X-ray structure determination. The polycrystalline compound was sealed in a thin-wall capillary under an inert atmosphere, and high-resolution powder diffraction patterns were collected at X16C beamline of the National Synchrotron Light Source, Brookhaven National Laboratory. A Si(111) channel-cut monochromator selected a 0.699275 Å highly parallel incident beam. The diffracted X-rays were analyzed by Ge(111) single-reflection crystal and detected using NaI scintillation counter. The wavelength and diffractometer zero position were calibrated by measuring a sample of NIST standard reference material 1976 (sintered plate of Al_2O_3). All measurements were done at room-temperature and the capillaries were spun during data collection for better averaging of powder pattern.

The TOPAS-Academic (TA) program was used to index, solve, and refine the crystal structure.[19-21] From the volume of the unit cell, the central Mn atom of the porphyrin molecule and the center of the TCNE were expected to reside on crystallographic inversion centers. After fixing the Mn atom and geometric center of the Me_2DCNQI molecule at two distinct inversion centers, simulated annealing was used to solve the structure. The process was repeated using all pairs of inversion centers to guarantee the best solution. Using this initial solution from simulated annealing, Rietveld refinement was used to improve the fits and optimize bond lengths, angles, and torsions.

Both of the molecules were defined as rigid bodies, with similar bonds and angles (e.g,. aromatic bonds, C-C single bonds) refined jointly to a single value. The MnTPP

was restricted to having D_{2h} symmetry, with the exception of torsion angles of the phenyl groups that were allowed to differ. Allowing deviation from this symmetry did not significantly improve the quality of the Rietveld fit.

Results and Discussion

Synthesis. Oxidation of $Mn^{II}TPP(py)$ with Me_2DCNQI forms $[Mn^{III}TPP][Me_2DCNQI]$, which forms crystals too small for a single crystal X-ray analysis. The IR ν_{CN} absorption occurs at 2101 cm^{-1} in agreement with 2103 cm^{-1} observed for [MnTmesPP][Me_2DCNQI] (TmesPP = tetramesitylporphinato),[8] and shifted -87 cm^{-1} from 2188 cm^{-1} for Me_2DCNQI[22] in accord with a one-electron reduction. Key structural and magnetic properties of $[Mn^{III}TPP][Me_2DCNQI]$ are listed and compared to similar compounds in Table 6.1.

Structure. The structure of [MnTPP][Me_2DCNQI] was determined by analysis of the synchrotron powder diffraction data based upon the chemical composition as discussed in the experimental procedure. The Rietveld refinement fit to the data was performed, and the crystallographic parameters are summarized in Table 6.2.

The structure of [MnTPP][Me_2DCNQI] is fully ordered with both the cation and anion residing on a center of symmetry (Figure 6.1). The intra-cation distances are similar to that reported for $[MnTPP]^{+}$.[2a,3b,4,8,24] The Me_2DCNQI radical is planar with an *exo*-cyclic methylene bond of 1.334(7) Å. This is only slightly longer than the neutral compound (1.319 Å)[24] and shorter than the analogous bond in [MnTmesPP][Me_2DCNQI] (1.356 Å),[8] but is consistent with the introduction of a negative charge into the compound. The bond length of the cyanimine (N-C≡N) groups can also be used to determine the ionicity of these bonds [N-C: 1.299(10) Å; N≡C:

Table 6.1. Summary of the IR, structural, and magnetic properties of [MnTPP][Me_2DCNQI]•zS and related compounds.

M^{III}(Por)	MnTPP	MnTmesPP	MnTmesPP	MnTmesPP	MnT$(OMe)_3$PP
Acceptor, A	Me_2DCNQI	Me_2DCNQI	$(MeO)_2$DCNQI	Me_2TCNQ	$TCNQF_4$
S	-	PhCl	*p*-xylene	*p*-xylene	*o*-$C_6H_4Cl_2$
z	0	4	2	2	3
ν_{CN}, cm^{-1}	2101	2103	2116	2184 2160	2196 2165
θ', K	13	24[b]	37[b]	23	29
J_{intra}/k_B, K	-40	-50	-90	-39	-71
J_{intra}, cm^{-1}	-28	-35	-63	-27	-49
χ'_{max} [a] (T_c), K (10 Hz)	4.3[c]	6.0	6.2	2.3	7.3
χT_{min}, K	100	150	270	115	215
ϕ	0.18	0.07	0.16	0.17	0.17
H_{cr}, Oe (2 K)	5600	9600	17800	-	17100
M, emuOe/mol (5 T, 2 K)	9400	10200	14200	-	14900
M_r, emuOe/mol (2 K)	6300	10200	14400	-	7200
Mn•••Mn, Intrachain, Å	12.83	12.99	12.80	11.43	12.69
Mn-N_{TCNE} Å	2.182	2.261	2.249	2.345 2.318	2.321
Interchain, Å, **I-II**	11.09	12.52	12.00	11.68	15.20
Mn•••Mn, Interchain, Å, **I-II**	12.42 13.24	12.67 16.69	12.04 16.77	11.76 15.46	15.36 15.40
Interchain, Å, **I-III**	7.79	15.05	13.12	14.45	15.20
Mn•••Mn, Interchain, Å, **I-III**	9.60 10.63	15.55 17.57	14.08 15.19	15.43 15.65	15.36 15.40
Interchain, Å, **I-IV**	11.83	-	14.87	15.11	-
Mn•••Mn, Interchain, Å, **I-IV**	11.94 18.69	-	16.11 16.27	15.66 16.78	-
Interchain, Å, **II-III**	14.95	12.52	20.27	21.50	18.68
Mn•••Mn, Interchain, Å, **II-III**	15.09 19.81	12.67 16.69	20.67 22.07	22.01 22.53	16.95 18.75
Mn-N-C, [o]	143.4	158.4	150.7	141.9 142.5	135.9
MnN_4- A, [o]	84.2	79.1	61.9	49.0 56.8	46.4
ref	this work	8	8	5	6

[a] The temperature at which $\chi'(T)$ has a maximum at 10 Hz.
[b] Regression fit from the data in reference.[8]
[c] An anomalous frequency-independent antiferromagnetic phase has a T_c = 9.6 K (see text).

Table 6.2. Summary of crystallographic parameters for [Mn^{III}TPP][Me_2DCNQI].

	[MnTPP][Me_2DCNQI]
a, Å	9.5949(2)
b, Å	10.63171(13)
c, Å	11.9382(4)
α, °	66.5119(15)
β, °	75.0132(15)
γ, °	78.5620(11)
V, $Å^3$	1072.67(5)
Z	1
Space group	$P\bar{1}$
ρ_{calc}, g/cm^3	1.3187
R_p, %	6.203
R_{wp}, %[a,b]	7.980
T, K	300
GOF (R_{wp}/R_{exp})[b,c]	1.877

[a] $$R_{wp} = \sqrt{\frac{\sum_i w_i (y_i^{calc} - y_i^{obs})^2}{\sum_i w_i (y_i^{obs})^2}}$$

[b] y_i^{calc} and y_i^{obs} are the calculated and observed intensities at the i^{th} point in the profile, normalized to monitor intensity. The weight w_i is $1/\sigma^2$ from the counting statistics, with the same normalization factor. *N* is the number of points in the measured profile minus number of parameters.

[c] $$R_{exp} = \sqrt{\frac{N}{\sum_i w_i (y_i^{obs})^2}}$$

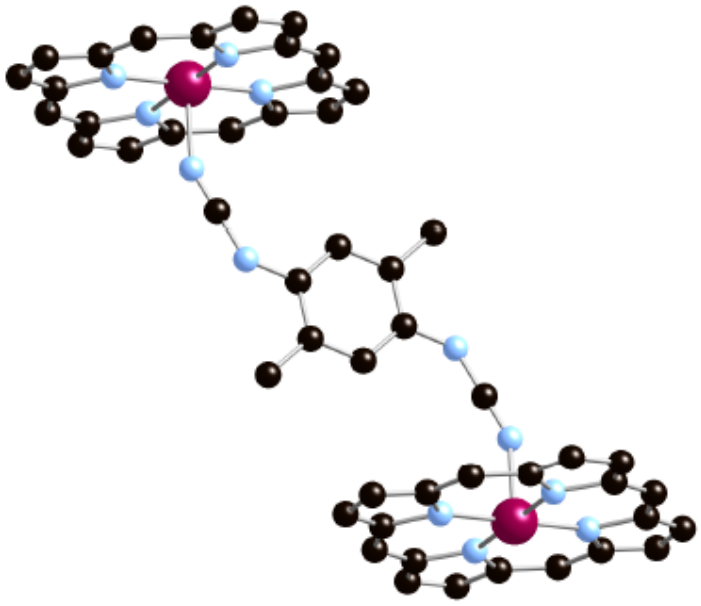

Figure 6.1. Segment of the chain structure for [MnTPP][Me_2DCNQI] (the phenyl rings are omitted for clarity).

1.160(12) Å], and are in good agreement with analogous bonds [N-C: 1.309(6) Å; N≡C: 1.163(6) Å] in [MnTmesP][Me_2DCNQI],[8] and in $[TCNQ]^{\bullet-}$.[25] This further supports the characterization of this compound as being $[Mn^{III}TPP]^{+}[Me_2DCNQI]^{\bullet-}$.

$[Me_2DCNQI]^{\bullet-}$ is uniformly *trans*-μ-*N*-σ-bound to two Mn^{III}'s forming parallel 1-D $\cdots D^{+}A^{\bullet-}D^{+}A^{\bullet-}\cdots$ [D = MnTPP; A = TCNE] as occurs for the entire family of $[Mn^{III}$(porphyrin)][TCNE] ferrimagnets (Figure 6.1).[2a] The $[Me_2DCNQI]^{\bullet-}$ N-Mn distance is 2.154(9) Å. The ∠Mn-N-C and dihedral angle between the mean $Mn(N_4)_{TPP}$ and the $[Me_2DCNQI]^{\bullet-}$ planes are 143.6(7)° and 84.18°, respectively. The ∠Mn-N-C was more similar to that seen in the Mn^{III}(porphyrin) chains linked with reduced Me_2TCNQ[5] and $TCNQF_4$.[6] The angle was smaller than those encountered for both [MnTmesP][Me_2DCNQI] [158.4(4)°] and [MnTmesP][$(MeO)_2$DCNQI] [150.7(2)°],[8] suggestive of poorer intrachain spin coupling.

The arrangements of the unique parallel chains are shown in Figure 6.2 for [MnTPP][Me_2DCNQI]. The chains pack more tightly than is observed for related compounds, as no solvent is present. The nearest chain pair (**I-III**, 7.79 Å) forms out-of-registry, allowing the large porphyrin planes to stagger and thus reducing steric interaction. The more distant **I-II** and **I-IV** chain pairs form out-of- and in-registry (Figure 6.3), respectively. Intrachain Mn•••Mn separation is 12.83 Å, very similar to the intra-Mn•••Mn separations for [MnTmesP][$(MeO)_2$DCNQI] (12.80 Å)[8] and shorter than the intrachain separation for [MnTmesP][Me_2DCNQI] (12.99 Å).[8] Interchain Mn•••Mn distances range from 9.60 (**I-III**) to 18.69 Å (**I-IV**). In general, the separations are slightly smaller than those observed for related compounds, consistent with the observation that these chains pack more tightly, to the exclusion of solvent molecules.

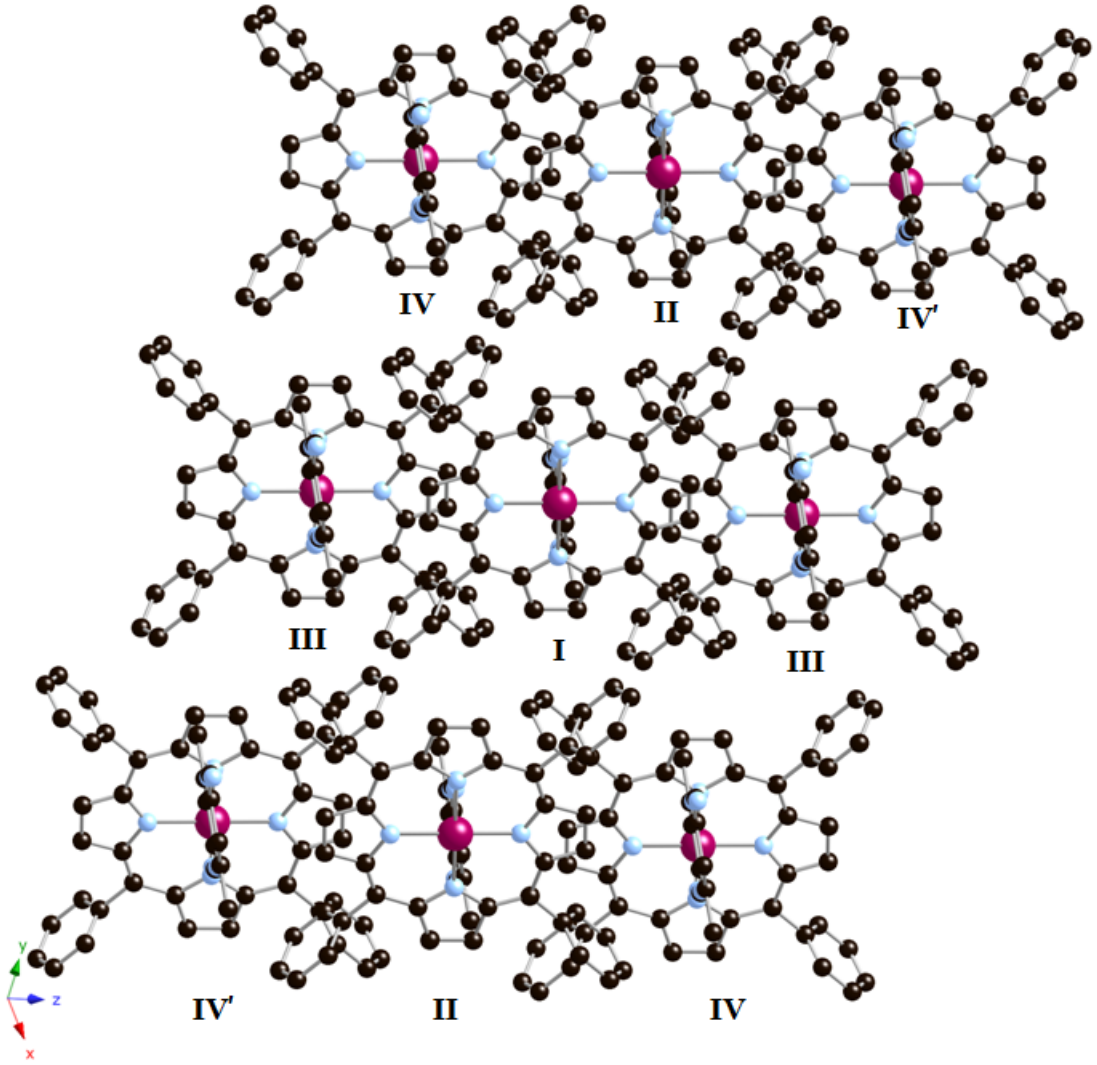

Figure 6.2. View along the chain (*b*) axis for [MnTPP][Me_2DCNQI] showing the interchain interactions.

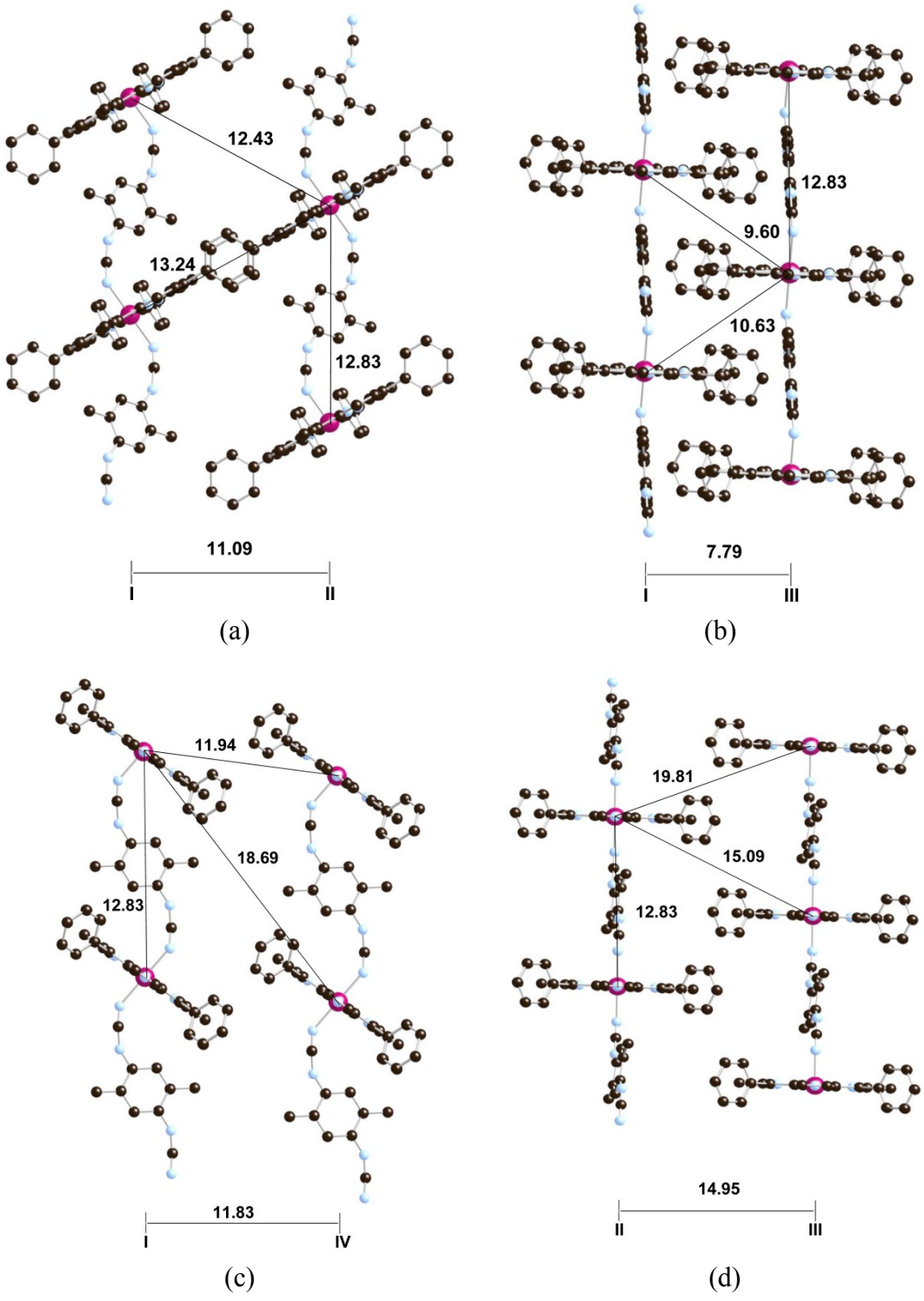

Figure 6.3. Interchain interactions [and important distances (Å)] between unique out-of-by out-registry chains of **I-II** (a), **I-III** (b), and **II-III** (d), and in-registry **I-IV** (c).

The overall structure can be thought of in terms of two repeating planes overlapping each, allowing more dense packing. The planes form in-registry to each other, but slip to accommodate the bulk of the porphyrin phenyl rings. However, there is neither a 2- nor 3-D lattice, as the 1-D chains are not cross-linked by bonds.

Magnetic studies. The 2 to 300 K molar magnetic susceptibility, $\chi(T)$, was measured for [MnTPP][Me_2DCNQI], and plotted as $\chi(T)$ (Figure 6.4) $\chi T(T)$ and $\chi^{-1}(T)$ (Figure 6.5). $\chi(T)$ increases with decreasing temperature, but reaches a maximum at 8.2 K, and has another shoulder at ~4.3 K. This suggests antiferromagnetic ordering. The 300 K χT-value is 2.86 emuK/mol. This is reduced from the expected spin-only value of 3.38 emuK/mol for and $S = 2$ and $S = 1/2$ spins due to antiferromagnetic coupling. This has been previously observed for TCNE analogs.[24a] $\chi T(T)$ remains relatively constant with decreasing temperature until ~70 K (Figure 6.5). Above 125 K, $\chi^{-1}(T)$ is linear and can be extrapolated to θ = -44 K, indicating strong antiferromagnetic coupling. At ~115 K, $\chi^{-1}(T)$ changes slope and the linear region between 20 and 100 K can be extrapolated to an effective θ,[26] θ', of 13 K, indicating short-range ferromagnetic coupling (Figure 6.5).

[MnTPP][Me_2DCNQI] has a minimum, *T*min, in the $\chi T(T)$ at 100 K, indicative of dominant antiferromagnetic coupling.[13] The $\chi T(T)$ data above ~70 K can be fit to the Seiden expression[12] for a uniform, isolated 1-D chain comprised of alternating quantum ($S = 1/2$) and classical ($g = 2$; $S = 2$) spin sites ($H = -2J\mathbf{S}i\bullet\mathbf{S}j$). The 1-D intrachain coupling, *J*intra, was determined from modeling $\chi T(T)$ by the Seiden expression with J_{intra}/k_B = -40 K (J_{intra} = -28 cm^{-1}) (Figure 6.5). The observed negative J_{intra} also indicates antiferromagnetic coupling. The Seiden model is not valid below ~70 K due to increased 3-D spin correlations for systems in which the intrachain coupling is weak. This is likely

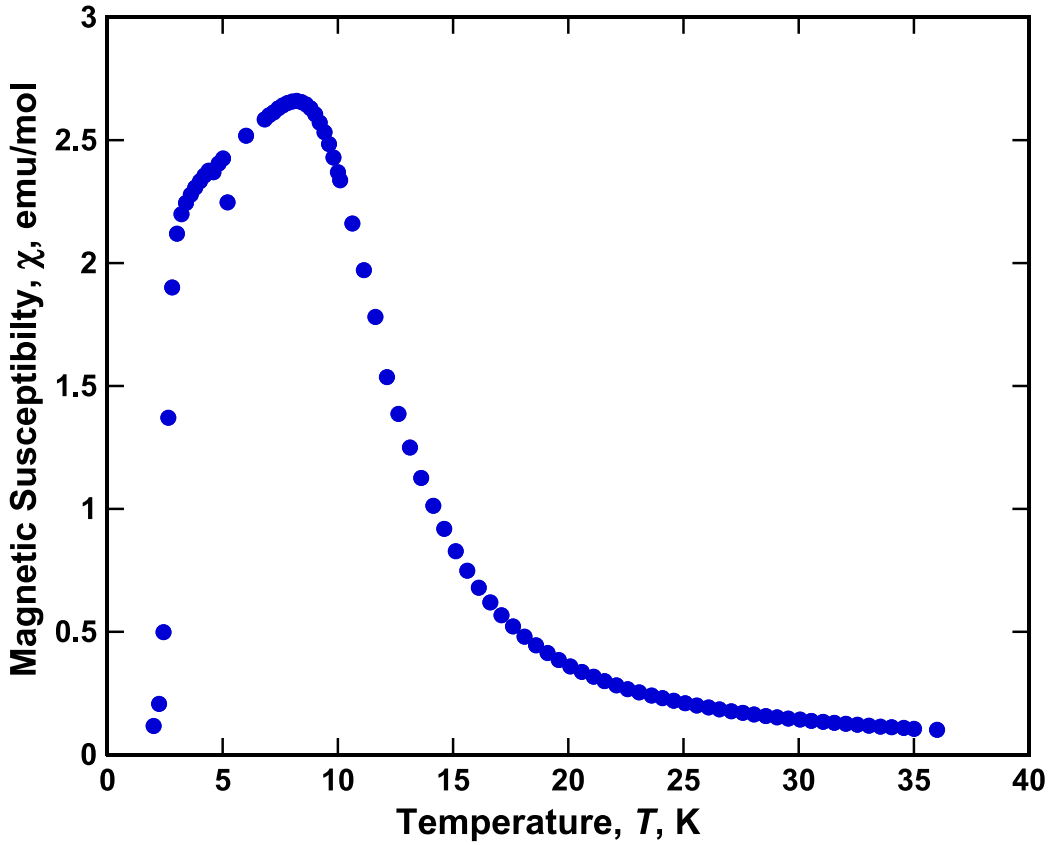

Figure 6.4. $\chi(T)$ for [MnTPP][Me_2DCNQI] at 1000 Oe applied field.

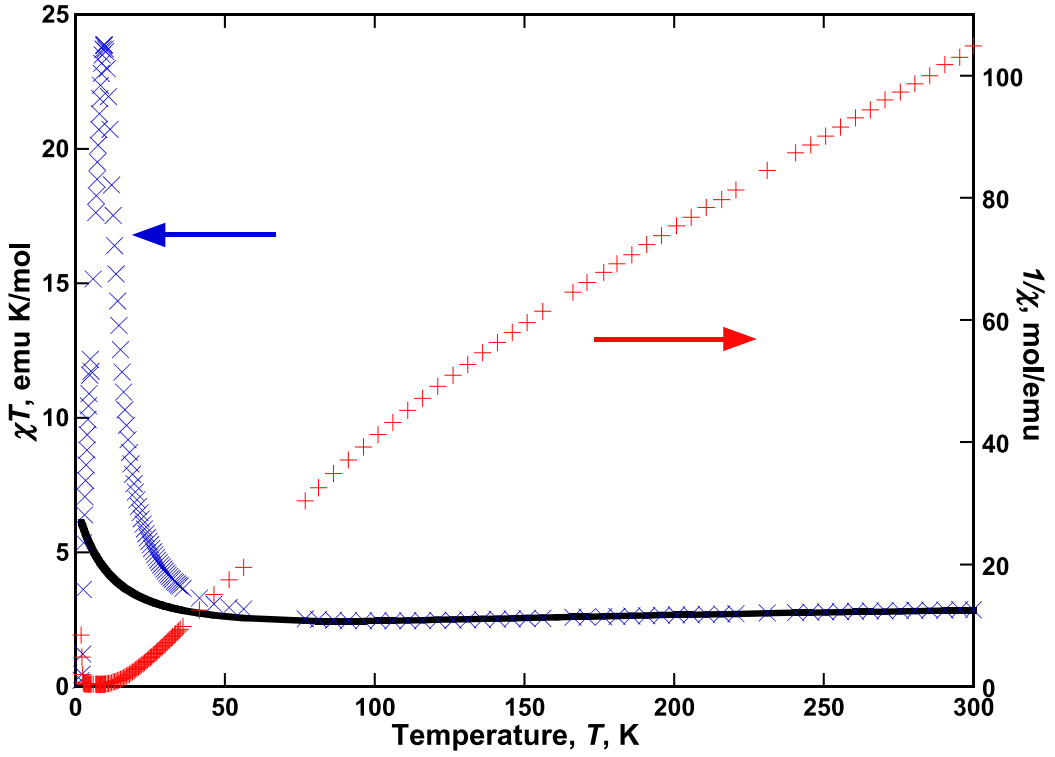

Figure 6.5. $\chi^{-1}(T)$ (+) and $\chi T(T)$ (x) and fit of the latter to the Seiden expression for [MnTPP][Me_2DCNQI].

due to next nearest neighbor interactions and the onset of long-range interchain coupling. Currently, no appropriate, alternative magnetic model exists. The Seiden model was modified[27] to include θ to account for the interchain interactions, and θ is -13 K indicating antiferromagnetic interchain coupling, which is weaker than the intrachain interactions, i.e., -40 K.

Isothermal field-dependent magnetization, $M(H)$, experiments reveal a 2-K magnetization at 90 kOe of 10650 emuOe/mol (9400 at 50 kOe) (Figure 6.6). For an antiferromagnetic $S_{tot} = 2 - 1/2 = 3/2$ system, the expected saturation magnetization, M_s, is 16755 emuOe/mol and for a ferromagnetic $S_{tot} = 2 + 1/2 = 5/2$ system, Ms is expected to be 27925 emuOe/mol. The magnitude of the magnetization at 90 kOe is lower than that expected for an antiferromagnetically coupled $S_{tot} = 2 - 1/2 = 3/2$ system; however, based on the slope of the $M(H)$ curve, saturation was not evident. Thus, [MnTPP][Me_2DCNQI] is a ferrimagnet. Hysteretic behavior is present at 2 K, with a coercivity of 5600 Oe, and remanent magnetization of 6300 emuOe/mol (Figure 6.6). The coercivity is much lower in value than that observed for the [MnTPP][TCNE] family of molecule-based magnets, which frequently have coercivities exceeding 25000 Oe.[10] This attenuated coercivity may be related to the reduced T_c for [MnTPP][Me_2DCNQI].

The reduced T_c is comparable to that observed for [MnTmesP][$(MeO)_2$DCNQI] and [MnTmesP][Me_2DCNQI].[8] These compounds have magnetization values of 14200 and 10200 emuOe/mol at 50 kOe, respectively, that exceed 9400 emuOe/mol for [MnTPP][Me_2DCNQI]. [MnTmesP][$(MeO)_2$DCNQI] and [MnTmesP][Me_2DCNQI] have remnant magnetizations of 14400 and 10200 emuOe/mol, and coercivities of 17800 and 9600 Oe, respectively.[8]

[MnTPP][Me_2DCNQI] exhibits responses to both the in-phase, real, $\chi'(T)$, and

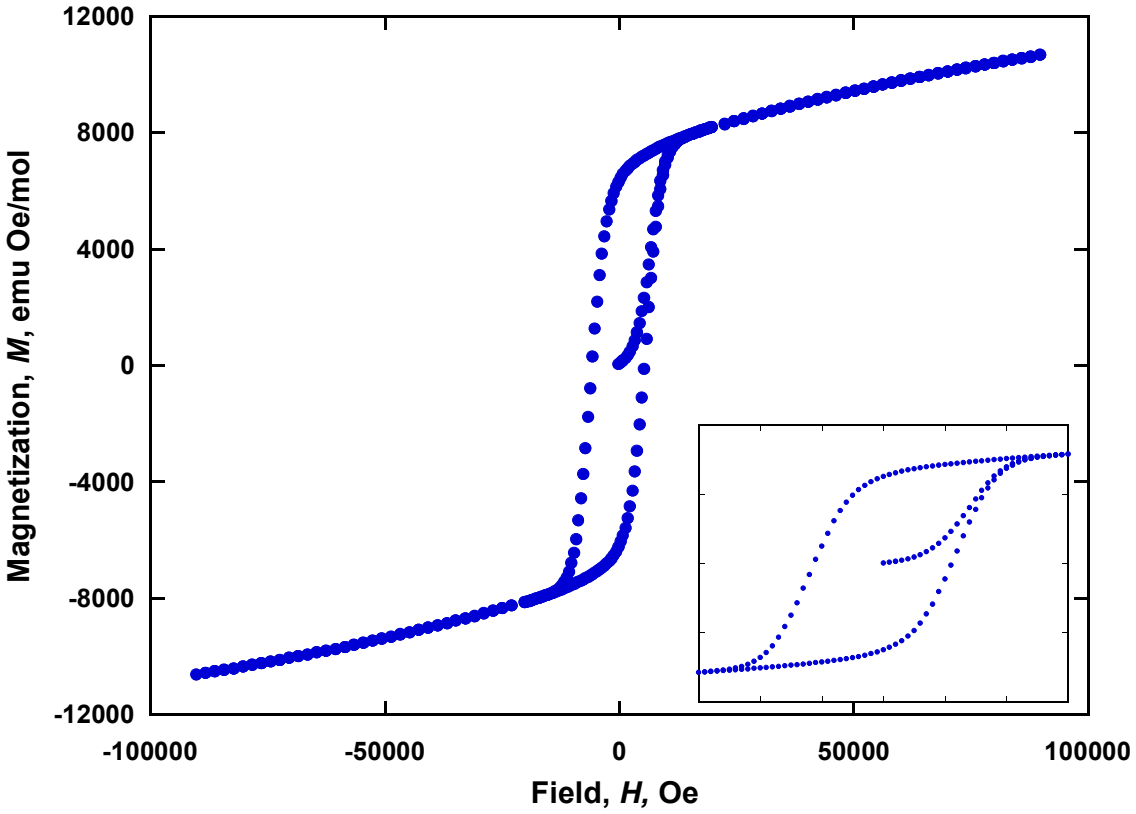

Figure 6.6. Hysteresis of [MnTPP][Me_2DCNQI] at 2 K.

out-of-phase, imaginary, $\chi''(T)$, ac susceptibilities (Figure 6.7). A large frequency-independent peak is observed centered at 9.6 K in $\chi'(T)$ for which there is no corresponding $\chi''(T)$ peak. This indicates antiferromagnetic ordering, and is anomalous with respect to related materials. At lower temperature, frequency-dependent peaks are observed for both $\chi'(T)$ and $\chi''(T)$. The latter is in accord with that reported for closely related TCNE[2a,18] as well as DCNQI materials.[5,6] For this family of materials, T_c is determined by the peak in the in-phase susceptibility at 10 Hz, and is estimated to be 4.3 K. The frequency (ω) dependence of the ac susceptibility indicates glassiness that is parameterized by ϕ [= $\Delta T_f/T_f\Delta\log\omega$][29] and is 0.18. This is consistent with typical spin-glasses[29] and related materials.[28] This value is higher than seen for [MnTmes][Me_2DCNQI] (0.07), but similar to that seen in [MnTmes][$(MeO)_2$DCNQI] (0.16).[8] The higher value of 0.18 is characteristic of greater disorder, as reported for [MnTP'P][TCNE]•2PhMe [TP'P = 3,5-di-*tert*-butyl-4-hydroxyphenylporphinato] that also has $\phi = 0.18$.[11]

Zero-field-cooled and field-cooled magnetic measurements were taken below 35 K at 5 Oe field, and reveal a bifurcation temperature, T_b, at 4.8 K, in accord with magnetic ordering as a ferrimagnet.

Antiferromagnetic ordering is suggested by the peaks in $\chi(T)$, and $\chi'(T)$ at 9.8 K, and absence of a $\chi''(T)$ absorption. Fisher noted that the temperature at which the maximum in $\chi(T)$ occurs lies above T_c,[29,30] and that T_c can be reliably determined from the temperature at which the maximum in $d\chi T/dT$ occurs.[31,32] The maximum in $d\chi T/dT$, T_c, occurs at 4.3 K.

Magnetostructural correlation. As discussed above, an inverse linear correlation between θ' and (a) the dihedral angle between the mean [Mn(porphyrin)]$^+$ and

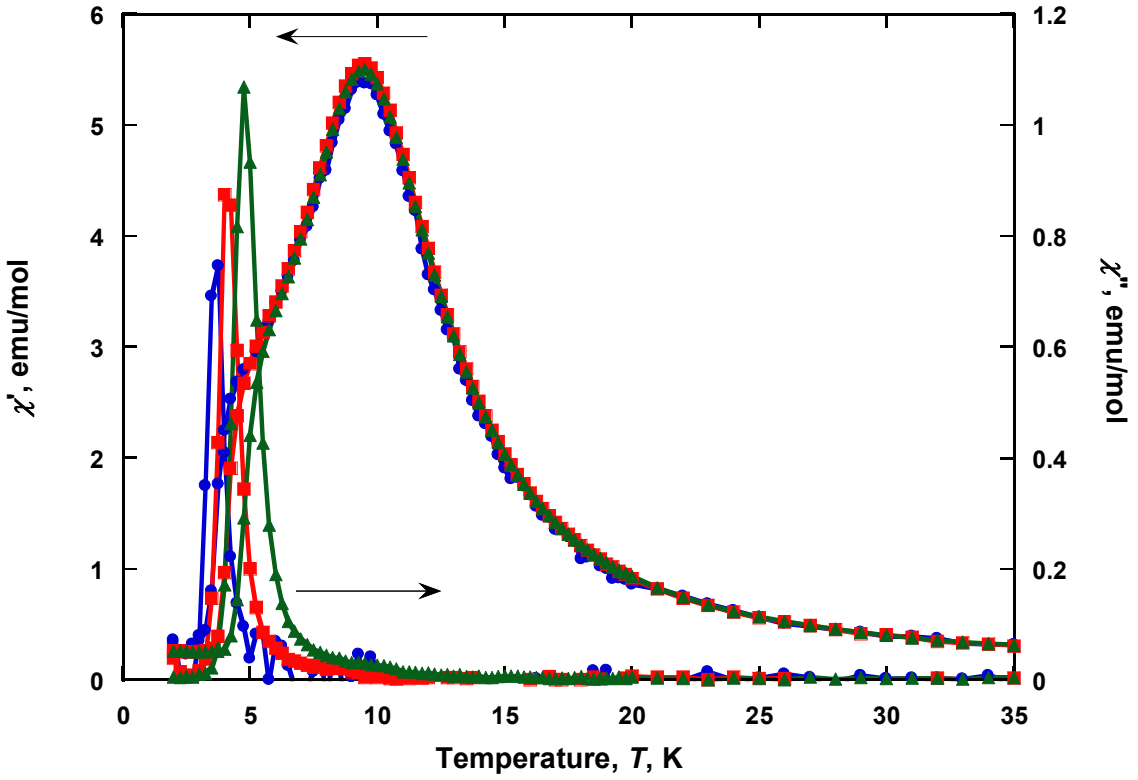

Figure 6.7. $\chi'(T)$ and $\chi''(T)$ for [MnTPP][Me_2DCNQI] at 10 (●), 100 (■), and 1000 (▲) Hz.

the $[TCNE]^{\cdot-}$ planes, and (b) the ∠Mn-$(N\text{-}C)_{TCNE}$ has been previously reported for a series of substituted [Mn(porphyrin)][TCNE] materials.[11] While this correlation works well for TCNE-based organic-based magnets, insufficient data are available to extend it to electron acceptors other than TCNE, and herein we add another example of an aromatic-based electron acceptor to extend the model.

Inclusion of data for [MnTPP][Me_2DCNQI], as well as for [MnTmesPP][Me_2DCNQI, [MnTmesPP][$(MeO)_2$DCNQI], ([MnTPP][TCNE], [MnTOMePP][TCNE] [TOMePP = tetrakis(4-methoxyphenyl)porphinato], [MnTFPP][TCNE] [TFPP = tetrakis(-2-fluorophenyl)porphinato], [MnTP'P][TCNE], and [MnTClPP][TCNE]•zS [TClPP = *meso*-tetrakis(4-chlorophenyl)porphinato; z = 0, 2; S = PhMe, CH_2Cl_2] with those for substituted [Mn(porphyrin)][TCNE] magnets show a strong inverse correlation between the dihedral angle and the value of θ' (Figure 6.8), with a correlation coefficient (R) equal to 0.98.[11b,33] This correlation exceeds that obtained for the dihedral angle and J_{intra} obtained from fits with the Seiden model (R = 0.80). The relationship between the ∠Mn-N-C and both θ' is similar (Figure 6.9), but has a poorer correlation with R = 0.84. The correlation of ∠Mn-N-C and J_{intra} is comparable with R = 0.80. When only [Mn(porphyrin)][TCNE] compounds are considered, the correlation between the dihedral angle and θ' is equally strong (R = 0.99), but the correlation between the dihedral angle and J_{intra} is somewhat worse (R = 0.78). In contrasted, the relationship between the ∠Mn-N-C and the magnetic parameters is greater within the TCNE series, with correlation coefficient (R) of 0.98 and 0.86 for correlations with θ' and J_{intra}, respectively.

These correlations indicate that the dihedral angle between the mean $Mn(N_4)_{TPP}$

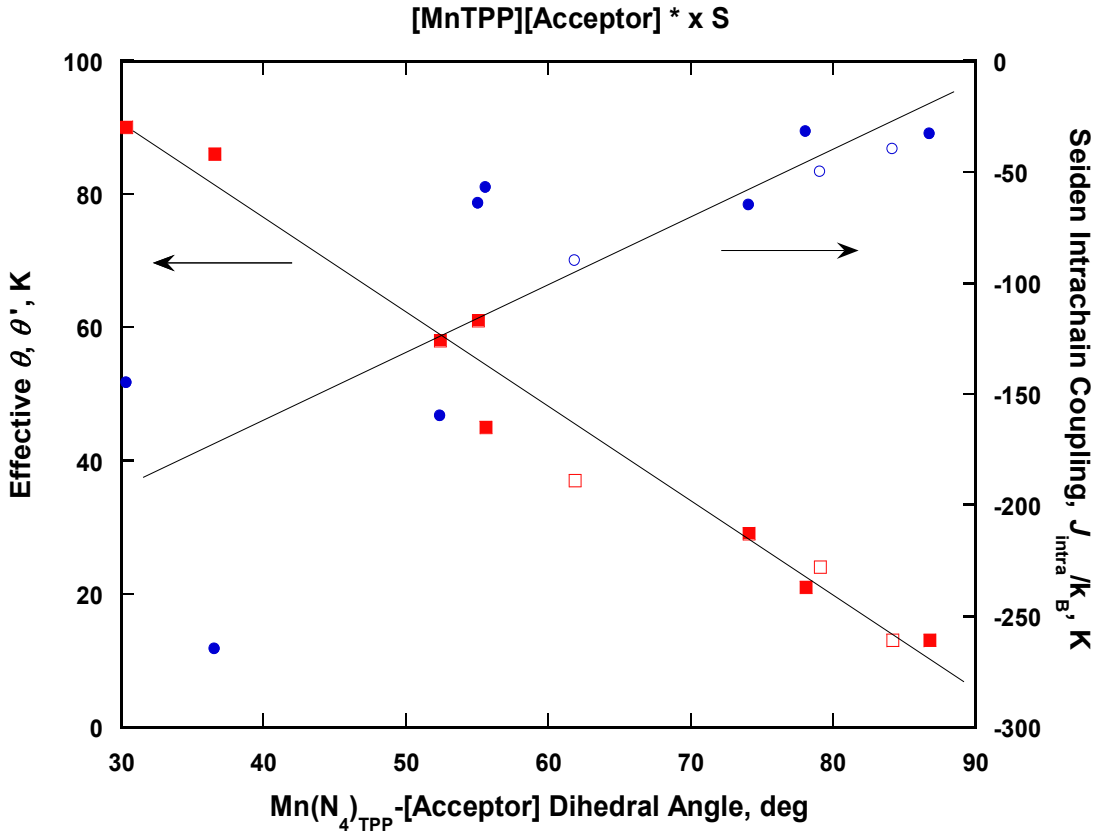

Figure 6.8. Inverse correlation between the dihedral angle and the θ' (■), and the direct correlation between the dihedral angle and J_{intra} coupling obtained from the Seiden fit (●) for a series of $[MnPor]^{+}$ cations and $[TCNE]^{\bullet-}$ (solid) aromatic DCNQI-based (hollow) radicals.

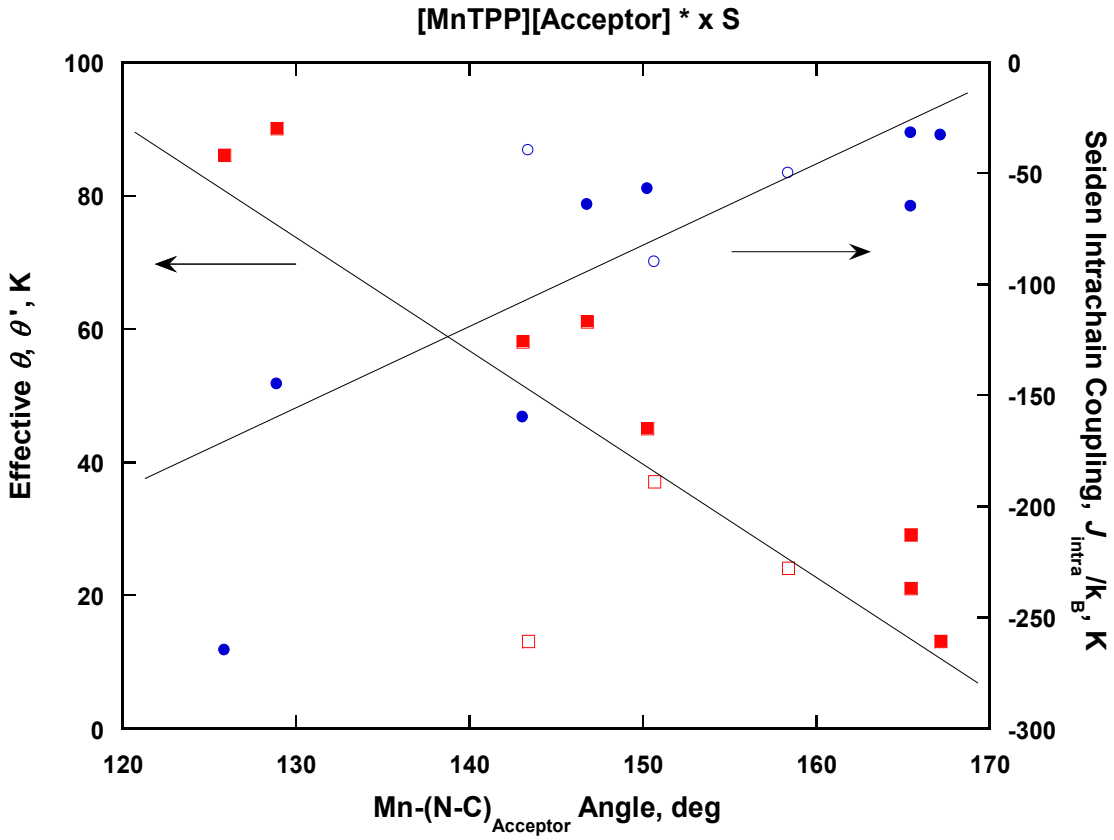

Figure 6.9. Inverse correlation between the ∠Mn-N-C and the θ' (■), and the direct correlation between the dihedral angle and J_{intra} coupling obtained from the Seiden fit (●) for a series of $[MnPor]^{+}$ cations and $[TCNE]^{\bullet-}$ (solid) aromatic DCNQI-based (hollow) radicals.

and $[Me_2DCNQI]^{\bullet-}$ planes is the most important parameter to consider for this compound when determining the dominant intrachain coupling within the chains. Lower values of this angle correlate with stronger coupling. This enhancement of intrachain coupling with decreasing angle is attributed to the dominate overlap leading to spin coupling arising from the Mn^{III} d_{z2}-like SOMO and the *z* component of the $[TCNE]^{\bullet-}$ π* (π_z*) SOMO (Figure 6.10). When $[TCNE]^{\bullet-}$ is perpendicular to the $Mn(N_4)_{TPP}$, there is no π_z* to overlap with the Mn^{III} d_{z2}-like SOMO. Upon reduction of this angle, π_z* becomes finite and increases, leading to greater overlap and spin coupling in accord with the observed increase of θ' and J_{intra}.

The identification of a correlation with T_c and structural parameters, however, remains elusive. Magnetic ordering is a bulk phenomenon that includes contributions from interchain coupling in addition to intrachain coupling. Further insight and modeling is needed to correlate the interchain couplings, in addition to the intrachain couplings, with T_c, and the structural data provided herein should be important in this future endeavor.

Conclusions

[MnTPP][Me_2DCNQI] forms chains of $S = 2$ $[Mn^{III}TPP]^+$ alternating with $S = 1/2$ μ-$[Me_2DCNQI]^{\bullet-}$ that lacks solvent. The dihedral angle between the mean $Mn(N_4)_{TPP}$ and $[TCNE]^{\bullet-}$ planes is almost perpendicular at 84.18° and thus, has weak intrachain overlap between the Mn^{III} d_{z2}-like and π_z*-$[TCNE]^{\bullet-}$ SOMOs, leading to weak intrachain chain coupling, J_{intra} = -40 K, as observed with respect to related magnetic materials. These data extend this model to strong electron acceptors in addition to TCNE and to electron acceptors that are aromatic. The reduced J_{intra} coupling contributes to the

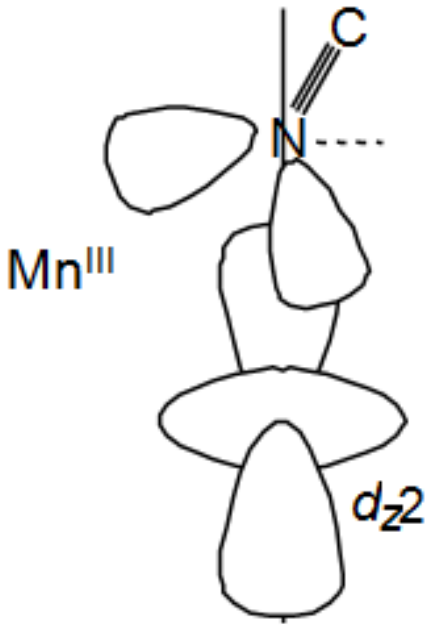

Figure 6.10. Illustration of the overlap leading to spin coupling arising from the Mn^{III} d_{z2}-like and π_z*-$[TCNE]^{\bullet-}$ SOMOs.

reduced T_c (4.3 K) as well as 2-K coercivity, H_{cr} (5600 Oe), which, except for [MnTmesPP][Me_2TCNQ][5] are among the lowest reported for this family of organic-based magnets. Materials with lower H_{cr} include [MnTFF][TCNE] (3600 Oe),[36] [MnT($OC_{12}H_{25}$)PP][TCNE] (5000 Oe),[36] and [MnTBrPP][TCNE] (4100 Oe).[1a,37]

In addition, [MnTPP][Me_2DCNQI] is an atypical member of this family of magnets as it has a second magnetic phase, antiferromagnetic, with a 9.6-K T_c, which is also anomalous, as it is frequency-independent. Similar responses have been seen in related [Mn(porphyrin)][TCNE] chains,[34] though the cause of the magnetic transition is not fully understood. A similar transition has also been studied for [MnOEP][$C_4(CN)_6$] where the first, antiferromagnetic transition is attributed to interlayer interactions and the second peak, exhibiting frequency dependency, is ascribed to weak 3-D ferromagnetic behavior.[35] Further study of this antiferromagnetic coupling is in progress.

References

(1) (a) Miller, J.S. *Adv. Mater.* **2002**, *14*, 1105. (b) Day, P. *Notes Rec. R. Soc. Lond.* **2002**, *56*, 95.

(2) (a) Miller, J.S. *Chem. Soc. Rev.* **2011**, *40*, 3266. (b) Miller, J.S.; Epstein, A.J. Chem. Commun. **1998**, 1319. (c) Blundell, S.J.; Pratt, F.L. *J. Phys.: Condens. Matter* **2004**, *16*, R771. (d) Crayston, J.A.; Devine, J.N.; Walton, J.C. *Tetrahedron* **2000**, *56*, 7829. (e) Ovcharenko, V.I.; Sagdeev, R.Z. *Russ. Chem. Rev.* **1999**, *68*, 345. (f) Kinoshita, M. *Phil. Trans. R. Soc. Lond. (A)* **1999**, *357*, 2855. (e) Miller, J.S.; Epstein, A.J. *Angew. Chem. Int. Ed. Engl.* **1994,** *33*, 385.

(3) (a) Rittenberg, D.K.; Sugiura, K.-i.; Arif, A.M.; Incarvito, C.D.; Rheingold, A.L.; Sakata, Y.; Miller, J.S. *Chem. Eur. J.* **2000**, *6*, 1811. (b) Sugiura, K.-i.; Arif, A.M.; Rittenberg, D.K.; Schweizer, J.; Öhrstrom, L.; Epstein, A.J.; Miller, J.S.; *Chem. Eur. J.* **1997**, *3*, 138. (c) Miller, J.S.; Vazquez, C.; Jones, N.L.; McLean, R.S.; Epstein, A.J. *J. Mater. Chem.* **1995**, *5*, 707.

(4) Brandon, E.J.; Rogers, R.D.; Burkhart, B.M.; Miller, J.S. *Chem. Eur. J.* **1998**, *4*, 1938.

(5) Sugiura, K.-i.; Mikami, S.; Johnson, M.T.; Miller, J.S.; Iwasaki, K.; Umishita, K.; Hino, S.; Sakata, Y. *J. Mater. Chem.* **2000**, *10*, 959.

(6) Johnson, M.T.; Arif, A.M.; Miller, J.S. *Eur. J. Inorg. Chem.* **2000**, 1781.

(7) Mikami, S.; Sugiura, K.-i.; Miller, J.S.; Sakata, Y. Chem. Lett. **1999**, 413.

(8) Sugiura, K.-i.; Mikami, S.; Johnson, M.T.; Raebiger, J.W.; Miller, J.S.; Iwatsaki, K.; Okada, Y.; Hino, S.; Sakata, Y. *J. Mater. Chem*. **2001**, *11*, 2152.

(9) Rittenberg, D.K.; Arif, A.M.; Miller, J.S. *J. Chem. Soc., Dalton Trans.* **2000**, 3939.

(10) Rittenberg, D.K.; Sugiura, K.-i.; Sakata, Y.; Mikami, S.; Epstein, A.J.; Miller, J.S. *Adv. Mater.* **2000**, *12*, 126.

(11) (a) Brandon, E.J.; Kollmar, C.; Miller, J.S. *J. Am. Chem. Soc.* **1998**, *120*, 1822. (b) Her, J.-H.; Stephens, P.W.; Bagnato, J.D.; Miller, J.S. *J. Phys. Chem. C* **2010**, *114*, 20614.

(12) Seiden, J. *J. Phys. Lett.* **1983**, *44*, 947.

(13) (a) Coronado, E.; Drillon, M.; Georges, R. *Research frontiers in magnetochemistry*; O'Connor C.J., Ed.; *Ferrimagnetic Chains: Models and Materials* **1993**, *26*, pp. 27-66. (b) Beltran, D.; Drillon, M.; Coronado, E.; Georges, R. *Stud. Inorg. Chem.* **1983**, *3*, 589. (c) Drillon, M.; Coronado, E.; Beltran, D.; Georges, R. *Chem. Phys.* **1983**, *79*, 449. (d) Verdaguer, M.; Julve, M.; Michalowicz, A.; Kahn, O. *Inorg. Chem.* **1983**, *22*, 2624. (e) Drillon, M.; Gianduzzo, J.C.; Georges, R. *Phys.* . **1983**, *96A*, 413.

(14) (a) Ribas-Ariño, J.; Novoa, J.J.; Miller, J.S. *J. Mater. Chem.* **2006**, *16*, 2600. (b) Brandon, E.J.; Miller, J.S. *NATO ARW supramolecular engineering of synthetic metallic materials: conductors and magnets*; Veciana, J.; Rovira, C.; Amabilino, D. Eds., **1998**, *C518*, 197.

(15) Adler, A.D.; Longo, F.R.; Finarelli, J.D.; Goldmacher, J.; Assour, J.; Korsakoff, L. *J. Org. Chem.* **1967**, *32*, 476.

(16) Jones, R.D.; Summerville, D.A.; Basolo, F. *J. Am. Chem. Soc*. **1978**, *100*, 416.

(17) Aumüller, A.; Hünig, A. *Liebigs Ann. Chem.* **1986**, 142.

(18) Brandon, E.J.; Rittenberg, D.K.; Arif, A.M.; Miller, J.S. *Inorg. Chem.* **1998**, *37*, 3376.

(19) Bruker AXS (2005): *TOPAS V3: General profile and structure analysis software for powder diffraction data.* - User's Manual, Bruker AXS, Karlsruhe, Germany.

(20) Coelho, A.A. J. Appl. Cryst. **2000**, *33*, 899.

(21) TOPAS-Academic is available at http://www.topas-academic.net.

(22) Bruno, I.J.; Cole, J.C.; Kessler, M.; Luo, J.; Motherwell, W.D.S.; Purkis, L.H.; Smith, B.R.; Taylor, R.; Cooper, R.I.; Harris, S.E.; Orpen, A.G. *J. Chem. Inf. Comput. Sci.* **2004**, *44*, 2133.

(23) Lunardi, G.; Pecile, C. *J. Chem. Phys.* **1991**, *95*, 6911.

(24) (a) Hibbs, W.; Rittenberg, D.K.; Sugiura, K.-i.; Burkhart, B.M.; Morin, B.G.; Arif, A.M.; Liable-Sands, L.; Rheingold, A.L.; Sundaralingam, M.; Epstein, A.J.; Miller, J.S. *Inorg. Chem.* **2001**, *40*, 1915. (b) Goldberg, I.; Krupitsky, H.; Stein, Z.; Hsiou, Y.; Strouse, C.E. *Supramolecular Chem 4* **1995**, 203. (c) Krupitsky, H.; Stein, Z.; Goldberg, I. *J. Inclus. Phenom. Mol.* **1995**, *20*, 211. (d) Goldberg, I. *Mol. Cryst. Liq. Cryst.* **1996,** *278*, 767. (e) Byrn, M.P.; Curtis, C.J.; Hsiou, Y.; Kahn, S.I.; Sawin, P.A.; Tendick, S.K.; Terzis, A.; Strouse, C.E. *J. Am. Chem. Soc.* **1993,** *115*, 9480. (f) Rittenberg, D.K.; Sugiura, K.-i.; Sakata, Y.; Guzei, I.A.; Rheingold, A.L.; Miller, J.S. *Chem. Eur. J.* **1999**, *5*, 1874. (g) Brandon, E.J.; Sugiura, K.-i.; Arif, A.M.; Liable-Sands, A.; Rheingold, A.L.; Miller, J.S. *Mol. Cryst., Liq. Cryst.* **1997**, *305*, 269. (h) Brandon, E.J.; Arif, A.M.; Burkhart, B.M.; Miller, J.S. *Inorg. Chem.* **1998**, *37*, 2792. (i) Brandon, E.J.; Arif, A.M.; Miller, J.S.; Sugiura, K.-i.; Burkhart, B.M. *Crystal Eng.* **1998**, *1*, 97. (j) Sugiura, K.-i.; Mikami, S.; Tanaka, T.; Sawada, M.; Manson, J.L.; Miller, J.S.; Sakata, Y. *Chem. Lett. 1997*, 1071. (k) Day, V.W.; Stults, B.R.; Tasset, E.L.; Marianelli, R.S.; Boucher, L.J. *Inorg. Nucl, Chem. Lett.* **1975**, *11*, 505. (l) Cheng, B.; Cukiernik, F.; Fries, P.; Pascal, H.; Marchon, J.-C.; Scheidt, W.R. *Inorg. Chem.* **1995**, *34*, 4627. (m) Guildard, R.; Perie, K.; Barbe, J.-M.; Nurco, D.J.; Smith, K.M.; Caemelbecke, E.V.; Kadish, K.M. *Inorg. Chem.* **1998**, *37*, 973. (n) Landrum, J.T.; Hatano, K.; Scheidt, W.R.; Reed, C.A. *J. Am. Chem. Soc.* **1980**, *102*, 6729. (o) Hill, C.L.; Williamson, M.M. *Inorg. Chem.* **1985**, *24*, 3024. (p) Fleischer, E.B. *Acc. Chem Res.* **1970**, *3*, 105. (q)

Scheidt, W.R.; Reed, C.A. *Chem. Rev.* **1981**, *81*, 543. (r) Turner, P.; Gunter, M.J.; Hambley, T.W.; White, A.H.; Skelton, B.W. *Inorg. Chem.* **1992**, *32*, 2297.

(25) Aumüller, A.; Erk, P.; Hünig, S.; Hädicke, E.; Peters, K.; von Schnering, H.G. *Chem. Ber.* **1991**, *124*, 2001.

(26) Liu, G.-X.; Huang, R.-Y.; Ren, X.-M. *J. Mol. Struct.* **2008**, *891*, 11.

(27) Böhm, A.; Vazquez, C.; McLean, R.S.; Calabrese, J.C.; Kalm, S.E.; Manson, J.L.; Epstein, A.J.; Miller, J.S. *Inorg. Chem.* **1996**, *35*, 3083.

(28) Dawe, L.N.; Turnbow, L.; Miglioi, J.M.; Taliaferro, M.L.; Shum, W.W.; Bagnato, J.D.; Zakharov, L.N.; Rheingold, A.L.; Arif, A.M.; Fourmigué, M.; Miller, J.S. *Inorg. Chem.* **2005**, *44*, 7530.

(29) Mydosh, J. Spin Glasses, Taylor and Francis, London, 1993.

(30) Fisher, M.E. *Philos. Mag.* **1962**, *7*, 1731.

(31) Ashcroft, N.W.; Mermin, N.D. Solid State Physics, W. B. Saunders and Co., **1976**, p. 701 ff.

(32) Aharen, T.; Greedan, J.E.; Ning, F.; Imai, T.; Michaelis, V.; Kroeker, S.; Zhou, H.; Wiebe, C.R.; Cranswick, L.M.D. *Phys. Rev. B* **2009**, *80*, 134423.

(33) Cage, B.; Nguyen, B.; Dalal, N. *Sol. State Commun.* **2001**, *119*, 597.

(34) R = correlation coefficient and is taken from regression fit of the linear correlation (Ref 11b). Correlation coefficient between the Mn(N4)TPP-[Acceptor] dihedral angle, φ, and θ' [$\theta' = 132.73 - 1.416\varphi$] and J [$J = -281.7 + 3.021\varphi$] is equal to 0.98 and 0.80 respectively. R between $\angle$Mn-N-C, ψ, and θ'[$\theta' = 288.01 - 1.635\psi$] and J [$J = -702.03 + 4.084\psi$] is 0.84 and 0.80, respectively.

(35) Rittenburg, D.K.; Miller, J.S. *Inorg. Chem.* **1999**, *38*, 4838.

(36) (a) Wynn, C.M.; Gírtu, M.A.; Miller, J.S.; Epstein, A.J. *Phys. Rev. B* **1997**, *56*, 14050. (b) Wynn, C.M.; Gírtu, M.A.; Sugiura, K.-i.; Brandon, E.J.; Manson, J.L.; Miller, J.S.; Epstein, A.J. *Synth. Met.* **1997**, *85*, 1695. (c) Wynn, C.M.; Gírtu, M.A.; Miller, J.S.; Epstein, A.J. *Phys. Rev. B* **1997**, *56*, 315. (d) Epstein, A.J.; Wynn, C.M.; Brinckerhoff, W.B.; Miller, J.S. *Mol. Cryst. Liq. Cryst.* **1997**, *305*, 321.

CHAPTER 7

CONCLUDING REMARKS AND FUTURE WORK

Concluding Remarks

Organic ligands have become an integral part of molecule-based magnetic systems. Research has shown that they can be used to tune and enhance magnetic properties. They play roles as scaffolds, spin-carriers, and the sole constituents of these magnetic systems.

The magnetic behavior of the dimeric form of *N*,*N*'-ethylenebis(salicylideniminato)cobalt(II) (Co^{II}(salen)) was reinvestigated due to evidence of multiple stable states in the magnetic data. The dimer was seen to exhibit magnetic tristability, which is associated with the dinuclear site, not a single-ion site as is typically seen. The singlet (S = 0) ground state arises from the antiferromagnetically coupled pair of the Co^{II} ions, each being in the single-ion, low-spin, S = 1/2 electron configuration. The triplet (S = 1) excited state arises from ferromagnetic coupling of the Co^{II} S = 1/2 ions. As the temperature increases, the thermal energy populates both the singlet and triplet states. This leads to increases in the $\chi T(T)$, approaching the Curie behavior for the two Co^{II}, S = 1/2 doublets at higher temperature because the exchange coupling, J, is less significant with respect to the thermal energy. The tristability found in these compounds is expected to have applications in molecular switches and memory storage.

In order to better understand the origin and properties of the tristability, a series of

functionalized salen-ligands were synthesized and examined for tristability. The results showed evidence of tristability in two additional compounds, [*N*,*N*'-bis(3,5-dinitrosalicylidene)-1,2-cyclohexanediaminato(2-)cobalt(II)] and [*N*,*N*-bis[[(2-hydroxyphenyl)methylene]-amino]-2-butenedinitrilato(2-)-cobalt(II)]. Crystal structures of these compounds have not yet been obtained, but spectroscopic and elemental analysis studies support the formation of the coordinated compounds. The presence of tristability in these compounds and the absence in other compounds is not currently understood, but is proposed to arise from interaction between metal sites within the dimers. Interaction between the dimers is noted to arise when the salen compound contains strong electron-withdrawing functionalities, such as the nitro- and cyano-groups. This may possibly lead to less electron density on the metal sites, encouraging dimerization. If this can be shown to be correct, it would provide a template for the synthesis of multistable materials, which have applications in molecular electronics.

Additionally, the properties of asymmetric cyanocarbon acceptors have been investigated. *N*,7,7-Tricyanoquinomethanimine (TCQMI) was of particular interest as the three nitrile groups would allow for better agreement of nitrile groups with octahedral metal center coordination sites. Reactions of TCQMI with precedented cationic building-blocks of molecular magnets, $FeCp^*_2$, $Fe(CO)_5$, and $V(CO)_6$, have shown mixed results. The expected structural motif of 1-D chains of alternating $[TCQMI]^{\bullet-}$ and $[FeCp^*_2]^+$ showed weak ferrimagnetic low-temperature ordering with a T_c of 3.4 K, within the range seen in related compounds. However, magnetic hystereses were not observed.

Additionally, the reaction of TCQMI with $M^{II}(CO)_x$ compounds led to amorphorous compounds which showed either weak ferromagnetic coupling or

paramagnetic behavior at low temperatures. These results indicate that TCQMI, specifically the cyanimine functional group, is incompatible with forming magnetic systems where direct bonding to metal centers is expected. This is consistent with the lack of ordered magnetic materials resulted from the reaction of DCNQI compounds with similar metal sources.

Further evidence of the unsuitability of cyanimine-bearing acceptors was encountered in the reaction of TCQMI with MnTPP(py). The resulting structure of $[Mn^{III}(TPP)]^{+}[TCQMI]^{\bullet-}$ consisted of a warped MnTPP with an average Mn-N distance of 2.023 Å, and a σ-$[TCQMI]_2^{2-}$ dimer. The $Mn^{III}NCNMn^{III}$ linkages with 6.204-Å Mn•••Mn separations are present, and the $S = 2$ Mn^{III}'s are not bonded to a radical. Thus, $[Mn^{III}TPP][TCQMI]$ is best formulated as $\{[Mn^{III}TPP]^{+}\}_2$-$[TCQMI]_2^{2-}$. The MnNCNMn linkages lead to 1-D chains that are cross-linked by the σ-$[TCQMI]_2^{2-}$ dimer. This leads to a honeycomb 2-D layered structure with 24-membered rings.

Magnetic ordering at low-temperature (T_c = 3.7 K) is observed. The origin of the canted antiferromagnetic/weak ferromagnetic ordering is attributed to the close proximity of the of the Mn^{III} sites. Similar behavior is seen in Mn^{III}(salen) sites bridged by hydrogencyanamide in a $\mu_{1,3}$-mode with ordering temperatures observed below 2.5 K. These results indicate that increased magnetic properties (higher T_c, hystereses) might be possible if the compound could be modified to inhibit dimerization. Since the dimerization appears to be typically observed at the -$C(CN)_2$ carbon of TCQMI, TCNE, and TCNQ, it is envisioned that replacing that carbon with an oxygen or nitrogen might be possible solutions. Two novel cyanocarbons, CDTQI and CDCQI, have been synthesized with this goal in mind. It is hoped these, or related compounds, may produce materials with large coercive fields that may be magnetic nearer to room-temperature. If

successful, these compounds would have applications in memory storage media.

[MnTPP][Me_2DCNQI] was also investigated for its interesting magnetic properties. A strong correlation between the dihedral angle formed by the mean $Mn(N_4)_{TPP}$ and $[TCNE]^{\bullet-}$ planes is significant as it indicates that intrachain overlap between the Mn^{III} d_{z2}-like and π_z*-$[TCNE]^{\bullet-}$ SOMOs leads to weak intrachain coupling. These data extend this model to aromatic electron acceptors other than TCNE.

In addition, [MnTPP][Me_2DCNQI] is an anomalous member of this family of magnets as it has a second magnetic phase, antiferromagnetic, with a 9.6-K T_c. This transition is also anomalous, as it occurs at higher temperature and is frequency-independent. Similar responses have been seen in related compounds, where the first, antiferromagnetic transition is attributed to interlayer interactions and the second peak, exhibiting frequency-dependency, is ascribed to weak 3-D ferromagnetic behavior.

Future Work

The success in forming new Co^{II}(salen) compounds exhibiting three reversible magnetic states has indicated a correlation between strong electron-withdrawing groups and tristability. As tristability has been previously linked with dimeric behavior, efforts are being made to solve the structure of the Co^{II}(salen) analogues. The structures are hoped to confirm the correlation between metal ligand bond distance and the transition temperatures found within the compounds as well as the correlation between electron-donating/withdrawing substituents and tristability. Additionally, an examination of the properties of compounds incorporating diaminomaleonitrile in the backbone as well as functionalized salicylaldehydes may produce further compounds the exhibit tristability and elucidate a means to better control the onset temperature and sharpness of the

transitions.

The use of TCQMI as a constituent in molecule-based magnetic systems indicates several drawbacks to this cyanocarbon acceptor. While it forms a stable radical anion with $Fe^{III}Cp^*_2$, reactions with other metal and organometallic agents lead to amorphous products with reduced ordering temperatures or dimerization of the ligand. However, low-temperature ordering with dimerized TCQMI and MnTPP has led to interest in cyanocarbons with the cyanimine moiety. Two quinone-based compounds possessing this moiety, but excluding the dicyanomethide carbon center (the point of dimerization), have been synthesized. Research into the chemistry of these compounds with appropriate metal centers is currently underway. These compounds are expected to exhibit higher ordering temperatures and hystereses.

Finally, further study is being made into the source of antiferro- and ferromagnetic ordering exhibited by [MnTPP][Me_2DCNQI]. Additionally, research into the reactions of other functionalized DCNQIs with manganese porphyrins is being conducted with the aim of extending our understanding of the magnetostructural correlations with a series of non-TCNE-based molecule-based magnetic systems.